UNCONVENTIONAL HYDROCARBON POTENTIAL OF THE GHAZIJ FORMATION, SOUTHERN INDUS BASIN, PAKISTAN

SULTAN HISHAM SULTAN ALKATIB

09-262242-020

BAHRIA UNIVERSITY ISLAMABAD

UNCONVENTIONAL HYDROCARBON POTENTIAL OF THE GHAZIJ FORMATION, SOUTHERN INDUS BASIN, PAKISTAN

A thesis submitted in fulfilment of the requirements for the award of the degree of Master of Science (Geology)

SULTAN HISHAM SULTAN ALKATIB

09-262242-020

Department of Earth and Environmental Sciences

BAHRIA UNIVERSITY ISLAMABAD

OCTOBER 2026

APPROVAL OF EXAMINATION

Scholar's Name: Sultan Hisham Sultan Alkatib

Registration No.: 98041

Program of Study: MS Geology

Thesis Title: "UNCONVENTIONAL HYDROCARBON POTENTIAL OF THE GHAZIJ FORMATION, SOUTHERN INDUS BASIN, PAKISTAN"

It is to certify that the above scholar's thesis has been completed to my satisfaction and, to my belief, its standard is appropriate for submission for examination. I have also conducted a plagiarism test of this thesis using HEC-prescribed software and found a similarity index of 17% that is within the permissible limit set by the HEC for the MS degree thesis. I have also found the thesis in a format recognized by the BU for the MS thesis.

NOTE: The Plagiarism report is attached at the end of the thesis.

Supervisor's Signature: _____

Date: /10/2026

Name: Dr. Adeeb Ahmed

AUTHOR'S DECLARATION

I, "Mr. Sultan Hisham Sultan Alkatib," hereby state that my MS thesis titled "UNCONVENTIONAL HYDROCARBON POTENTIAL OF THE GHAZIJ FORMATION, SOUTHERN INDUS BASIN, PAKISTAN" is my own work and has not been submitted previously by me for the award of any degree by this university "Bahria University Islamabad Campus" or anywhere else in the country/world.

At any time, if my statement is found to be incorrect even after my graduation, the University has the right to withdraw/cancel my MS degree.

Scholar Name: Sultan Hisham Sultan Alkatib

Sign.: _____

Date: /10/2026

PLAGIARISM UNDERTAKING

I solemnly declare that the research work presented in the thesis titled "UNCONVENTIONAL HYDROCARBON POTENTIAL OF THE GHAZIJ FORMATION, SOUTHERN INDUS BASIN, PAKISTAN" is solely my research work with no significant contribution from any other person. Small contribution/help wherever taken, have been duly acknowledged, and the complete thesis has been written by me.

I understand the zero-tolerance policy of HEC and Bahria University towards plagiarism. Therefore, I, as the author of the above-titled thesis, declare that no portion of my thesis has been plagiarized, and any material used as reference is properly referred/ cited.

I understand that if I am found guilty of any formal plagiarism in the above-titled thesis, even after award of MS degree, the university reserves the right to withdraw, revoke my MS degree, and that HEC and the University have the right to publish my name on the HEC/University website on which names of the scholars are placed who submitted plagiarized thesis.

Scholar/Author's Sign.: _____

Name of the Scholar: Sultan Hisham Sultan Alkatib

DEDICATION

To my parents, especially my father, Dr. Hisham Alkatib, whose example, wisdom, and sacrifices have shaped the person I have become;

To my mother, Mrs. Kareema Alsaidi; my beloved siblings (Noor, Huda, and Natheer), Waqas, and my dearest Sbbaa, whose love, encouragement, and unwavering support have been a constant source of strength throughout my journey;

With love and gratitude, I dedicate this work to you all.

ACKNOWLEDGMENT

I am profoundly grateful to my supervisor, Dr. Adeeb Ahmed, Assistant Professor, Department of Earth and Environmental Sciences, Bahria University, Islamabad, for his invaluable guidance, supervision, and encouragement, which were instrumental in shaping and completing this thesis. I also sincerely thank my co-supervisor, Dr. Samina Jahandad, General Manager, Hydrocarbon Development Institute of Pakistan (HDIP), for her generous support and assistance with the research and laboratory work.

I am grateful to my teachers, Dr. Mumtaz Ali Khan, Dr. Muhammad Raiees Amjad, Mr. Tausif Ahmad, and Mr. Masood Anwar, for their valuable academic guidance and encouragement. I would also like to sincerely thank my thesis examiners for their valuable time, insightful comments, and constructive feedback, which greatly helped improve the quality of this work. I would also like to thank Dr. Syed Umair Ullah Jamil, Head of Department, Department of Earth and Environmental Sciences, Bahria University, Islamabad, for his support and cooperation throughout my studies.

I thank Bahria University, Islamabad, for the academic environment and support; the Centre of Research Excellence – Earth, Climate and Environment, Bahria University, Islamabad, for facilitating research resources; the Directorate General of Petroleum Concessions (DGPC), Pakistan, for access to geological and well data; and the Hydrocarbon Development Institute of Pakistan (HDIP) for laboratory access and analytical support.

Heartfelt thanks to my colleagues and friends for their cooperation and companionship throughout this journey, and to my family for their unconditional love, patience, and unwavering support, without which this work would not have been possible.

Finally, I sincerely thank Pakistan and its people for welcoming me and enabling my higher education here. The kindness and hospitality I experienced have left a lasting impression, and I am grateful for the friendships and memories gained.

ABSTRACT

The Ghazij Formation in the Southern Indus Basin, Pakistan, is a shale-dominated Eocene sequence containing carbonate-rich limestone intervals whose source rock quality and unconventional reservoir potential remain poorly characterized. This study integrates geochemical and petrographic analysis of the Ghazij Formation in Zamzama-5 and Mehar-1 to evaluate the quantity, quality, and thermal maturity of organic matter and to assess its unconventional hydrocarbon reservoir potential. Total organic carbon (TOC) analysis, Rock-Eval pyrolysis, X-ray fluorescence (XRF), X-ray diffraction (XRD), and scanning electron microscopy with energy dispersive X-ray spectroscopy (SEM-EDS) were applied to drill-cutting samples from Zamzama-5. Mehar-1 was evaluated by TOC and visual cutting examination only, as all samples fell below the 0.5 wt.% analytical threshold. XRF and XRD indicate carbonate-dominated limestone at Zamzama-5, ranging from calcareous quartzose limestone at shallow depths to a purer limestone at depth. Clinochlore as the only clay phase (4–5%) and a diagenetic dolomite-to-ankerite transition at the deepest interval. TOC values of 2.71–5.05 wt.% indicate very good to excellent source rock quality, exceeding the 2% unconventional hydrocarbon threshold throughout. Rock-Eval pyrolysis identifies Type III indigenous gas-prone kerogen (HI: 87–183 mg HC/g TOC), with the production index indicating immature to early mature conditions in the sampled intervals. SEM-EDS identifies five pore types defining a multi-scale pore system, with interparticle pores at shallower depths and more conspicuous natural microfractures at the deepest sample. Mineralogy-based brittleness indices of 29.5–39.6% and 90.3–96.8% indicate a favourable mineralogical brittleness framework for hydraulic fracture stimulation. However, the sampled Ghazij intervals are currently immature to early mature, representing the principal limitation to their present thermogenic hydrocarbon potential. More thermally mature Ghazij intervals may occur in deeper parts of the Southern Indus Basin and require investigation using samples from more deeply buried wells. At Mehar-1, TOC values of 0.32–0.45 wt.% and mixed shale-limestone cuttings confirm a lean organic-poor facies equivalent. The Ghazij limestone at Zamzama-5 exhibits the principal organic, mineralogical, and pore-system characteristics favourable for an unconventional tight carbonate gas play, but its present immature to early mature thermal state remains the principal limitation. It is therefore proposed as a target for further investigation, particularly in deeper parts of the Southern Indus Basin where more mature intervals may occur.

TABLE OF CONTENTS

CHAPTER	TITLE	PAGE
	APPROVAL OF EXAMINATION	i
	AUTHOR'S DECLARATION	ii
	PLAGIARISM UNDERTAKING	iii
	DEDICATION	iv
	ACKNOWLEDGMENT	v
	ABSTRACT	vi
	TABLE OF CONTENTS	vii
	LIST OF TABLES	x
	LIST OF FIGURES	xi
	LIST OF ABBREVIATIONS	xvii
1	**INTRODUCTION**	1
	1.1 Background	1
	1.2 Location of the Study Area	7
	1.3 Literature Review	8
	1.4 Research Gap	10
	1.5 Research Question	10
	1.6 Study Objectives	11
	1.7 Significance of the Study	11
2	**REGIONAL GEOLOGIC AND TECTONIC FRAMEWORK**	13

2.1 Regional Tectonic Setting 13
2.2 Geologic Setting of the Lower Indus Basin 15
2.3 Stratigraphy of Southern Indus Basin 17
2.3.1 The Ghazij Formation: age, extent, and lithofacies 20
2.4 Well-based Stratigraphic Framework 23
2.4.1 Stratigraphy of Zamzama-5 24
2.4.2 Stratigraphy of Mehar-1 25

3 METHODOLOGY 27

3.1 Research Workflow 27
3.2 Sample Material and Preparation 30
3.2.1 Cutting sample selection 30
3.2.2 Sample preparation 34
3.3 Organic Geochemical Analysis 35
3.3.1 Total organic carbon (TOC) analysis 36
3.3.2 Rock-Eval pyrolysis 388
3.4 Mineralogical and Elemental Analysis 40
3.4.1 X-ray diffraction (XRD) 41
3.4.2 X-ray fluorescence (XRF) 4242
3.5 Microscopic and Pore Structure Analysis 45
3.5.1 Scanning electron microscopy and energy dispersive x-ray spectroscopy (SEM-EDS) 45
3.6 Integrated Analytical Workflow 48

4 RESULTS AND DISCUSSION 49

4.1Lithological Characterization of the Ghazij Formation (XRF-Based) 50
4.2 XRD Mineralogical Composition of the Ghazij Formation 52
4.2.1 Carbonate mineralogy 54

4.2.2 Siliciclastic and accessory phases 55
4.3 Organic Richness (TOC) and Source Rock Quality 56
4.4 Kerogen Type and Hydrocarbon Generation Potential 59
4.5 Thermal maturity (T_{max} and production index) and its reliability 61
4.6 Petroleum Source Rock Potential of the Ghazij Formation 64
4.7 SEM-EDS Petrographic Characterization of the Ghazij Formation 666
4.7.1 Micro-scale mineral identification by EDS 67
4.7.2 Matrix fabric and organic matter distribution 71
4.7.3 Pore types 72
4.7.4 Depth-related evolution of the pore system 777
4.8 Cross-validation of XRF, XRD and SEM-EDS 799
4.9 Unconventional Hydrocarbon Reservoir Potential of the Ghazij Formation 81
4.9.1 Organic richness criterion 81
4.9.2 Mineralogical criterion: brittleness index 82
4.9.3 Pore fabric criterion: multi-scale pore network 85

CONCLUSIONS 8787
RECOMMENDATIONS 8989
REFERENCES 90

LIST OF TABLES

TABLE NO.	TITLE	PAGE
2.1	Borehole stratigraphy of Zamzama-5.	24
2.2	Borehole stratigraphy of Mehar-1.	25
3.1	Details of the sample's distribution within the Ghazij Formation in the selected wells.	31
4.1	Major oxide composition (wt.%) of the Ghazij Formation, Zamzama-5, determined by (XRF).	50
4.2	XRD mineral composition (%) of the Ghazij Formation, Zamzama-5.	54
4.3 (a)	Total organic carbon (TOC), Zamzama-5.	56
4.3 (b)	Total organic carbon (TOC), Mehar-1.	57
4.4	Rock-Eval pyrolysis parameters, Zamzama-5 (Ghazij Formation).	59
4.5	Summary comparison of source rock characteristics, Zamzama-5 vs. Mehar-1.	64
4.6	Depth-related pore system evolution, Ghazij limestone, Zamzama-5.	77
4.7	Cross-validation of mineral phases across XRF, XRD and SEM-EDS, Ghazij Formation, Zamzama-5.	79
4.8	Brittleness index calculations, Ghazij Formation, Zamzama-5.	84

LIST OF FIGURES

FIGURE NO.	TITLE	PAGE
1.1	Petroleum resource triangle (Zou, 2017).	2
1.2	Tectono-stratigraphic map of Pakistan, showing the location of the study area (After Qureshi et al., 2023).	7
2.1	General stratigraphic column for Kirthar Fold Belt of the Lower Indus Basin (after Khalid et al., 2023).	18
3.1	Schematic representation of the integrated research methodology adopted for the study. The workflow summarizes the sequence of sample selection, preparation, and laboratory analysis including TOC, Rock-Eval pyrolysis, XRD, XRF, and SEM-EDS, providing a comprehensive unconventional source rock evaluation of Ghazij Formation.	29
3.2	Representative drill-cutting samples from Mehar-1 well. The upper interval sample (2357–2360 m) consists of 75% light grey carbonate chips with 25% granular to flaky shale pieces (a). Middle interval sample (2393–2396 m) shows an increase in granular shale to about 90% of the sample with minor 10% calcareous chips (b). Lower interval (2432–2435 m) is dominated by dark grey shale fragments (approximately 80%) with approximately 20% light-grey carbonate chips (c).	32
3.3	Representative drill-cutting samples from the Zamzama-5 well. The upper interval (2240–2250 m)	33

	consists predominantly of fine- to medium-grained angular carbonate fragments (a). The middle interval (2300–2310 m) exhibits a similar carbonate dominant appearance with relatively uniform particle size and morphology (b). The lower interval (2370–2380 m) consists predominantly of carbonate fragments with only minor variation in color and grain characteristics (c).	
3.4	Representative stages and reference materials used during the TOC sample preparation and analysis: (a) weighing of the powdered sample in a crucible on an analytical balance; (b) crucible containing samples after being treated with hydrochloric acid placed on the hot plate and tungsten shaving added to them; (c) tungsten shavings used as a combustion accelerator; (d) carbon rings used for instrument calibration; and (e) certified standard sample used to verify analytical accuracy and precision.	37
3.5	TOC instrument used at HDIP, the Jinyibo CS-8820S Carbon and Sulfur Analyzer.	38
3.6	Rock-Eval 6 instrument with the hydrogen generator and a zoom in at the autosampler holding samples' crucibles.	39
3.7	Standard XRD sample holder with sample loaded and levelled ready for XRD analysis.	41
3.8	Rigaku SmartLab SE multipurpose θ-θ X-ray diffractometer used for XRD analysis at HDIP lab.	42
3.9	Pressed pellets of the Zamzama-5 samples.	43

3.10	The Shimadzu EDX-7200 Energy-Dispersive X-Ray Fluorescence (ED-XRF) spectrometer used for XRF analysis at HDIP.	44
3.11	Quorum sputter coater used for sputter coating the samples with a thin layer of gold-palladium alloy.	46
3.12	Carl Zeiss EVO 10 scanning electron microscope equipped with an Oxford Xplore 30 Energy Dispersive X-ray Spectroscopy (EDS) system used at HDIP.	47
4.1	XRD diffractograms and mineral proportion pie charts for (a) Pr-23027, (b) Pr-23033 and (c) Pr-23040, Ghazij Formation, Zamzama-5.	53
4.2	The distribution of TOC with respect to burial depth in both Zamzama-5 and Mehar-1 wells (plotted using the guidelines of Peters et al., 2005; Peters and Cassa, 1994).	58
4.3	Modified Van Krevelen Diagrams of the tested Zamzama-5 Samples, (a) HI vs. OI to identify kerogen type. (b) HI vs. T_{max} to identify kerogen type and maturity (Adopted from Peters and Cassa, 1994).	60
4.4	Production Index (PI) vs. depth plot showing maturation stages of the studied Zamzama-5 samples.	62
4.5	(a) Cross plot of HI vs. TOC suggests good to excellent gas generation potential, (b) S1 vs. S2 plot shows indigenous samples for Zamzama-5.	66
4.6	SEM-EDS analysis of Pr-23027 (2240–2250 m), Ghazij Formation, Zamzama-5. (a) Secondary electron image at 25µm scale showing EDS spot locations. (b) Spectrum 8: calcite-dominated matrix with minor illite clay. (c) Spectrum 9: pure detrital quartz grain (Si 43.8%, O 52.0%). (d) Spectrum 10: mixed quartz-	68

	calcite zone with barite (Ba 2.0%) as an accessory diagenetic phase.	
4.7	SEM-EDS analysis of Pr-23033 (2300–2310 m), Ghazij Formation, Zamzama-5. (a) Secondary electron image at 50µm scale showing EDS spot locations. (b) Spectrum 7: purest calcite composition in the dataset (Ca 55.4%). (c) Spectrum 8: illite clay phase (Al 16.3%, K 8.3%) with no carbonate contribution. (d) Spectrum 9: calcite-clay interface with elevated Fe (7.8%) interpreted as pyrite.	69
4.8	SEM-EDS analysis of Pr-23040 (2370–2380 m), Ghazij Formation, Zamzama-5. (a) Secondary electron image at 25µm scale showing EDS spot locations. (b) Spectrum 8: illite clay with minor calcite (Al 9.5%, K 1.8%, Ca 7.2%) and trace smectite indicated by Na (0.6%). (c) Spectrum 9: mixed illite-calcite zone with detrital rutile indicated by Ti (0.5%). (d) Spectrum 10: most clay-rich composition in the dataset (Al 9.8%, Fe 6.3%) with near-absent Ca (1.3%), representing pore-lining illite-smectite films.	70
4.9	Organic matter distribution and associated porosity, Ghazij limestone, Zamzama-5. (a) Pr-23027 (2240–2250 m): wavy organic matter films coating carbonate grain surfaces (red arrow) with nano-scale pores developed within the organic matter (yellow arrows), representing potential sites for gas storage. (b) Pr-23033 (2300–2310 m): yellow arrows indicate organic matter-hosted and intercrystalline pores; red arrows indicate pyrite framboids within organic coating, consistent with reducing/anoxic depositional conditions.	72

4.10	Micron-scale interparticle microporosity, Pr-23027 (2240–2250 m), Ghazij limestone, Zamzama-5. Rounded micrite grains at 2µm scale with interparticle pores visible between grain boundaries (arrows), representing the primary matrix storage porosity at this depth.	73
4.11	Nano-scale interparticle porosity, Pr-23033 (2300–2310 m), Ghazij limestone, Zamzama-5. Sub-micrometre pores between micrite grains at 1µm scale (arrows), indicating progressive pore size reduction with depth due to compaction and carbonate cementation.	74
4.12	Intercrystalline porosity, Pr-23033 (2300–2310 m), Ghazij limestone, Zamzama-5. Pores developed between interlocking crystalline carbonate patches at 2µm scale (arrows), representing a secondary storage pore type contributing to overall pore network connectivity at this depth.	75
4.13	Microfracture porosity, Pr-23040 (2370–2380 m), Ghazij limestone, Zamzama-5. (a) Open microfracture cutting diagonally across the matrix at 10µm scale (Mag 783X) (arrows). (b) Continuation of fracture network with partial calcite or clay diagenetic infill along fracture walls (arrows), confirming natural fracture origin and representing a potential permeability pathway at this depth.	76
4.14	Depth-related evolution of pore types, Ghazij limestone, Zamzama-5. (a) Pr-23027 (2240–2250 m): micron-scale interparticle pores at approximately 2 µm scale (arrows). (b) Pr-23033 (2300–2310): nano- to submicron-scale interparticle pores at 1 µm scale (arrows), accompanied by organic-matter-hosted and	78

intercrystalline pores. (c) Pr-23040 (2370–2380): natural, microfracture at 10 μm scale (arrows), representing a potential high-permeability pathway through the tight carbonate matrix.

LIST OF ABBREVIATIONS

%	-	Percentage
°C	-	Degree Celsius
BI	-	Brittleness Index
DCM	-	Dichloromethane
DGPC	-	Directorate General of Petroleum Concessions
EDS	-	Energy-Dispersive X-ray Spectrometer
FID	-	Flame Ionization Detector
g	-	Gram
GP	-	Generation Potential
HC	-	Hydrocarbon
HCl	-	Hydrochloric Acid
HI	-	Hydrogen Index
IR	-	Infrared
km	-	Kilometre
m	-	Metre
mg	-	Milligram
NDIR	-	Non-dispersive Infrared
OBM	-	Oil-Based Mud
OI	-	Oxygen Index
PI	-	Production Index
Ro/ VR	-	Ro – Vitrinite Reflectance
RTKB	-	Rotary Table Kelly Bush
SEM	-	Scanning Electron Microscope
TOC	-	Total Organic Carbon
wt.	-	Weight
XRD	-	X-ray Diffraction
XRF	-	X-ray Fluorescence
μm	-	Micrometre

CHAPTER 1

INTRODUCTION

1.1 Background

Petroleum source rocks constitute the foundation of every petroleum system, controlling the generation, composition, and distribution of hydrocarbons within sedimentary basins (Peters and Cassa, 1994). Their ability to accumulate, preserve, and thermally transform the organic matter governs the formation of economically recoverable oil and gas resources and therefore plays a critical role in hydrocarbon exploration. For decades, petroleum exploration has primarily targeted conventional accumulations in which hydrocarbons migrate from mature source rocks into structurally or stratigraphically trapped reservoir units. However, advances in petroleum geoscience have shown that many fine-grained sedimentary successions possess the capacity to function simultaneously as the source, reservoir, and seal of hydrocarbons, giving rise to unconventional petroleum systems in which generated hydrocarbons remain largely retained within the host formation (Tissot and Welte, 1984; Law and Curtis, 2002; Jarvie, 2012). Consequently, the characterization of source rocks has evolved from simply identifying hydrocarbon

generating intervals to understanding the complex geological processes that control hydrocarbon generation, storage, retention, and productibility (Jarvie, 2012).

The petroleum resource triangle (Fig. 1.1) illustrates the global distribution of hydrocarbon resources, with conventional reservoirs occupying the apex, representing high resource quality and extractability but accounting for only approximately 20% of total global petroleum reserves. The remaining 80% is comprised of unconventional resources, which form the broad base of the triangle. Although unconventional accumulations are characterized by lower resource quality and require more complex extraction techniques, their sheer volumetric abundance makes them a critical component of the global energy supply. This reality has driven a significant shift in exploration focus toward unconventional plays, including tight carbonates, shale gas, and coalbed methane, particularly in regions where conventional reserves are maturing.

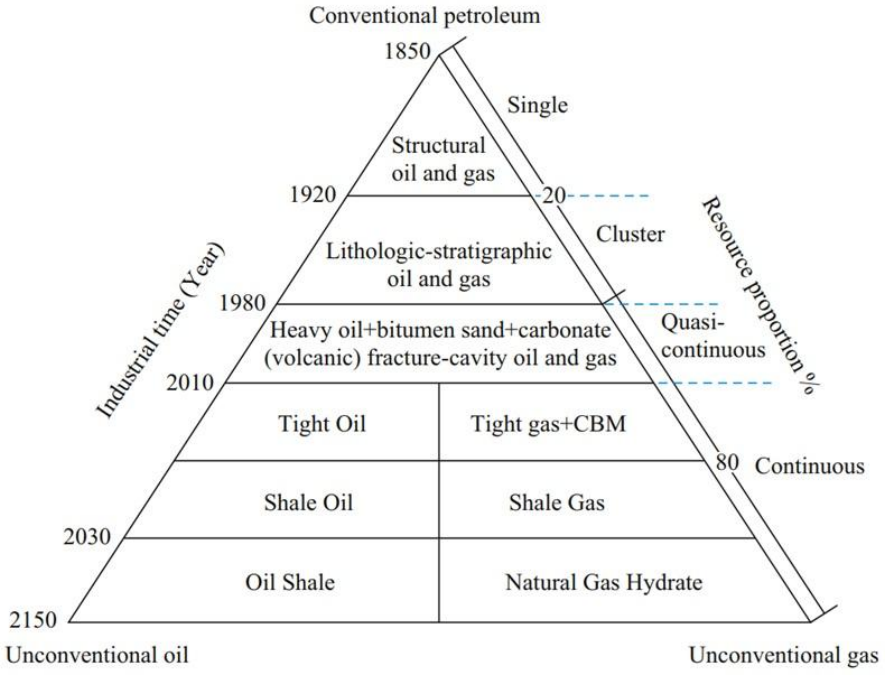


Figure 1.1 Petroleum resource triangle (Zou, 2017).

The evaluation of unconventional petroleum systems differs from that of the conventional systems in the sense that it requires an integrated understanding of both the organic and inorganic components of the host rock. Organic richness determines the

quantity of hydrocarbons that may be generated, whereas kerogen type and thermal maturity govern the nature and timing of hydrocarbon generation. Simultaneously, mineralogical composition governs mechanical characteristics, brittleness, fracture propagation, and diagenetic evolution, all of which affect reservoir quality and production potential. At the microscopic scale, pore morphology, mineral fabrics, and the spatial distribution of organic matter regulates hydrocarbon storage and migration pathways within low permeability rocks. These interdependent geological factors cannot be adequately characterized using a single analytical technique, making multidisciplinary investigations essential for the reliable assessment of unconventional petroleum resources (Peters and Cassa, 1994; Peters et al., 2005; Hackley and Cardott, 2016).

Recent developments in petroleum geochemistry and reservoir characterization have emphasized the importance of integrating complementary analytical techniques to reduce the uncertainty in source rock evaluation. Organic geochemical analysis, particularly total organic carbon (TOC) and Rock-Eval pyrolysis, provide a primary framework for assessing organic richness, kerogen type, thermal maturity, and hydrocarbon generation potential. Mineralogical investigations using X-ray diffraction (XRD) identify the crystalline constituents of the rock, whereas the X-ray fluorescence (XRF) provides quantitative bulk elemental composition that assists in evaluating lithological variability, depositional conditions, and mineralogical trends. At the microscale, scanning electron microscopy coupled with energy dispersive X-ray spectroscopy (SEM-EDS) allows direct visualization of mineral fabrics, pore systems, and organic matter occurrence while providing phase-specific elemental composition from selected microscopic domains. When combined, these datasets provide a more comprehensive characterization of the source rock by linking its organic richness and hydrocarbon generating capacity with mineralogical composition, elemental variability, and microscale textural and pore characteristics. Such an integrated approach is particularly valuable for evaluating unconventional source rocks, where organic matter distribution, mineralogy, brittleness, pore development, and thermal maturity collectively control hydrocarbon generation, storage, and producibility (Loucks et al., 2009; Slatt and O'Brien, 2011; Peters et al., 2005).

The Lower Indus Basin of Pakistan represents one of South Asia's most prolific hydrocarbon provinces and hosts numerous producing oil and gas fields within Mesozoic and Cenozoic sedimentary successions (Wandrey et al., 2004). Although exploration within the basin has been historically concentrated on conventional reservoirs, several fine-grained stratigraphic intervals have long been recognized as potential petroleum source rocks capable of supporting unconventional hydrocarbon systems. Regional geological investigations and international resource assessments have identified multiple organic rich formations within the basin, including the Lower Goru, Mughal Kot, Sembar, and Ghazij Formations, highlighting the considerable yet incompletely understood unconventional hydrocarbon potential of southern Pakistan (Ahmad et al., 2012; EIA, 2015; Schenk et al., 2017). Despite these assessments, integrated geological investigations remain comparatively limited, and many potentially prospective source rock intervals continue to be evaluated using incomplete isolated datasets.

Among these stratigraphic units, the Early Eocene Ghazij Formation occupies a particularly important position within the petroleum system of the Southern Indus Basin (Wandrey et al., 2004; Johnson et al., 1999). The formation is regionally extensive and exhibits considerable lithological variability, reflecting changes in depositional environment and sediment supply across the basin (Johnson et al., 1999; Warwick et al., 1998). Previous investigations have primarily addressed the formation's regional stratigraphy, sedimentology, paleoenvironment, tectonic evolution, and conventional hydrocarbon significance, whereas comparatively limited work has integrated organic geochemistry, mineralogy, and microscopic characterization to evaluate its unconventional petroleum potential (Kazi, 1968; Johnson et al., 1999; Warwick et al., 1998). As a result, important relationships between organic matter characteristics, mineralogical composition, diagenetic evolution, pore development, and thermal maturation remain insufficiently constrained. This lack of integrated characterization limits the understanding of both the source rock quality and unconventional reservoir behavior of the Ghazij Formation and in turn introduces uncertainty into future exploration strategies within the Southern Indus Basin.

The evaluation of unconventional petroleum systems has progressively evolved from simple source rock screening to comprehensive geological characterization. While total organic carbon (TOC) and Rock-Eval pyrolysis remain the foundation of source rock assessment, they alone cannot adequately explain the geological controls responsible for organic matter enrichment, mineralogical evolution, or reservoir behavior. Organically rich intervals possessing similar TOC values may exhibit very different hydrocarbon generation potentials, brittleness, pore development, and production performance due to variations in mineral composition, diagenetic history, and burial evolution. Hence, modern unconventional resource evaluation increasingly relies on integrating organic geochemistry with mineralogical and petrographic analyses to establish the relationships between depositional environment, post-depositional alteration, thermal maturation, and reservoir quality. Such multidisciplinary approaches provide a more robust understanding of petroleum systems than individual analytical methods interpreted in isolation and have become fundamental in the evaluation of fine-grained hydrocarbon-bearing formations worldwide (Jarvie, 2012; Peters et al., 2016; Hackley and Cardott, 2016).

In Pakistan, however, relatively few studies have adopted this integrated methodology for evaluating potential unconventional source rocks. Furthermore, exploration efforts within Pakistan have remained predominantly focused on conventional accumulations, while comprehensive investigations of potential unconventional source rocks remain comparatively limited. Existing investigations of the Lower Indus Basin have predominantly focused on regional geology, basin evolution, conventional petroleum systems, or the hydrocarbon potential of some promising stratigraphic units within the Lower Indus Basin (Ahmad et al., 2012 & 2013; EIA, 2015). Additionally, most available investigations have considered individual datasets independently, making it difficult to establish the relationships between organic matter characteristics, mineral assemblages, pore development, and burial evolution that collectively determine unconventional reservoir quality. Addressing these knowledge gaps is essential for improving the geological understanding of the Ghazij Formation and refining future exploration strategies within the Southern Indus Basin.

The complexity of the Ghazij Formation further emphasizes the need for an integrated evaluation. Lithological variability within the formation reflects changes in depositional conditions, sediment provenance, and diagenetic evolution that directly influence both organic matter preservation and reservoir properties. Organic richness alone cannot determine unconventional prospectivity if mineralogical composition is unfavorable for fracture development, while favorable mineralogy alone cannot compensate for insufficient organic matter or inadequate thermal maturity. Likewise, microscopic pore development and mineral-organic relationships provide critical information regarding hydrocarbon storage that cannot be inferred from bulk geochemical analyses alone. Understanding how these geological parameters interact is therefore essential for accurately assessing the petroleum significance of the Ghazij Formation and identifying the factors controlling its spatial variability within the Southern Indus Basin.

To address these knowledge gaps, the present study applies an integrated analytical workflow to drill-cutting samples obtained from the Zamzama-5 and Mehar-1 wells, targeting the Early Eocene Ghazij Formation. Organic geochemical characterization was undertaken using total organic carbon (TOC) analysis and Rock-Eval pyrolysis to evaluate organic richness, kerogen type, thermal maturity, and hydrocarbon generation potential. Mineralogical and elemental compositions were investigated using X-ray diffraction (XRD) and X-ray fluorescence (XRF), while scanning electron microscopy coupled with energy dispersive X-ray spectroscopy (SEM-EDS) was employed to examine mineral fabrics, pore systems, and the distribution of organic matter at the microscale.

By integrating multiple analytical approaches within a single evaluation framework, this research provides a more comprehensive understanding of the petroleum characteristics of the Ghazij Formation than has previously been available. The study not only assesses its organic richness and source rock quality but also examines the mineralogical, petrographic, and thermal controls governing its unconventional reservoir potential. The findings are expected to contribute to the geological understanding of the Southern Indus Basin, and to provide a scientific basis for future exploration of the Ghazij Formation.

1.2 Location of the Study Area

The study area (Fig. 1.2) is on the west side of the boundary between the Kirthar Fold Belt and Kirthar Foredeep, which stretches between Quetta and Karachi, forming a north-south trending folded zone that is bound by Sibi trough and Indus Platform to the east, and bounded by Bela-Zhob ophiolite-and-thrust belt to the north and west (Kazimi and Jan, 1997).

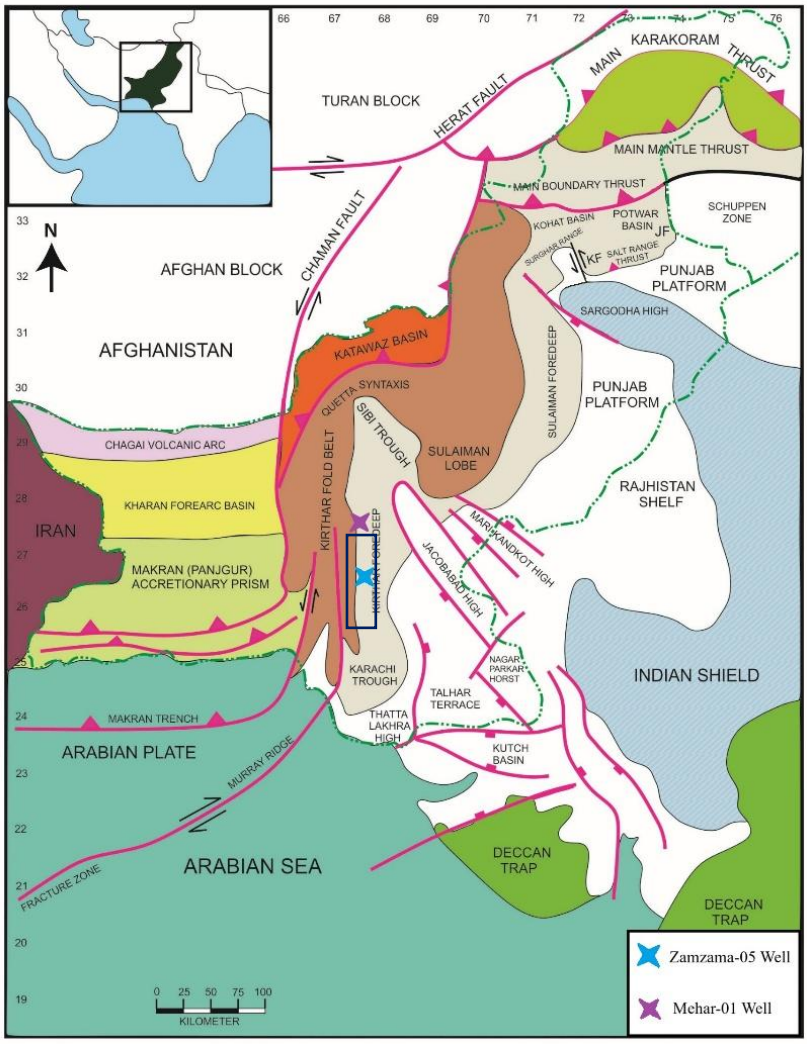


Figure 1.2 Tectono-stratigraphic map of Pakistan, showing the location of the study area (After Qureshi et al., 2023).

The two wells chosen for this study are Mehar-1, and Zamzama-5, parts of Mehar and Zamzama gas fields respectively. Zamzama-5 is located at 67°40’14.208” E; 26°40’03.564” N which is about 13 km to the southwest of Dadu city in Dadu district. Mehar-1 is located at 67°33’17.7769” E; 27°27’04.2842” N which is 88 km northwest of Zamzama-5.

1.3 Literature Review

Previous published studies suggest that the Eocene’s Ghazij Formation in the Lower Indus Basin is a good source rock of both gas and light oil, with enough maturity to have even reached oil window in the trough area (Amjad et al., 2022). It was also suggested that the hydrocarbon generation potential extends into the southern part of the basin, namely in the Khairpur-Jacobabad High region (Kadri, 1995). Ghazij shale samples from the Kirthar sub-Basin and parts of Kutch Basin were documented to have TOC up to 6.9 wt.%, with many samples in the 0.5–3.5 wt.% range, and vitrinite reflectance (VR) near 0.65–1.3, which shows Ghazij intervals to contain organically rich pods that have reached oil to gas maturity windows (Raza et al., 1990). Detailed field-based sedimentological, lithostratigraphic and petrographic analysis of the Ghazij Formation in the Sor Range area near Quetta District (west of Sulaiman Thrust), provided a depositional model for the Ghazij Formation in different tectonic settings, describing a deltaic system with a pro-delta shale (Lower Member), delta-front distributary channels and coals (Middle Member), and a wave- and storm-influenced upper delta (Upper Member) (Kakar and Kassi, 1997). The presence of a conglomerate horizon, locally reaching approximately 17 m in thickness, records a significant increase in coarse clastic input during deposition of the Ghazij Formation. The conglomerate contains predominantly limestone clasts derived from older Jurassic-Paleocene sedimentary successions, together with subordinate quartz arenite, volcanic, quartzite, and phyllite fragments (Kakar and Kassi, 1997). The conglomerate

facies, together with the transition from marine to paralic and terrestrial deposits, has been interpreted as evidence of tectonic uplift and changing paleogeography associated with an Early Eocene collision along the northwestern margin of the Indian subcontinent (Warwick et al., 1998; Johnson et al., 1999). These changes prompted increased clastic influx and the development of a prograding deltaic to continental depositional system within the Ghazij basin (Warwick et al., 1998). The resulting transition from marine to deltaic and terrestrial environments indicates substantial spatial and temporal variability in sediment supply and depositional conditions, which would have influenced the distribution and preservation of organic matter within the Ghazij Formation.

The Ghazij and associated shales were recognized by Wandrey et al. (2004) to be a significant contributor within the composite Sembar-Goru/Ghazij total petroleum system. Hydrocarbon generation began 65–40 Ma ago, and peaked during the Eocene-Miocene, coinciding with trap development. The Ghazij Formation, though regionally secondary to the Sembar, provides additional unconventional source potential in the fold belt and foreland settings of southern Pakistan. Additionally, Ghazij shales in Pirkoh area exhibit variable source rock potential, with TOC values up to 2.5 wt.% (Amjad et al., 2022) with burial and maturity modelling showing immature to marginally mature shales with (Ro 0.5–0.9%), while deeper Ghazij intervals in the Bambor syncline entered the gas window with (Ro 0.9–1.3%), and the seismic attributes analysis identified bright spots and gas-prone zones, supporting the role of Ghazij Formation as a potential unconventional hydrocarbon source rock in Kirthar Fold Belt. Another geochemical study published by Ahmed et al. (2025) provides critical, direct geochemical data for Ghazij Formation shales in Southern Indus Basin showing they possess good to excellent organic richness, with TOC values ranging from 1.55–6.06 wt.%. Rock-Eval Pyrolysis indicated these shales contain type II/III kerogen (HI: 136–430 mg HC/g TOC), which is characteristic of mixed oil- and gas-prone organic matter.

1.4 Research Gap

Despite the growing body of literature on the Ghazij Formation as a source rock in the Southern Indus Basin, existing studies have focused predominantly on the shale-dominated facies of the formation, characterizing its organic richness, kerogen type, and thermal maturity in shale intervals across the Kirthar sub-Basin, Pirkoh area, and Bombar syncline. No published study has systematically evaluated the carbonate-rich limestone facies of the Ghazij Formation as a potential source rock and unconventional reservoir target using an integrated geochemical, mineralogical, and petrographic approach. Furthermore, while regional petroleum system studies recognized the Ghazij Formation as a contributor to the Sembar-Goru/Ghazij composite total petroleum system, the lateral variability in source rock quality between carbonate and shale-dominated facies within the same formation remains poorly constrained in the Southern Indus Basin. The mineralogical controls on reservoir quality, pore-fabric evolution, and rock brittleness of the Ghazij limestone; all critical parameters for unconventional play evaluation, have not been previously investigated. This study addresses these gaps directly by applying XRF, XRD, TOC, Rock-Eval Pyrolysis, and SEM-EDS to the Ghazij limestone interval in Zamzama-5 and Mehar-1 in the Southern Indus Basin.

1.5 Research Question

This study is guided by two principal research questions. First, what are the quantity, quality and thermal maturity of organic matter in the carbonate-rich limestone facies of the Ghazij Formation in the Southern Indus Basin, and how does source rock potential vary laterally between Zamzama-5 and Mehar-1? Second, what are the

mineralogical composition, diagenetic history, and petrographic pore characteristics of the Ghazij limestone at Zamzama-5, and do these properties satisfy the established criteria for an unconventional tight carbonate gas reservoir? These questions directly inform the study objectives of this research.

1.6 Study Objectives

The objectives of the research are

a) To determine the quantity, quality and thermal maturity of organic matter in the Ghazij Formation across the study area.
b) To characterize the mineralogical and pore fabric properties of the Ghazij Formation and evaluate its potential as an unconventional hydrocarbon reservoir.

1.7 Significance of the Study

This study makes an original contribution to the understanding of the Ghazij Formation by characterizing, for the first time, the source rock quality and unconventional reservoir properties of its carbonate-rich limestone facies in the Southern Indus Basin. While previous studies focused exclusively on the shale-dominated facies, this study demonstrates that the Ghazij limestone possesses very good to excellent organic richness, indigenous gas-prone kerogen, and a multi-scale pore network consistent with an unconventional tight carbonate gas reservoir, significantly broadening the exploration

potential of the formation beyond its conventional shale source rock role. The lateral comparison between Zamzama-5 and Mehar-1 provides the first direct geochemical evidence of facies-controlled variability in source rock quality within the formation at the field scale. More broadly, by proposing the Ghazij limestone as a prospective unconventional tight carbonate gas play, this study contributes to the diversification of the domestic hydrocarbon resource base and provides a scientific foundation for future exploration targeting carbonate-hosted unconventional gas in the Southern Indus Basin.

CHAPTER 2

REGIONAL GEOLOGIC AND TECTONIC FRAMEWORK

2.1 Regional Tectonic Setting

In Pakistan, two major sedimentary basins, the Indus Basin and the Balochistan Basin, evolved independently across the ages, and started converging during the Cretaceous and Paleocene periods. Additionally, the Pishin Basin, also known as the Kakar-Khorasan Basin, was formed during the Early Tertiary period, but the formation of this basin has its own history. The tectonic evolution of the Indus Basin and Balochistan Basin is closely related to the collision between the Indian and Eurasian plates that eventually resulted in the formation of the Median Basin plate (Ahmad and Afzal 2012; Raza et al., 1989). The Indus Basin occupies most of eastern Pakistan and extends across multiple provinces, namely Punjab, Sindh, and Khyber Pakhtunkhwa. Geographically the basin extends across 1,600 km southwestward from the Indian subcontinent and covers nearly 300,000 km^2 (Shah, 2009).

Structurally, the Indus Basin is subdivided into the Upper and Lower Indus Basins, where the Sargodha High separates the Upper Indus Basin from the Lower Indus Basin. The Upper Indus Basin is further subdivided into the Potwar and Kohat Basins, which are

separated by the Jhelum Fault and the Indus River (Raza et al., 1989; Kazmi and Abbasi, 2008). The Upper Indus Basin is characterized by mountainous topography associated with compressional tectonics, while the Lower Indus Basin consists predominantly of plains formed under extensional tectonic conditions (Shah, 2009).

The tectonic development of the Lower Indus Basin reflects the northward drift of the Indian Plate after its separation from the Antarctic and Australian plates during the Cretaceous period (Nosheen and Giao, 2017). During this phase, transform faulting along with the Ninety-East Ridge and the accumulation of flysch sediments occurred around the Indian Plate margins (Wandrey et al., 2004). Continuous northward movement during the Late Cretaceous eventually led to the closure of the Tethys Sea through an oblique collision between the Indian and Eurasian plates, initiating the formation of the Sulaiman-Kirthar Fold Belt (Jadoon et al., 1994).

Sedimentation within the Lower Indus Basin was strongly influenced by tectonic and depositional changes associated with plate movement. The Goru Sandstone and Sembar Shale of the Southern Indus Basin were deposited over eroded material derived from the western shelf.

Following the late Cretaceous regression and deposition of the Pab Sandstone, continued northward movement of the Indian Plate progressively intensified the closure of the Tethys and initiated oblique convergence with the Eurasian margin. By the Paleocene-Early Eocene, collision-related tectonic uplift along the northwestern margin of the Indian Plate modified the regional paleogeography and generated new sediment source area. These changes caused a transition from marine shelf deposition to progressively more proximal paralic and terrestrial environments, culminating in the deposition of the Ghazij Formation as a prograding clastic wedge during the Early Eocene (Warwick et al., 1998; Johnson et al., 1999; Wandrey et al., 2004).

2.2 Geologic Setting of the Lower Indus Basin

The Lower Indus Basin is subdivided into the Central and Southern Indus Basins and represents the larger portion of the Indus Basin system, occupying nearly 250,000 km^2 of the total basin area (Shah, 2009). The Southern Indus Basin lies south of the Sukkur rift, which remained undivided until the Middle Cretaceous when the Khairpur-Jacobabad High developed as a significant tectonic feature separating the Central and Southern Indus Basins (Shah et al., 2023).

The Southern Indus Basin comprises five main tectono-stratigraphic units: the Thar Platform, Karachi Trough, Kirthar Foredeep, Kirthar Fold Belt, and Offshore Indus. Both the Thar Platform and Karachi Trough extend offshore into the Offshore Indus and the Arabian Sea. Geographically, the basin is bounded by the Indian Shield to the east and the marginal zone of the Indian Plate to the west (Khan and Liu, 2019).

The oldest rocks encountered within the basin are Triassic in age, as identified in the Jhat Pat and Nabisar wells (Khan and Liu, 2019). Jurassic and Lower Cretaceous stratigraphy is represented by the Chiltan Limestone and Sembar Formation, which displays relatively homogeneous lithologies across the Khairpur-Jacobabad High, indicating that the Central and Southern Indus basins remained connected prior to the Middle Cretaceous (Fatmi and Zeiss, 1994). Similarly, the sand facies of the Goru Formation extend toward the Kandhkot and Giandari regions, further supporting stratigraphic continuity across the basin (Dar et al., 2023).

Evidence from the Khairpur and Jhat Pat wells demonstrates significant erosional or non-depositional intervals over the Khairpur-Jacobabad High. In the Khairpur-02 well, substantial portions of the Lower Cretaceous and Paleocene sequences are absent, while in the Jhat Pat well, the entire Cretaceous and Paleocene sections are missing, with the Eocene strata directly overlying the Jurassic Chiltan Limestone. Paleocene facies south of the High differ markedly from northern facies and are dominated by clastic sediments derived from

nearby positive tectonic elements such as the Khairpur-Jacobabad High and the Nibisar Arc (Kazimi and Jan, 1997).

The Thar Platform is a gently sloping monocline controlled primarily by basement topography and bordered by the Indian Shield to the east, the Kirthar and Karachi troughs to the west, and the Mari-Bugti Inner Folded Zone to the north (Mughal and Akhter, 2021). The Karachi Trough represents an onshore extension of the Arabian Sea and is characterized by thick Early Cretaceous sedimentary successions and numerous closely spaced anticlines, several of which host hydrocarbon accumulations such as the Hundi, and the Kothar gas fields (Khalid et al., 2023).

One of the notable features of the Karachi trough is the continuous deposition of the Korara Shales across the Cretaceous-Paleogene (K/T) boundary, particularly within the Danian interval, suggesting the absence of a depositional hiatus during this period (Sahir, 2018). Westward, the Kirthar Foredeep forms a north-south trending depression filled with up to 15,000 m of sediments and bounded by faults along its eastern margin adjacent to the Thar Platform. Sedimentation within the foredeep is considered to have been largely continuous and significantly contributes to source rock maturation potential within the basin (Shah, 2009).

The Kirthar Fold Belt extends approximately 350 km in a north-south orientation and is subdivided into several lithostratigraphic and structural zones, including the eastern Pab and western Kirthar zones (Kazimi and Jan, 1997). Structurally, the belt contains complex tectonic features such as the Khuzdar Knot, a major syntaxial bend characterized by zigzag fold axes convex towards the north. This feature extends nearly 70 km in length and 50 km in width and is structurally controlled by the northeast-southwest trending Diwani Fault (Bannert and raza, 1992).

2.3 Stratigraphy of Southern Indus Basin

The Southern Indus Basin preserves a thick and regionally extensive sedimentary succession that records the long-term evolution of the northwestern margin of the Indian Plate. The stratigraphic column of the Kirthar Fold Belt in the Lower Indus Basin is illustrated in Figure 2.1. The succession is predominantly marine from the Mesozoic into Cenozoic, with continental deposits becoming increasingly important during the later stages of basin development. In the deeper parts of the basin, approximately 13–16 km of Jurassic to Tertiary sedimentary rocks have accumulated, reflecting prolonged subsidence and sedimentation. These strata comprise diverse carbonate and siliciclastic lithologies deposited under changing marine shelf, marginal-marine, and continental conditions (Shah, 2009). The stratigraphic record therefore documents a broad transition from extensive Mesozoic marine sedimentation, through increasingly differentiated Paleogene depositional systems, to the predominantly regressive and continental conditions of the Neogene and Quaternary. Of particular relevance to the present study is the Paleocene-Eocene succession, during which changes in basin configuration and sediment supply promoted the accumulation of thick fine-grained intervals, including the Ghazij Formation.

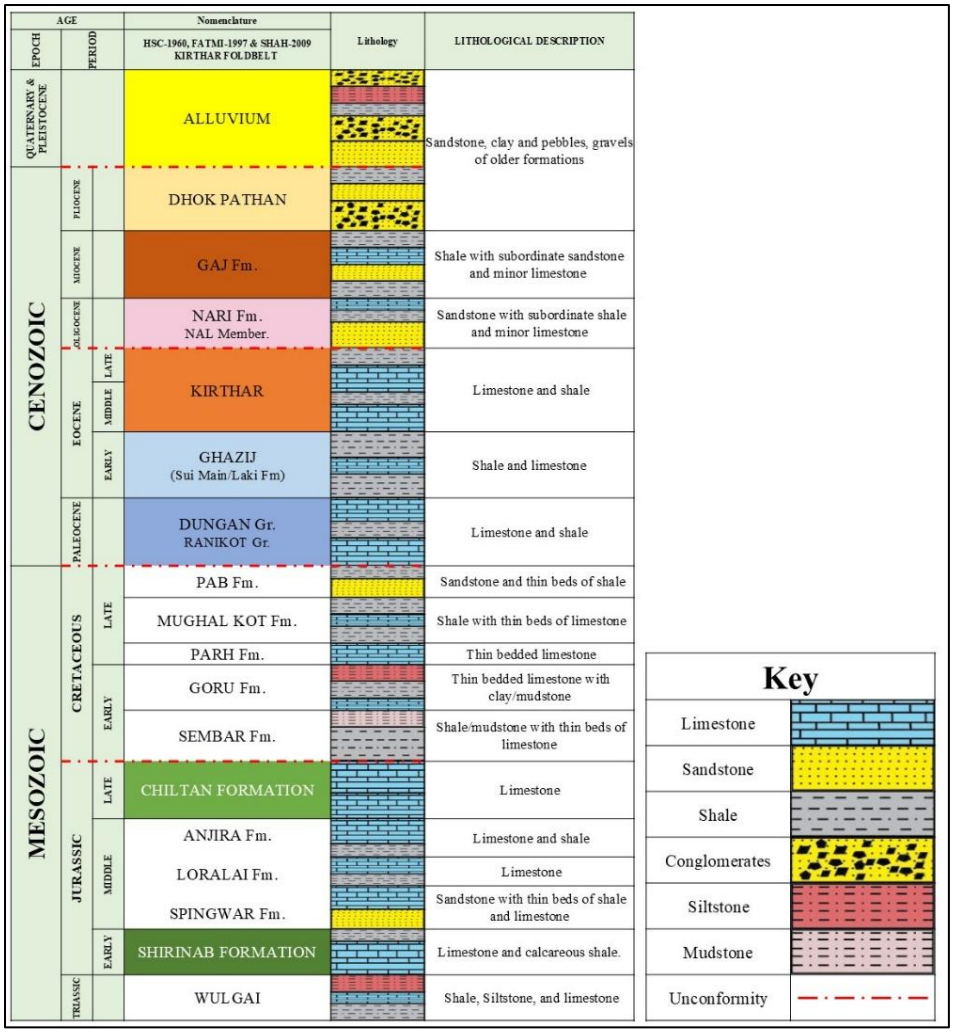


Figure 2.1 General stratigraphic column for Kirthar Fold Belt of the Lower Indus Basin (after Khalid et al., 2023).

The Mesozoic succession is well developed and comprises several thousand meters of predominantly calcareous and argillaceous sedimentary rocks. Jurassic strata consist mainly of thick marine limestone and shale, with subordinate sandstone in their lower parts, and locally exceed 3,000 m in thickness. A regional withdrawal of the sea near the end of the Middle Jurassic was followed by renewed marine transgression during the Late Jurassic, after which marine sedimentation continued into the Early Cretaceous. Consequently, the Jurassic-Cretaceous boundary is regarded as transitional in parts of the basin (Shah, 2009).

The Cretaceous succession records continued subsidence and marine deposition accompanied by changes in siliciclastic supply and depositional conditions. The lower succession includes the shale-rich Sembar Formation, followed by the Goru Formation and the carbonate-dominated Parh Formation, while the Upper Cretaceous includes the Mughal kot Formation, Fort Munro Limestone, and Pab Sandstone. Together, these units record changes from argillaceous marine sedimentation to carbonate deposition and increasingly prominent siliciclastic systems (Shah, 2009). Their distribution and thickness were partly influenced by extensional structures developed during the late Jurassic-Early Cretaceous rifting, which produced fault-controlled accommodation patterns in southern Sindh (Ahmed et al., 2018).

The transition into the Paleogene marks an important change in the stratigraphic development of the Southern Indus Basin. Paleocene strata are conventionally represented by the Ranikot Group, comprising the Khadro, Bara, and Lakhra formations. These units exhibit marked lateral and vertical variations between siliciclastic and carbonate facies. The Khadro Formation comprises mixed sandstone, shale, and limestone. The Bara Formation is dominated by sandstone with subordinate shale and coal. The Lakhra Formation consists dominantly of limestone with subordinate shale (Shah, 2009; Malkani and Mahmood, 2017). The early Cenozoic succession of southern Pakistan is traditionally organized into the Ranikot, Laki, and Kirthar stratigraphic intervals, which broadly record successive Paleocene and Eocene stages of basin development (Shah, 2009). This interval is also significant within the regional petroleum system because Upper Cretaceous to Eocene sandstones and limestones constitute major reservoir units, while intervening fine-grained successions provide important sealing and source intervals (Wandrey et al., 2004).

The Eocene succession is particularly important to the present study because it records substantial lateral variation in depositional environments and lithofacies. Where shallow-marine carbonate deposition persisted in some parts of the basin, while adjacent depocenters accumulated thicker shale-rich successions, reflecting differences in accommodation and siliciclastic input. Within this framework, the Early Eocene Ghazij Formation occupies an important stratigraphic position above the Paleocene succession and below the younger Eocene units. It is predominantly fine-grained, although sandstone,

limestone, and other subordinate lithologies occur regionally. The formation therefore represents a major phase of fine-grained siliciclastic accumulation between the mixed Paleocene depositional systems and younger Eocene successions that are locally dominated by shallow marine carbonates (Shah, 2009). The lateral variability of the Paleogene succession was also influenced by inherited structures that remained active or were reactivated during the early Eocene, contributing to local variations in accommodation and sediment accumulation (Ahmed et al., 2018).

After the Eocene, the stratigraphic record shifts toward marine regression and increasing siliciclastic sedimentation. Oligocene strata are represented mostly by the Nari formation and associated units, which records continued marine deposition during a broader transition toward increasingly regressive conditions. During the Miocene and Pliocene, the southward retreat of the sea progressively transformed large parts of the basin from marine to estuarine and fluvial environments, although marine conditions persisted longer in the southern and coastal areas. The youngest succession is dominated by continental clastic deposits associated with uplift, erosion, and basin filling, followed by unconsolidated alluvial, aeolian, floodplain, lacustrine, and coastal sediments (Shah, 2009, Kadri, 1995).

2.3.1 The Ghazij Formation: age, extent, and lithofacies

The Ghazij Formation is an Early Eocene sedimentary succession that is widely developed along the western margin of the Indus basin. Its age has been established primarily from foraminiferal assemblages and regional stratigraphic relationships, although precise geological time limits assigned to the formation vary across different parts of its extensive outcrop belt. Biostratigraphic evidence generally places Ghazij within the Early Eocene, whereas regional chronostratigraphic studies indicate that deposition

broadly occurred during the Early Eocene interval represented across the western and southern parts of the Indus Basin (Afzal et al., 2009; Shah, 2009, Johnson et al., 1999).

Regionally the Ghazij Formation is exposed discontinuously across the Sulaiman Range, Kirthar Range, Axial Belt, and adjoining areas of western Pakistan (Shah, 2009). Johnson et al. (1999) documented an intermittent outcrop belt extending for approximately 750 km along the western margin of the Axial Belt and demonstrated substantial regional variation in the formation's thickness and lithofacies architecture. Southward along the Kirthar range, Ghazij exposures continue intermittently to approximately 23 km south of Karkh, where the southernmost exposed occurrence is abruptly interrupted by faulting. Further south in Sindh area, approximately time-equivalent Early Eocene strata are represented by the Laki and associated formations rather than by the Ghazij lithostratigraphic nomenclature (Johnson et al., 1999). The broad regional distribution of the Ghazij Formation, along with its documented lateral variability, reflects deposition across a geographically extensive and spatially heterogeneous sedimentary system.

The thickness of the Ghazij Formation varies considerably across its regional extent. Shah (2009) reported thicknesses ranging from approximately 160 m in parts of the Kirthar Range to more than 2,000 m in the Sulaiman region, while Johnson et al. (1999) documented similarly pronounced variations among measured and previously reported sections. The lower part alone has been reported to range from approximately 914 m near Duki to 2,134 m near Johan, although structural complications make accurate thickness determination difficult in some localities (Johnson et al., 1999). Such variations indicate substantial lateral changes in accommodation, sediment supply, preservation, and post depositional deformation. The formation generally overlies Paleocene carbonate strata, mainly the Dungan Formation or its regional equivalents, and is overlain by middle Eocene carbonate successions, including the Kirthar Formation and equivalent units (Shah, 2009; Johnson et al., 1999). The lower contact is commonly sharp but may become transitional or gradational in some areas, whereas the nature of the upper contact also varies regionally because of local erosion, structural disturbance, and lateral facies changes (Johnson et al., 1999).

A major characteristic of the Ghazij Formation is its systematic regionally variable vertical lithofacies organization. In the Sulaiman lobe and northern Kirthar Range, Johnson et al. (1999) recognized three principal subdivisions in Ghazij Formation as follows: a lower muddy marine part, a middle coal bearing part, and an upper muddy nonmarine part. These subdivisions correspond broadly to the natural stratigraphic zones recognized by earlier scholars and provide a useful regional framework for describing the internal architecture of the Ghazij Formation. The lower part is generally the thickest subdivision and commonly exceeds 1,000 m. It consists predominantly of greenish-grey calcareous mudstone and shale, with relatively uncommon, isolated sandstone bodies. The middle part is considerably thinner, generally ranging from approximately 30–300 m, and is more lithologically heterogenous, comprising grey mudrock and sandstone together with locally developed carbonaceous shale, coal, and limestone. The upper part may reach approximately 533 m in thickness and is dominated by multicolored mudrock with subordinate isolated sandstone bodies and in some localities, a conglomeratic unit near its base (Johnson et al., 1999).

The lower subdivision is dominated by thick successions of calcareous mudstone and shale, locally containing sandy intervals and thin, very fine-grained sandstones beds. Sandstone is generally subordinate and occurs as thin tabular or broader lenticular bodies (Johnson et al., 1999). The middle subdivision displays the greatest lithological heterogeneity within the formation. In addition to mudrock, it contains sandstone bodies of variable geometry and internal organization, together with carbonaceous shale, coal, limestone, claystone, and local coquina. The relative abundance and distribution of these lithologies vary substantially between localities. Comparable local scale variability has also been documented in earlier sedimentological studies of the Ghazij Formation (Kazi, 1968; Kassi, 1987; Johnson et al., 1999). In contrast, the upper subdivision is dominated by variegated calcareous mudrock with less abundant sandstone and locally developed conglomerate, although the proportions and character of these lithologies also change laterally (Johnson et al., 1999).

Within the broader petroleum system framework of the Indus Basin, the Ghazij Formation is therefore not lithologically uniform unit, but a laterally and vertically

heterogenous succession dominated by fine-grained rocks and interrupted by variable sandstone, carbonate, carbonaceous, and locally coal bearing intervals (Wandrey et al., 2004; Shah, 2009; Johnson et al., 1999). This heterogeneity is particularly relevant to the present study because the Ghazij Formation is investigated in the subsurface at the Zamzama and Mehar fields, where the lithofacies architecture established from regional outcrops may not be reproduced identically. Accordingly, evaluation of the formation in the study wells requires direct integration of well-based lithological, geochemical, and mineralogical data rather than sample extrapolation from exposed reference sections. The vertical and lateral variability outlined above also provides the stratigraphic framework for interpreting the depositional environments of the Ghazij Formation, discussed in the following subsection.

2.4 Well-based Stratigraphic Framework

Regional studies have documented substantial changes in the thickness, facies organization, and stratigraphic expression of the Ghazij succession along the Sulaiman-Kirthar trend (Johnson et al., 1999; Shah, 2009). For this reason, the subsurface stratigraphic position of the Ghazij Formation in the present study was established directly from the reported formation tops of the Zamzama-5 and Mehar-1 wells rather than inferred from regional outcrop sections.

The two wells provide separate subsurface records of the Cenozoic succession in the Southern Indus Basin. In Zamzama-5, drilling and logging depths were measured from the rig floor, located 44 m above mean sea level, whereas depths in Mehar-1 were measured from the Rotary Table Kelly Bush (RTKB), located 119.6 m above mean sea level. Original reported well depths are retained throughout the well-specific descriptions because the formation tops in each well were recorded relative to the corresponding well reference datum. This approach preserves the internal consistency of the primary well records. The

complete stratigraphic successions and reported formation tops are presented in tables (2.1) and (2.2).

2.4.1 Stratigraphy of Zamzama-5

Zamzama-5 reached a reported total drilled depth of 3,871 m and penetrated a stratigraphic succession extending from recent alluvial deposits to Upper Cretaceous strata. The complete succession and reported formation tops are presented in (Table 2.1). Within the Paleogene succession, the Ghazij Formation occurs between the overlying Kirthar Limestone and underlying Laki Formation.

Table 2.1 Borehole stratigraphy of Zamzama-5.

Formation	Age	Depth (m)	Thickness (m)
Alluvium	Recent	0	68
Siwalik	Miocene-Pleistocene-Pliocene	68	1,324
Gaj	Miocene	1,392	108
Nari	Oligocene	1,500	575
Kirthar Limestone	Eocene	2,075	167
Ghazij Formation	Eocene	2,242	132
Laki	Eocene	2,374	399
Dunghan	Paleocene	2,773	406
Girdo	Paleocene	3,179	354
Khadro	Paleocene	3,533	53.6
Pab Sandstone	Late Cretaceous	3,586.6	229.4
Fort Munro	Late-Early Cretaceous	3,816	55

The Ghazij formation extends from 2,242 to 2,374 m and occupies a gross vertical interval of 132 m. This stratigraphic position is broadly consistent with the regional occurrence of the Ghazij within the Paleogene succession, although the nomenclature and correlation of adjacent units vary geographically across the basin. The interval encountered in Zamzama-5 is substantially thinner than many of the classic exposed Ghazij successions described in the preceding sections, further reflecting the pronounced regional thickness variability of the formation. In the absence of well-specific lithological logs, core descriptions, or Biostratigraphic data, no attempt is made to subdivide the interval into the lower, middle, and upper lithofacies associations recognized in the regional outcrop studies. The reported formation tops therefore provide the principal basis for defining the Ghazij interval in this well.

2.4.2 Stratigraphy of Mehar-1

The complete succession and reported formation tops for Mehar-1 are presented in (Table 2.2). Within the Paleogene succession, the Ghazij Formation occurs between the overlying Kirthar Limestone and underlying Sui Main Limestone.

Table 2.2 Borehole stratigraphy of Mehar-1.

Formation	Age	Depth (m)	Thickness (m)
Alluvium	Recent	0	17
Siwalik	Miocene-Pleistocene-Pliocene	17	813
Gaj	Miocene	830	445
Upper Nari	Oligocene	1,275	576
Lower Nari	Oligocene	1,851	152
Kirthar Limestone	Eocene	2,003	354

Ghazij Formation	Eocene	2,357	87
SUI main Limestone	Eocene	2,444	618
Dunghan	Paleocene	3,062	166
Ranikot	Paleocene	3,228	332
Pab Sandstone	Late Cretaceous	3,560	113
Mughal Kot	Late Cretaceous	3,673	132

The Ghazij Formation extends from 2,357 to 2,444 m and occupies a gross vertical interval of 87 m. Its upper stratigraphic relationship is the same as in Zamzama-5, whereas the lower bounding unit differs between the two wells. The Ghazij interval in Mehar-1 is 45 m thinner than the 132 m interval recorded in Zamzama-5. This well scale contrast is consistent with the pronounced regional thickness variability documented for the Ghazij succession (Johnson et al., 1999; Shah, 2009).

Taken together, the two wells demonstrate that the Ghazij Formation occurs as a distinct Eocene stratigraphic interval beneath the Kirthar Limestone but varies in thickness and in what formation underlies it. Its gross vertical interval decreases from 132 m in Zamzama-5 to 87 m in Mehar-1, while the underlying unit is Laki Formation in the former and is Sui Main Limestone in the latter. The available well data does not allow for detailed lithofacies correlation or internal subdivision of the Ghazij interval between the two boreholes. Nevertheless, the observed differences provide a well-based stratigraphic framework for the investigated intervals, while the source, distribution, and analytical selection of the cutting samples are described in Chapter 3.

CHAPTER 3

METHODOLOGY

3.1 Research Workflow

The methodological workflow adopted in this study follows an integrated source-rock evaluation approach that is widely applied in petroleum geochemistry, in which organic geochemical, mineralogical, elemental geochemical, and microscopic datasets are combined to provide a comprehensive characterization of unconventional reservoirs (Peters and Cassa, 1994; Muktadir et al., 2021). For this study, the two wells, Zamzama-5 and Mehar-1, were selected based on the availability of drill-cutting samples, the complete penetration of the Early Eocene Ghazij Formation, and the accessibility of supporting geological and stratigraphic information.

The evaluation of the unconventional hydrocarbon source rock potential of the Early Eocene Ghazij Formation in the Southern Indus Basin in this study was designed according to a sequential and multidisciplinary analytical workflow, starting with the selection of representative wells penetrating the formation, followed by identification of the target stratigraphic interval using the reported formation tops. Representative drill-cutting samples were subsequently selected from the Ghazij interval and prepared for

laboratory analysis in accordance with standard source rock evaluation procedures, where appropriate sample selection and preparation constitute the foundation of reliable geochemical interpretation (Peters et al., 2016; Peters and Cassa, 1994).

Total organic carbon (TOC) analysis was initially performed on all collected samples to quantify organic richness and to serve as a primary screening tool for selecting representative samples for further analysis. This sequential approach follows the widely adopted exploration workflow in which TOC measurements preceded more detailed programmed pyrolysis to optimize the evaluation of source rock quantity and quality (Peters and Cassa, 1994; Behar et al., 2001). Selected Samples were then subjected to rock-Eval Pyrolysis to determine kerogen type, hydrocarbon generation potential, and thermal maturity. In parallel, representative samples were analyzed using X-ray diffraction (XRD) and X-ray fluorescence (XRF) to characterize mineralogical composition and elemental geochemistry, while scanning electron microscopy coupled with energy-dispersive X-ray spectrometry (SEM-EDS) was employed to investigate pore morphology, mineral textures, and the spatial occurrence of organic matter. This integrated combination of geochemical, mineralogical, and microscopic techniques has become a standard approach for evaluating unconventional shale source rocks because it provides complementary information on both geochemical properties and reservoir characteristics.

Finally, the results obtained from all analytical techniques were integrated to develop a comprehensive understanding of the organic, mineralogical, geochemical, and microstructural characteristics of the Ghazij Formation. The combined interpretation of these datasets provides the basis for evaluating its unconventional hydrocarbon source rock potential and for assessing the geological factors controlling its prospectivity within the Southern Indus Basin. The methodological sequence adopted in this study is summarized in Figure 3.1.

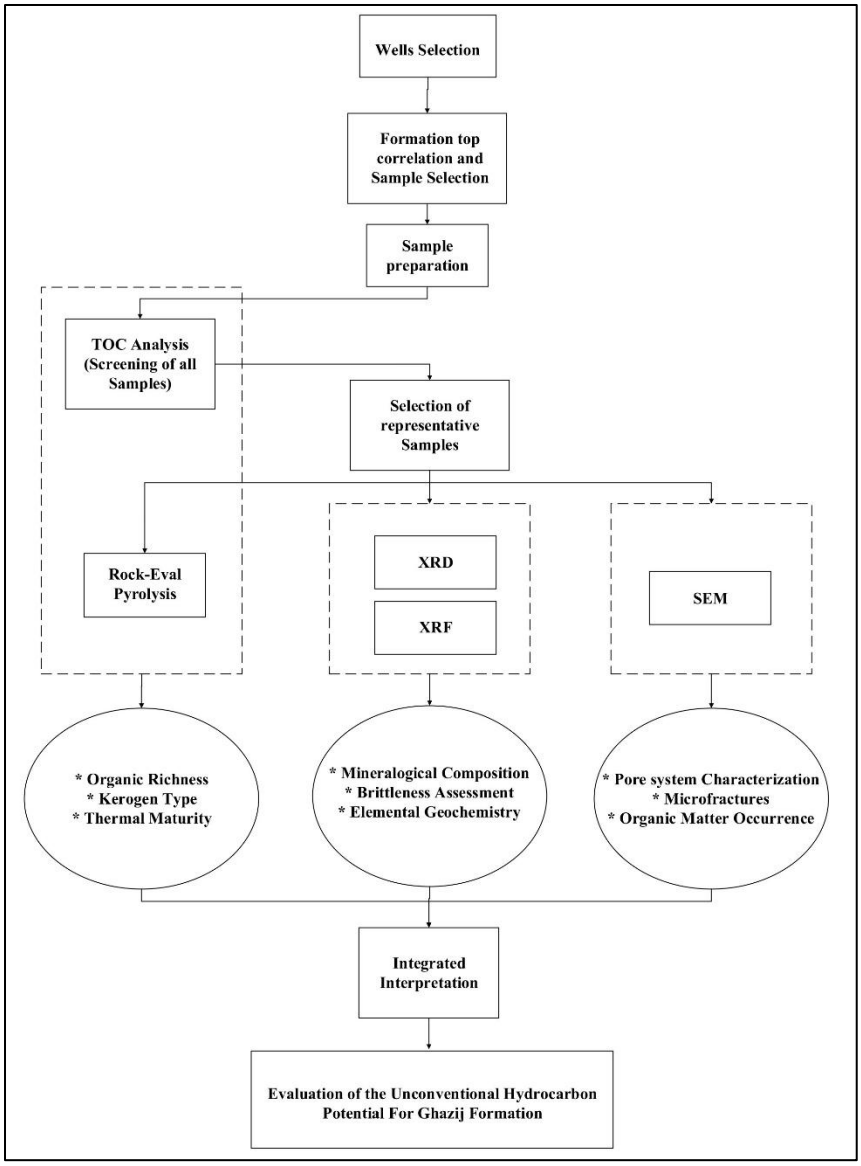


Figure 3.1 Schematic representation of the integrated research methodology adopted for the study. The workflow summarizes the sequence of sample selection, preparation, and laboratory analyses including TOC, Rock-Eval pyrolysis, XRD, XRF, and SEM-EDS, providing a comprehensive unconventional source rock evaluation of Ghazij Formation.

3.2 Sample Material and Preparation

In this study, drill-cutting samples were collected from two representative wells, Zamzama-5 and Mehar-1, located within the Southern Indus Basin, Pakistan. The Ghazij Formation occurs between depths 2242–2374 m in Zamzama-5 and 2357–2444 m in Mehar-1, corresponding to gross formation thickness of approximately 132 m and 87 m, respectively. A total of 24 drill-cutting samples were investigated in this study, comprising 14 samples from Zamzama-5 and 10 samples from Mehar-1.

The drill-cutting samples were obtained from the Petroleum Core House (PETCORE) of the Hydrocarbon Development Institute of Pakistan (HDIP) following official approval granted by the Directorate General of Petroleum Concessions (DGPC). All laboratory analyses were conducted at the laboratories of HDIP.

Following sample acquisition, the Ghazij Formation interval in each well was identified using the reported formation tops. The samples were washed and air dried before subsequent preparation in accordance with the analytical requirements of each laboratory technique prior to organic geochemical, mineralogical, elemental geochemical, and microscopic characterization. The procedures adopted for cutting sample selection, and sample preparation are described in the following sections.

3.2.1 Cutting sample selection

The sampling strategy ensured to obtain material from upper, middle, and lower portions of the Ghazij Formation while maintaining adequate coverage across the entire sampled interval. Sample selection was primarily based on stratigraphic position and the

availability of sufficient drill-cutting material to perform the planned laboratory analysis. This approach ensured that the selected samples captured the vertical variability of the formation while providing a representative dataset for integrated organic geochemical, mineralogical, elemental geochemical, and microscopic investigations, the distribution of the selected samples within the Ghazij Formation intervals of both wells is illustrated in Table 3.1.

Table 3.1 Details of the samples' distribution within the Ghazij Formation in the selected wells.

Wells	Lab No.	Depth Interval	No. of samples
Zamzama-5	Pr-23027	2240–2250	14
	Pr-23028	2250–2260	
	Pr-23029	2260–2270	
	Pr-23030	2270–2280	
	Pr-23031	2280–2290	
	Pr-23032	2290–2300	
	Pr-23033	2300–2310	
	Pr-23034	2310–2320	
	Pr-23035	2320–2330	
	Pr-23036	2330–2340	
	Pr-23037	2340–2350	
	Pr-23038	2350–2360	
	Pr-23039	2360–2370	
	Pr-23040	2370–2380	
Mehar-1	Pr-22826	2357–2360	10
	Pr-22827	2369–2372	
	Pr-22828	2375–2378	
	Pr-22829	2384–2387	
	Pr-22830	2393–2396	
	Pr-22831	2402–2405	
	Pr-22832	2411–2414	

	Pr-22833	2420–2423	
	Pr-22834	2429–2432	
	Pr-22835	2432–2435	

Prior to laboratory preparation, all selected drill-cutting samples were subjected to visual examinations to document their lithological appearance, fragment morphology, color, and particle characteristics. Representative photographs from the upper, middle, and lower sections of the Ghazij Formation in each well are presented in Figures 3.2 and 3.3, providing a visual reference for the analyzed material before laboratory characterization.

The representative cuttings from Mehar-1 (Fig. 3.2 a, b, and c) exhibit moderate lithological variability throughout the sampled Ghazij Formation interval. The upper interval (Figure 3.2a) is dominated by light grey carbonate chips with subordinate granular to flaky dark grey shale fragments. In contrast, the middle interval (Figure 3.2b) consists predominantly of fine-grained, granular shale fragments with only minor calcareous chips. The lower interval (Figure 3.2c) displays a mixed lithology, comprising abundant dark grey shale fragments interspersed with light grey carbonate ships. These observations provide an initial qualitative assessment of the recovered drill-cuttings prior to sample preparation and laboratory analyses.

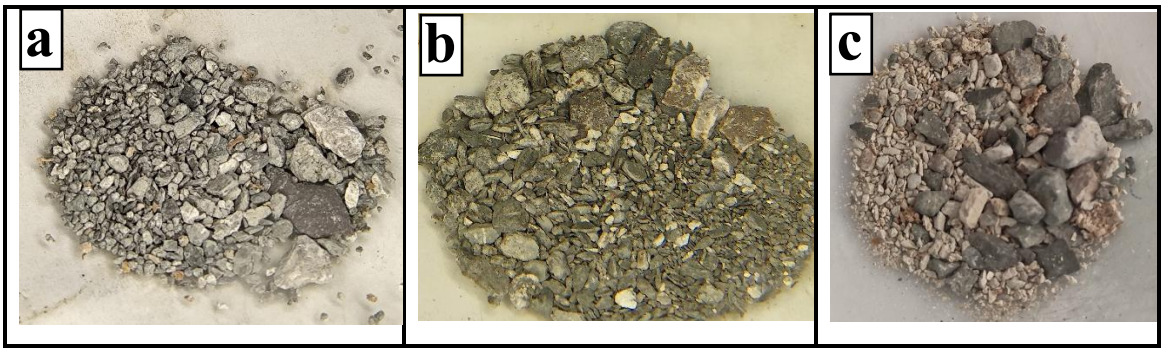


Figure 3.2 Representative drill-cutting samples from Mehar-1 well. The upper interval sample (2357–2360 m) consists of 75% light grey carbonate chips with 25% granular to flaky shale pieces (a). Middle interval sample (2393–2396 m) shows an increase in granular

shale to about 90% of the sample with minor 10% calcareous chips (b). Lower interval (2432–2435 m) is dominated by dark grey shale fragments (approximately 80%) with approximately 20% light-grey carbonate chips (c).

In contrast, the cuttings from Zamzama-5 (Fig. 3.3 a, b, and c) consist predominantly of light grey to grey, fine to medium grained angular carbonate fragments exhibiting relatively uniform particle size and morphology throughout the sampled interval. Compared with Mehar-1, the Zamzama-5 cuttings display a more homogeneous visual appearance with limited variation in color and fragment morphology between upper, middle, and lower intervals.

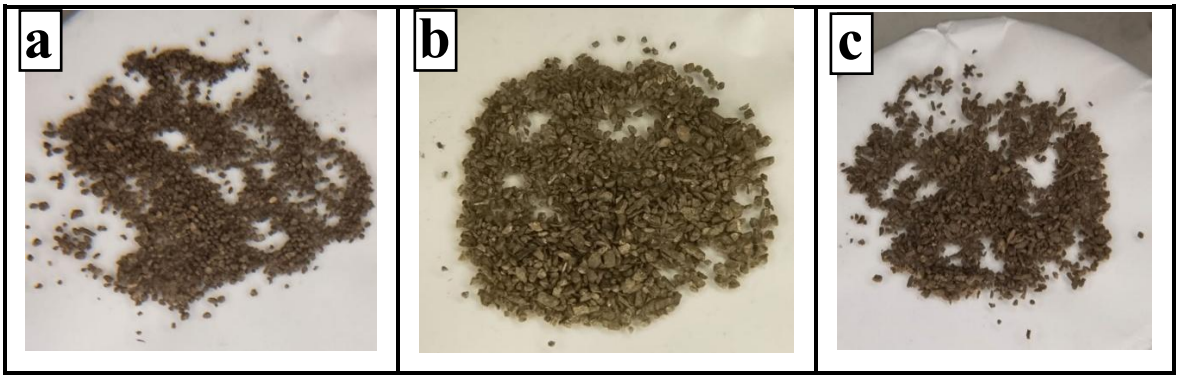


Figure 3.3 Representative drill-cutting samples from the Zamzama-5 well. The upper interval (2240–2250 m) consists predominantly of fine- to medium-grained angular carbonate fragments (a). The middle interval (2300–2310 m) exhibits a similar carbonate dominant appearance with relatively uniform particle size and morphology (b). The lower interval (2370–2380 m) consists predominantly of carbonate fragments with only minor variation in color and grain characteristics (c).

Overall, the visual examination demonstrates distinct lithological differences between the two investigated wells. Mehar-1 is characterized by abundant dark shale fragments interspersed with subordinate carbonate chips, while Zamzama-5 is dominated by comparatively homogenous carbonate-rich fragments. Although these observations are

qualitative, they provide important visual framework for interpreting the subsequent laboratory analysis results.

3.2.2 Sample preparation

The selected drill-cutting samples were prepared following standard laboratory procedures to ensure that the material was suitable for subsequent analysis. Sample preparation was designed to remove contaminants introduced during drilling while preserving representative formation material for laboratory characterization, because different drilling mud systems were used during drilling operations, the preparation procedures were adapted accordingly. After the samples were acquired from PETCORE, they were individually labelled according to their respective well name and sampling depth.

The Zamzama-1 drill-cutting samples were recovered from intervals using an oil-based drilling mud (OBM). Consequently, these samples required additional cleaning to remove residual drilling fluids prior to laboratory analysis. The samples were initially washed with dichloromethane (DCM) to dissolve residual oil-based mud adhering to the cuttings. They were subsequently cleaned in an ultrasonic bath (sonication) to further remove fine residues and contaminants from the sample surfaces. After cleaning, the samples were oven-dried overnight until completely free of solvent and moisture.

In contrast, the Mehar-1 drill-cuttings were not contaminated by oil-based drilling mud and therefore did not require solvent cleaning or ultrasound treatment. These samples were thoroughly washed on a washing station with distilled water to remove loose drilling residues and surface impurities and then air-dried under controlled conditions until free of moisture.

Following drying, all samples from both wells were carefully examined under a magnifying lens. Visible foreign material, including residual drilling mud aggregates,

wooden chips, husks, and other non-geological debris introduced during drilling operations, were manually removed using forceps to ensure that only representative formation cuttings were retained for analysis. This handpicking process minimized the possibility of contamination and improved the reliability of the results.

Following cleaning, representative portions of each sample were gently crushed and homogenized using a mortar and pestle. To prevent cross contamination, the mortar and pestle were thoroughly cleaned with DCM and wiped with a clean lint-free cloth between samples. The prepared powdered samples were used for total organic carbon (TOC), Rock-Eval pyrolysis, X-ray diffraction (XRD), and X-ray fluorescence (XRF) analysis. For scanning electron microscopy coupled with energy-dispersive X-ray spectroscopy (SEM-EDS), representative cleaned drill-cutting fragments were retained in their original form to preserve their natural surface morphology, pore structure, and mineral-textural relationship prior to microscopic examination.

3.3 Organic Geochemical Analysis

Organic geochemical analyses were conducted to evaluate the source rock characteristics of the Ghazij Formation by determining the organic richness, hydrocarbon generation potential, kerogen type, and thermal maturity. These parameters provide the fundamental geochemical information required to assess the petroleum generation capacity and quality of potential source rocks. Total organic carbon (TOC) analysis was employed as the initial screening method to quantify the abundance of organic matter, while Rock-Eval pyrolysis was subsequently performed on selected samples to assess their hydrocarbon generation potential, kerogen type, and thermal maturity of the organic matter. The principal parameters considered were S1, S2, S3, Tmax, TOC, Hydrogen Index (HI), Productivity Index (PI), and Oxygen Index (OI). The combined interpretation of TOC

and Rock-Eval data represent the standard approach for source rock evaluation in petroleum geochemistry and forms the basis for classifying source rock quality and generative potential (Peters, 1986; Peters and Cassa, 1994). The analytical procedures adopted for both methods are described in the following sections.

3.3.1 Total organic carbon (TOC) analysis

Total organic carbon (TOC) analysis was performed as the initial organic geochemical screening technique to quantify the organic richness of the samples and identify intervals suitable for further source rock evaluation. Approximately 100 mg ±5 mg of each powdered sample was weighed into ceramic crucibles using an analytical balance (Fig. 3.4 a). To remove inorganic carbon, the samples were treated with 10% hydrochloric acid (HCl). The crucibles were then placed on a hot plate with temperature not exceeding 40 °C for approximately 1 hour, and then they were oven-dried for approximately 24 hours to remove all residual moisture.

TOC measurements were carried out using Jinyibo CS-8820S Carbon and Sulfur Analyzer (Fig. 3.5). The instrument operates on the principle of high-temperature combustion coupled with non-dispersive infrared (NDIR) detection. During analysis, the samples (Fig. 3.4 b) were combusted in a stream of high-purity oxygen at temperatures between 1500 and 1800 °C, assisted by a pure iron flux accelerator (Fig. 3.4 c) to ensure complete oxidation of organic carbon to carbon dioxide (CO_2) and carbon monoxide (CO), which are transported through dust and moisture removal systems before being quantified by the NDIR detector, allowing the instrument to calculate the TOC contents as weight percent of the sample. Instrument calibration was done using standard (carbon and sulfur in steel) rings and the calibration then verified using a certified reference standard (Fig. 3.4 d and e) after every ten sample analyses to ensure analytical accuracy and consistency.

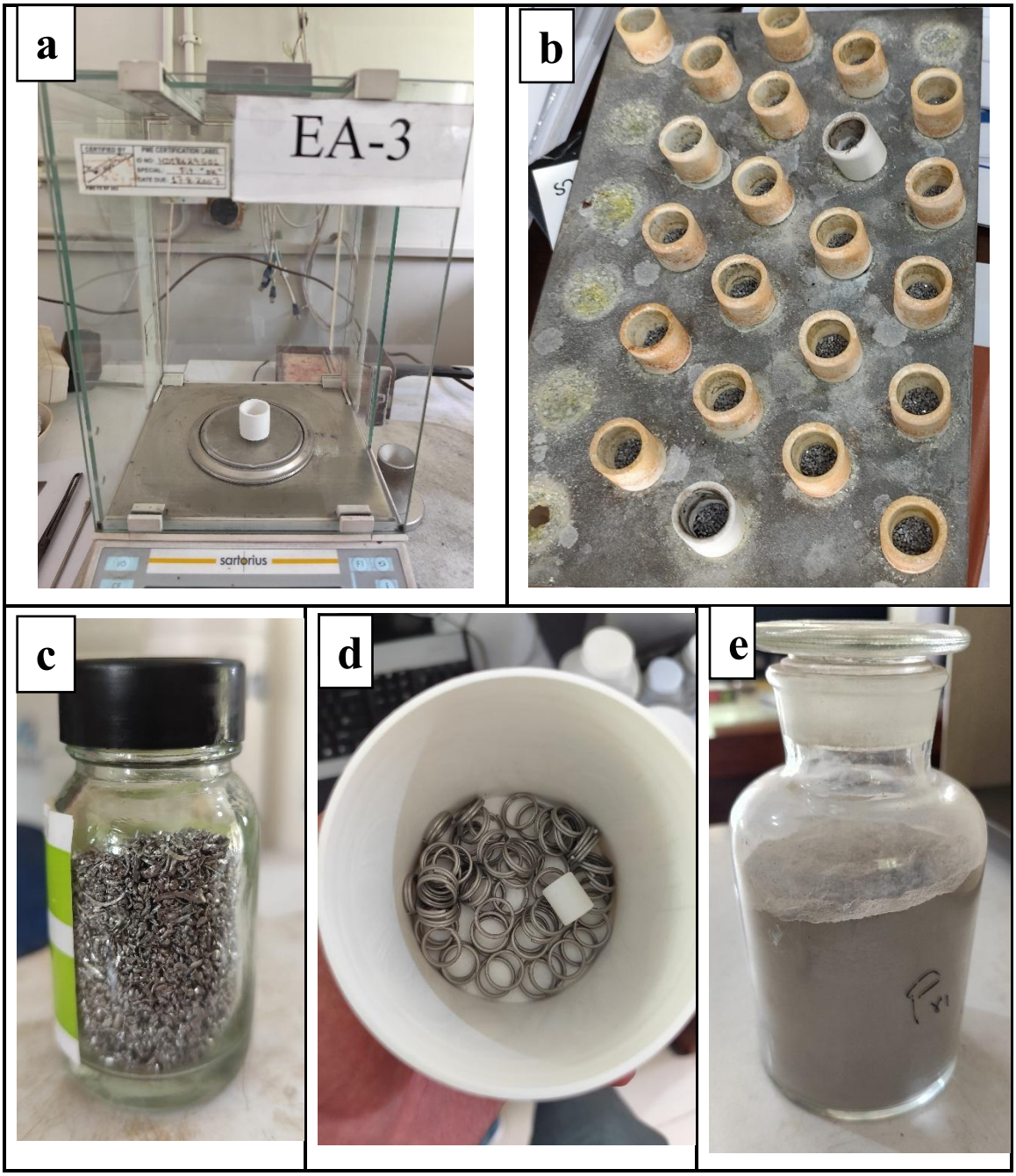


Figure 3.4 Representative stages and reference materials used during the TOC sample preparation and analysis: (a) weighing of the powdered sample in a crucible on an analytical balance; (b) crucible containing samples after being treated with hydrochloric acid placed on the hot plate and tungsten shaving added to them; (c) tungsten shavings used

as a combustion accelerator; (d) carbon rings used for instrument calibration; and (e) certified standard sample used to verify analytical accuracy and precision.

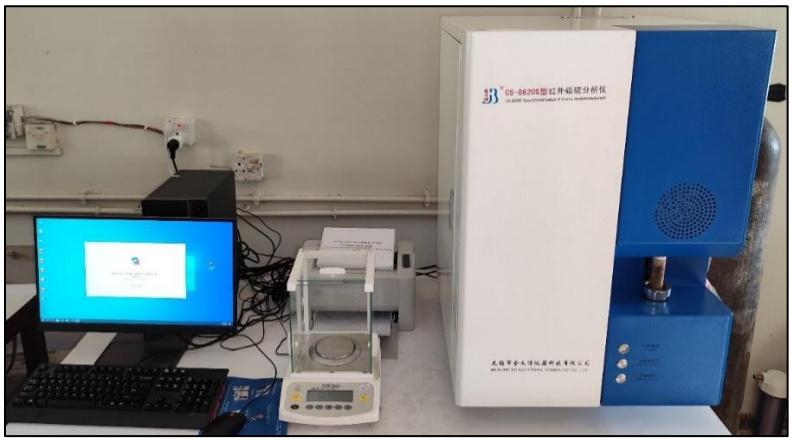


Figure 3.5 TOC instrument used at HDIP, the Jinyibo CS-8820S Carbon and Sulfur Analyzer.

3.3.2 Rock-Eval pyrolysis

Rock-Eval pyrolysis was performed to evaluate the hydrocarbon generation potential, kerogen type, and thermal maturity of the selected samples. Only samples from the Zamzama-5 well were subjected to Rock-Eval analysis using Rock-Eval 6 instrument at HDIP (Fig. 3.6). Approximately 60–65 mg of each powdered sample was weighed into Rock-Eval crucibles and analyzed under programmed heating conditions. The samples were initially pyrolyzed in an inert nitrogen atmosphere by heating from 300 °C to 600 °C at a rate of 25 °C per minute, subsequently the Flame Ionization Detector (FID) response would be recorded for each sample, generating characteristic S1, S2, and S3 peaks that represent the emission of organic compounds during each stage of heating.

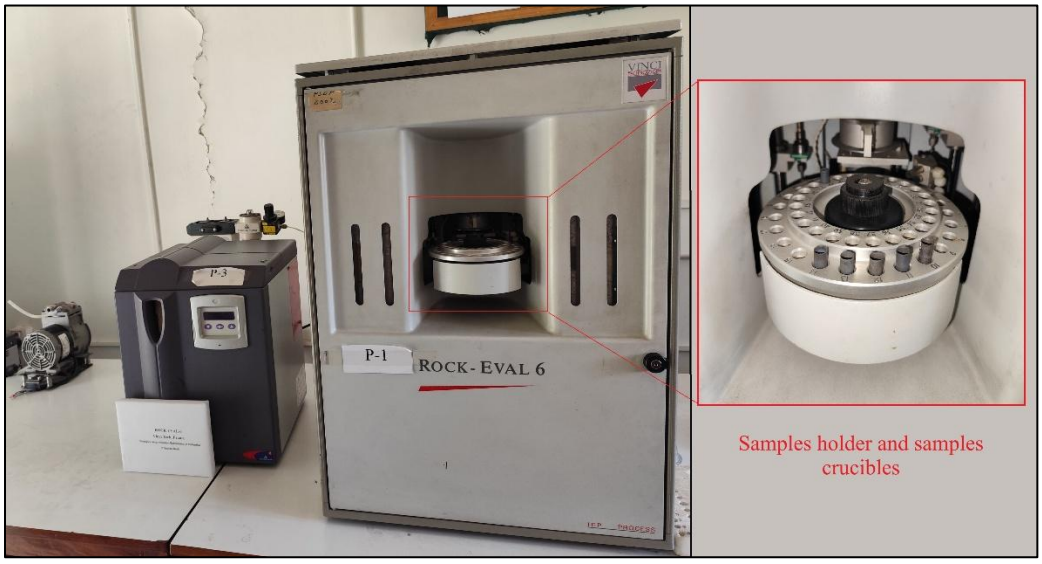


Figure 3.6 Rock-Eval 6 instrument with the hydrogen generator and a zoom in at the autosampler holding samples' crucibles.

The S_1 peak represents the free hydrocarbons already present within the rock, S2 corresponds to hydrocarbons generated through the thermal cracking of kerogen, and S3 represents carbon dioxide generated from the bonding of carbon to the oxygen-bearing functional groups contained in the kerogen. The temperature corresponding to the maximum S2 peak (T_{max}) was recorded for each sample and used as an indicator of thermal maturity. From the TOC and Rock-Eval data, additional parameters were calculated to further characterize the source rock, including the hydrogen index ($HI = \frac{S_2}{TOC} * 100$), oxygen index ($OI = \frac{S_3}{TOC} * 100$), production index ($PI = \frac{S_1}{S_1+S_2}$), Generic Potential ($GP = S_1 + S_2$), following the methodology of Peters (1986) and Peters and Cassa (1994).

3.4 Mineralogical and Elemental Analysis

Mineralogical and elemental analysis provide essential information for interpreting lithological characteristics. In fine grained sedimentary rocks, mineral composition exerts a significant influence on depositional processes, diagenetic evolution, mechanical behavior, and reservoir properties. Knowing the relative abundance of certain minerals is an important factor in determining rock brittleness, fracture development, and the overall behavior of formations. Similarly, elemental composition provides complementary information that assists in identifying lithological variations, mineral assemblages, and geochemical characteristics within the studied interval (Moore and Reynolds, 1997; Rollinson, 1993).

X-ray diffraction (XRD) and X-ray fluorescence (XRF) are widely recognized as complementary analytical techniques for the characterization of sedimentary rocks. In this study, the XRD was used to identify and quantify the mineralogical composition of the selected samples, including the relative proportions of major mineral phases such as calcite, quartz, dolomite/ankerite, feldspar, clay minerals, and other detected phases, whereas the XRF was used to characterize the elemental composition of the selected samples, with the analytical results reported in conventional oxide weight-percent form. The resulting major and trace element/oxide data were used to evaluate the geochemical and mineralogical characteristics of the samples. The combined interpretations of mineralogical and elemental data enhance the reliability of lithological characterization and have been widely adopted in studies of unconventional shale reservoirs and source rocks (Hupp and Donovan, 2018). Furthermore, mineralogical information provides a valuable framework for assessing rock brittleness and supporting the interpretation of organic geochemical and microscopic observations, thereby contributes to a more comprehensive evaluation of the unconventional hydrocarbon source rock potential (Ji et al., 2012). The detailed methodologies are discussed in the following subsections.

3.4.1 X-ray diffraction (XRD)

X-ray diffraction analysis was conducted on three representative samples from the Ghazij Formation in the Zamzama-5 well, corresponding to the upper (2240–2250 m), middle (2300–2310 m), and lower (2370–2380 m) intervals of the formation. The samples were ground into a fine powder using a vibratory disc mill down to (75 μm), then they were loaded into a standard powder sample holder (Fig. 3.7) and gently levelled to obtain a flat and uniform sample surface suitable for diffraction analysis. Maintaining a smooth, flush surface minimizes specimen displacement errors and improves diffraction accuracy.

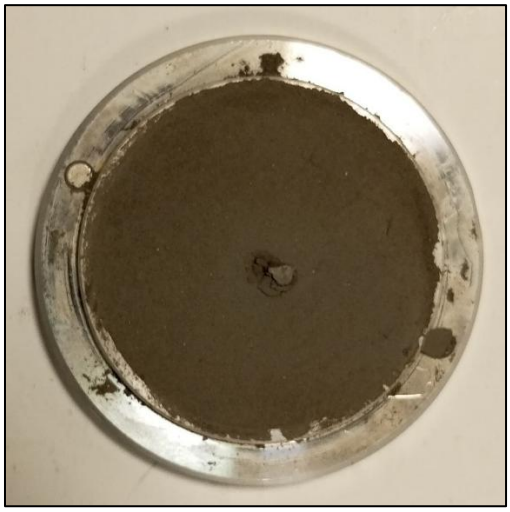


Figure 3.7 Standard XRD sample holder with sample loaded and leveled ready for XRD analysis.

The analyses were performed using a Rigaku SmartLab SE multipurpose θ–θ X-ray diffractometer (Fig. 3.8) employing Cu-Kα radiation (λ = 1.5406 Å) operated at 30 kV and 30 mA. Diffraction patterns were collected over a 2θ range of 10°–90° with a step size of 0.02°. Instrument control, data acquisition, and phase identification were carried out

using Rigaku SmartLab Studio II software. The identified mineral assemblages were subsequently used for mineralogical characterization of the Ghazij Formation.



Figure 3.8 Rigaku SmartLab SE multipurpose θ–θ X-ray diffractometer used for XRD analysis at HDIP lab.

3.4.2 X-ray fluorescence (XRF)

X-ray fluorescence (XRF) analysis was performed on the same three representative powdered samples below 75 microns in particle size from the Ghazij Formation in the

Zamzama-5 well that were selected for the XRD analysis. Prior to the analysis, the powdered samples were pressed into homogeneous pellets (Fig. 3.9) using a 15-ton hydraulic press with boric acid as a binder with a ratio of (1:10 of sample to boric acid) to produce stable, uniform discs suitable for XRF measurements and aid the pellet formation without introducing significant spectral interferences. The analyses were carried out under vacuum conditions to improve the detection sensitivity of low atomic number elements.

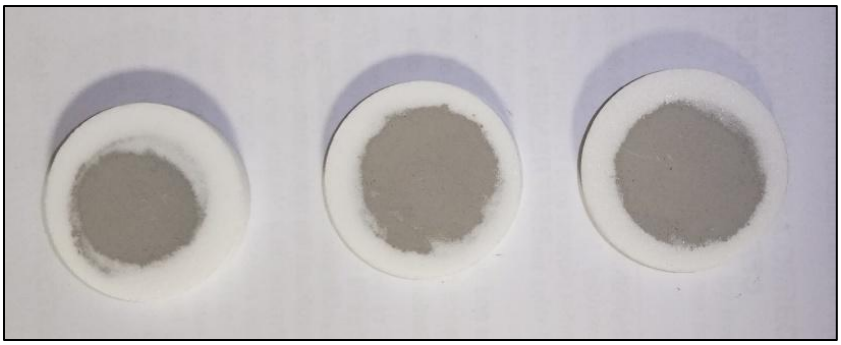


Figure 3.9 Pressed pellets of the Zamzama-5 samples.

Elemental analyses were conducted at the XRF Laboratory of the HDIP, using a Shimadzu EDX-7200 Energy-Dispersive X-Ray Fluorescence (ED-XRF) spectrometer (Fig. 3.10) equipped with a 10 mm collimator and a Rhodium (Rh) target. The instrument was operated at 15 kV for low energy elements (Na-Sc and S-Ca) and 50 kV for higher energy elemental groups (Ti-U, Cr-Fe, Zn-Pb, and Rb-Sb). Acquisition energy ranges of 0–20 keV and 0–40 keV were employed for low and high energy elemental groups respectively, providing accurate determination of major, trace, and selected rare earth elements.



Figure 3.10 The Shimadzu EDX-7200 Energy-Dispersive X-Ray Fluorescence (ED-XRF) spectrometer used for XRF analysis at HDIP.

Instrument calibration and quality control were verified using the certified reference materials OREAS 461 and OREAS 755, which were analyzed under the same operating conditions as the unknown samples. Each sample was measured in duplicate, and the average values were used for subsequent geochemical interpretation to improve analytical precision and minimize random measurement errors. This analytical technique allowed for precise quantification of the major and trace elements present in each sample, which provided a comprehensive geochemical profile.

The XRF measurements determine elemental concentrations, which are conventionally reported as equivalent oxide weight percentages (wt.%). Accordingly, elements such as Si, Al, Fe, Ca, Mg, Na, K, Ti, Mn, and P are reported as SiO_2, Al_2O_3, Fe_2O_3, CaO, MgO, Na_2O, K_2O, TiO_2, MnO, and P_2O_5, respectively.

3.5 Microscopic and Pore Structure Analysis

Microscopic characterization was performed to examine the morphology, pore structure, and mineral textures of the Ghazij Formation at the microscale. Scanning electron microscopy (SEM), coupled with energy dispersive X-ray spectroscopy (EDS), enables high resolution imaging of rock surfaces while simultaneously providing localized elemental composition. The combined use of SEM and EDS facilitates the identification of local mineral phases, textural relationships, pore types, and diagenetic features that cannot be resolved using bulk mineralogical techniques alone. Consequently, SEM-EDS serves as an important complementary technique for interpreting mineralogical and geochemical observations in unconventional source rocks.

3.5.1 Scanning electron microscopy and energy dispersive x-ray spectroscopy (SEM-EDS)

Scanning electron microscopy (SEM), coupled with energy dispersive X-ray spectroscopy (EDS) was performed on three representative drill-cutting samples from the upper (2240–2250 m), middle (2300–2310 m), and lower (2370–2380 m) intervals of the Ghazij Formation in the Zamzama-5 well. Small rock fragments were mounted on standard aluminum stubs using conductive carbon tape and sputter-coated with a thin conductive layer of gold-palladium (Au 80%, Pd 20%) using a Quorum sputter coater (Fig. 3.11) to minimize charging during electron beam exposure.



Figure 3.11 Quorum sputter coater used for sputter coating the samples with a thin layer of gold-palladium alloy.

Microscopic imaging was carried out at the SEM laboratory at HDIP using a Carl Zeiss EVO 10 scanning electron microscope equipped with an Oxford Xplore 30 energy dispersive X-ray spectroscopy (EDS) system (Fig. 3.12). Surface morphology was examined using the Everhart-Thornley Secondary Electron (SE) detector, which provides high resolution images of surface topography and microtextural features. Elemental point analyses were subsequently performed on selected microscopic regions using the integrated Oxford EDS system to determine the elemental composition of individual mineral phases and associated microstructures.

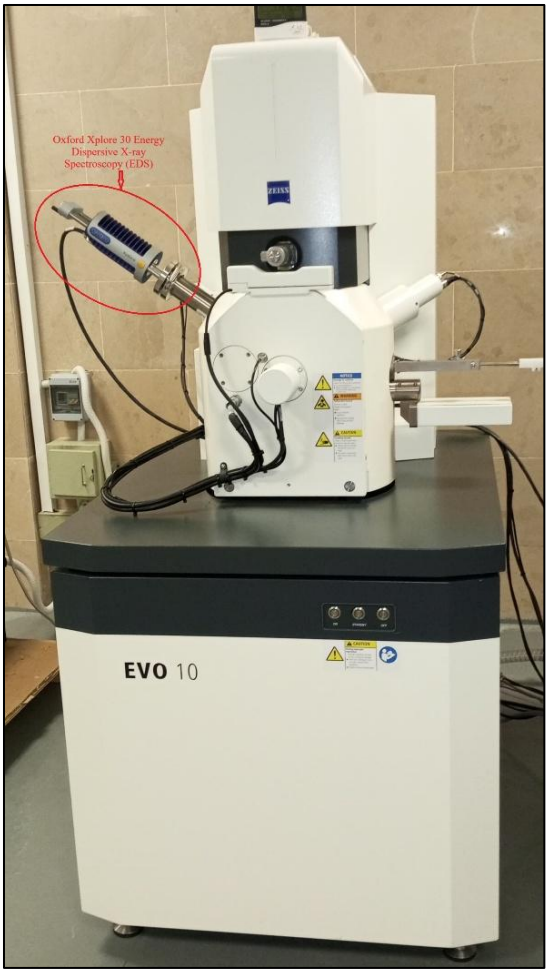


Figure 3.12 Carl Zeiss EVO 10 scanning electron microscope equipped with an Oxford Xplore 30 Energy Dispersive X-ray Spectroscopy (EDS) system used at HDIP.

Because the samples were sputter-coated with a gold-palladium layer and mounted using conductive carbon tape, characteristic peaks corresponding to Au, Pd, and C were present in the EDS spectra. These peaks represent procedural artifacts rather than constituents of the rock samples and were therefore excluded from the final elemental interpretation.

3.6 Integrated Analytical Workflow

The analytical workflow adopted in this study followed a progressive source rock evaluation workflow, in which TOC analysis served as the initial screening method for selecting samples for subsequent geochemical, mineralogical, and microscopic investigations. This approach is consistent with established petroleum geochemical practice, where TOC is first used to assess organic richness before undertaking more detailed analysis such as Rock-Eval Pyrolysis, XRD, XRF, and SEM-EDS. Furthermore, analytical techniques are selected according to the characteristics and objectives of the samples investigated to ensure reliable geological interpretation (Carvajal-Ortiz and Gentzis, 2018; Jarvie, 2015).

Following the source rock classification of peters and Cassa (1994), samples with TOC values below 0.5 wt.% are classified as poor source rocks and generally considered unsuitable for detailed source rock characterization. All ten samples analyzed from the Mehar-1 well yielded TOC values ranging from 0.32 to 0.45 wt.%, remaining below this threshold throughout the sampled interval. Consequently, further Rock-Eval pyrolysis, XRD, XRF, and SEM-EDS analyses were not performed on these samples, and their characterization in this study is based on TOC measurements and visual examination of the drill-cuttings.

In contrast, all fourteen samples analyzed from the Zamzama-5 well exhibited TOC values exceeding 2.56 wt.%, corresponding to very good to excellent source rock quality according to the classification of Peters and Cassa (1994). Based on these results, seven representative samples (Pr-23027, Pr-23029, Pr-23031, Pr-23033, Pr-23035, Pr-23038, and Pr-23040) were selected for Rock-Eval pyrolysis to assess the hydrocarbon generation potential, kerogen type, and thermal maturity. And three representative samples (Pr-23027, Pr-23033, and Pr-23040) were selected for XRD, XRF, and SEM-EDS analyses. These samples represent the upper, middle, and lower parts of the Ghazij Formation respectively, and were selected to evaluate potential vertical variations in mineralogical composition, elemental geochemistry, microstructural characteristics, and pore fabric across the studied interval.

CHAPTER 4

RESULTS AND DISCUSSION

This chapter presents an integrated geochemical, mineralogical, and pore fabric evaluation of the Ghazij Formation as penetrated by Zamzama-5 and Mehar-1 in the Southern Indus Basin. The analytical dataset comprises X-ray fluorescence (XRF) major oxide geochemistry, X-ray diffraction (XRD) mineralogy, total organic carbon (TOC) analysis, Rock-Eval pyrolysis parameters (S1, S2, S3, T_{max}, genetic potential, hydrogen index, oxygen index, and production index), and scanning electron microscopy coupled with energy dispersive X-ray spectroscopy (SEM-EDS). The Ghazij Formation is regionally a shale-dominated sequence in the Southern Indus Basin; this study specifically targets a carbonate-rich limestone interval within the formation at Zamzama-5, while cutting examination at Mehar-1 confirms that well penetrates the shale-dominated regional facies of the same formation. Results, interpretation and discussion are presented together under each heading, following the natural sequence of source rock and reservoir evaluation.

4.1 Lithological Characterization of the Ghazij Formation (XRF-Based)

Table 4.1 presents the major oxide composition of three Ghazij Formation samples from Zamzama-5 (Pr-23027, Pr-23033 and Pr-23040), corresponding to the top, middle and base of the sampled interval at 2240–2250 m, 2300–2310 m and 2370–2380 m, respectively.

Table 4.1 Major oxide composition (wt.%) of the Ghazij Formation, Zamzama-5, determined by (XRF).

Oxide	Depth: 2240–2250 m	Depth: 2300–2310 m	Depth: 2370–2380 m
CaO	43.041	61.505	69.930
SiO_2	22.845	14.593	9.176
Al_2O_3	5.159	3.472	2.009
Fe_2O_3	14.406	6.795	4.775
BaO	4.364	5.557	7.019
SO_3	3.517	3.060	2.764
K_2O	2.342	1.408	0.985
Cl	0.860	1.139	1.389
MgO	1.451	0.837	1.341
TiO_2	1.263	0.576	—
MnO	0.291	0.177	—
SrO	0.329	0.805	0.580
CuO	—	0.030	—
ZrO_2	0.046	—	—
Rb_2O	0.027	0.015	0.009
ZnO	0.027	0.018	0.012
Y_2O_3	0.011	—	—

Ir_2O_3	0.010	0.006	0.003
PbO	0.004	0.002	0.004
Br	0.003	0.003	0.004

CaO is the dominant oxide at all three depths, increasing from 43.04% at 2250 m to 69.93% at 2380 m. Converting CaO to an equivalent calcite ($CaCO_3$) content (using the stoichiometric ratio of 0.56 g CaO per gram $CaCO_3$) yields approximately 77%, 110% and 125% $CaCO_3$-equivalent for the three samples, respectively (Deer, Howie and Zussman, 2013). Values exceeding 100% indicate that calcium is not held exclusively as calcite, indicating that the CaO content cannot be interpreted as calcite alone; the accompanying SO_3 (2.76–3.52%) and the steadily increasing BaO (4.36–7.02%) suggest a minor but growing contribution from gypsum/anhydrite and barite ($BaSO_4$) to the carbonate-dominated matrix with depth (Tucker, 2001; Boggs, 2012).

Al_2O_3, the most diagnostic proxy for detrital clay content, remains low throughout the interval (5.16%, 3.47% and 2.01%), well below the 15-25% typically associated with shale (Ross and Bustin, 2009; Jarvie, 2012). This rules out a shale classification for the entire sampled section. SiO_2 (22.85% → 9.18%) and Fe_2O_3 (14.41% → 4.78%) decrease in step with the Al_2O_3 decline and the CaO increase, consistent with a simple dilution trend: as the proportion of carbonate increases downhole, the detrital quartz-clay-iron oxide fraction is proportionally diminished, rather than reflecting an independent compositional change (Tucker, 2001; Boggs, 2012).

On the basis of dominant CaO, subordinate SiO_2, and consistently low Al_2O_3, the Ghazij interval in Zamzama-5 is classified as a limestone, becoming progressively purer in carbonate (and correspondingly more depleted in clastic input) with depth. Its further classification as a bituminous or lean limestone, is established in section 4.3 once the organic richness data are considered.

4.2 XRD Mineralogical Composition of the Ghazij Formation

X-ray diffraction (XRD) analysis was performed on the same three samples used for XRF, providing quantitative mineral phase identification to complement the bulk elemental data. Five principal mineral phases were identified: calcite, quartz, dolomite/ankerite, barite, and clinochlore/orthoclase. Quantitative mineral proportions are summarized in Table 4.2 and illustrated in Figure 4.1.

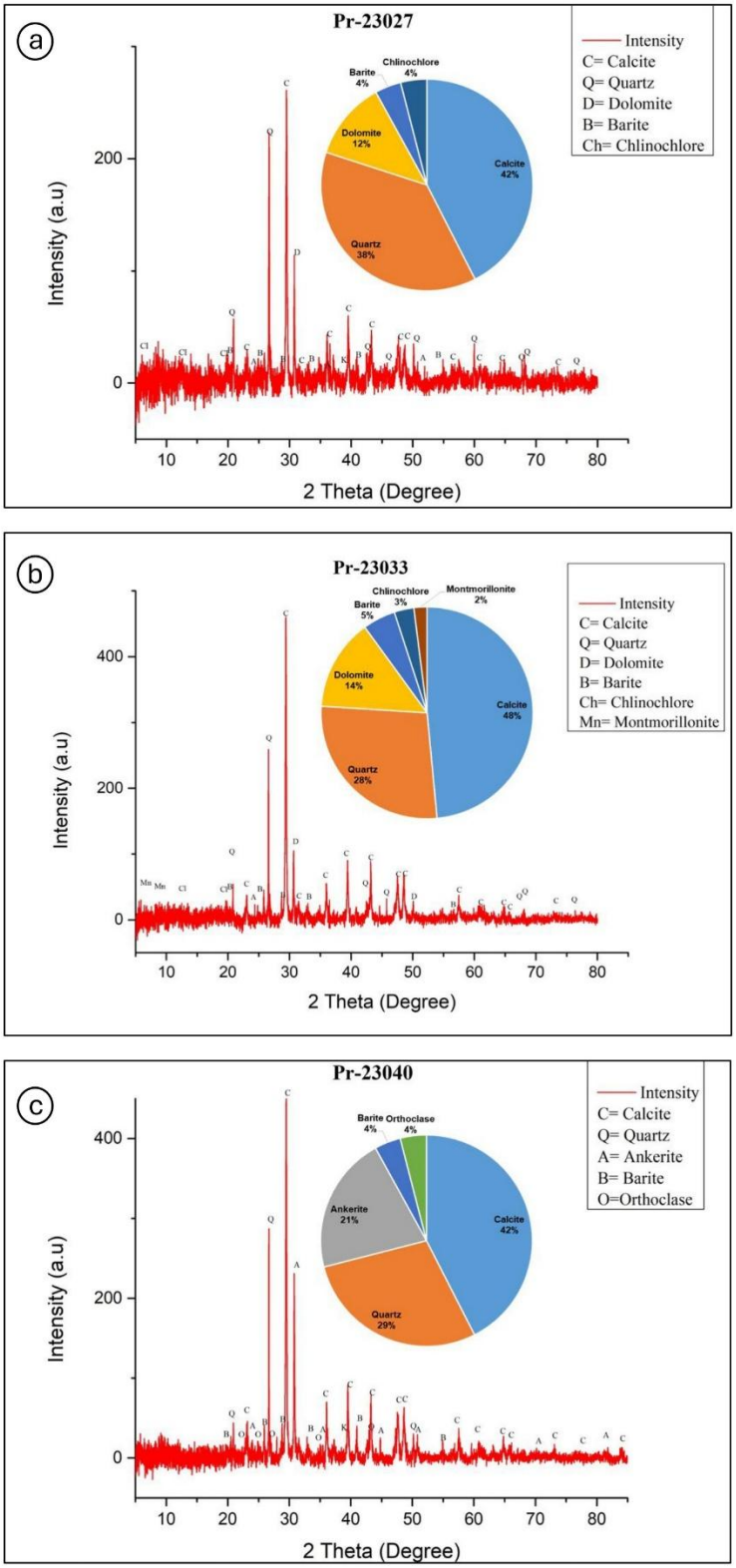


Figure 4.1 XRD diffractograms and mineral proportion pie charts for (a) Pr-23027, (b) Pr-23033 and (c) Pr-23040, Ghazij Formation, Zamzama-5.

Table 4.2 XRD mineral composition (%) of the Ghazij Formation, Zamzama-5.

Mineral	Pr-23027 (2240–2250 m)	Pr-23033 (2300–2310 m)	Pr-23040 (2370–2380 m)
Calcite	42%	48%	42%
Quartz	38%	28%	29%
Dolomite	12%	14%	—
Ankerite	—	—	21%
Barite	4%	5%	4%
Clinochlore	4%	5%	—
Orthoclase	—	—	4%

4.2.1 Carbonate mineralogy

Calcite is the dominant mineral phase at all three depths (42–48%), confirming the carbonate-dominated lithological classification established by XRF. Strong calcite diffraction peaks at approximately 29.4° 2θ are the most prominent reflections in all three diffractograms. Calcite content increases from 42% at 2250 m to 48% at 2310 m before returning to 42% at 2380 m, broadly consistent with the CaO trend in XRF.

Dolomite is identified as a secondary carbonate phase in Pr-23027 and Pr-23033 (12% and 14% respectively), representing partial dolomitization of the primary calcite matrix during burial diagenesis, a common process in carbonate sequences that modifies reservoir porosity through selective dissolution and replacement (Moore and Wade, 2013; Tucker, 2001).

The most significant carbonate mineralogy finding is the complete replacement of dolomite by ankerite (21%) in the deepest sample Pr-23040. Ankerite, $Ca(Fe,Mg,Mn)(CO_3)_2$, forms when iron progressively replaces magnesium in dolomite during burial under reducing conditions, a process termed ankeritization (Immenhauser, 2022; Moore and Wade, 2013). Its occurrence at 21% directly accounts for the elevated Fe signals (Fe 4.4–6.3%) recorded in EDS spectra of Pr-23040 and the Fe_2O_3 in bulk XRF. The dolomite-to-ankerite transition with depth indicates increasing burial diagenetic overprint and reducing pore fluid conditions at the deepest sampled interval, consistent with the anoxic depositional environment established from organic geochemical data in Section 4.4.

4.2.2 Siliciclastic and accessory phases

Quartz is the second most abundant mineral at all three depths (29–38%), with the highest proportion at the shallowest sample Pr-23027 (38%). At this depth, near-equal proportions of calcite (42%) and quartz (38%) classify the rock as a calcareous quartzose limestone rather than a pure limestone, refining the earlier XRF-based classification. With increasing depth, quartz decreases to 28–29%, consistent with the dilution trend observed in XRF where SiO_2 decreases as carbonate content increases.

Barite ($BaSO_4$) is a minor but consistent accessory phase at 4–5% across all three depths, directly confirming the elevated BaO in XRF (4.36–7.02%) and Ba signals in EDS. Its consistent presence across all depths indicates barite as a pervasive diagenetic or authigenic phase throughout the interval (Boggs, 2012; Tucker, 2001).

Clinochlore, a magnesium-aluminium chlorite, is identified at 4–5% in Pr-23027 and Pr-23033 (Deer, Howie and Zussman, 2013). Its low abundance is consistent with the

low Al_2O_3 values in XRF and confirms that clay minerals are a volumetrically minor constituent of the rock framework. Importantly, clinochlore is a non-swelling chlorite, which is significantly less damaging to permeability than swelling clays such as smectite or mixed-layer illite-smectite, a mineralogical characteristic that is generally considered more favourable for reservoir quality than swelling minerals because chlorite does not undergo hydration induced volume expansion and therefore has a lower potential to impair pore connectivity (Worden and Morad, 2003; Zhao et al., 2022). In Pr-23040, clinochlore is absent and replaced by orthoclase (K-feldspar, 4%), a detrital or authigenic feldspar consistent with K and Al signals in EDS spectra of this sample.

4.3 Organic Richness (TOC) and Source Rock Quality

Table 4.3 presents TOC values for the Ghazij Formation in Zamzama-5 and in Mehar-1.

Table 4.3(a) Total organic carbon (TOC), Zamzama-5.

Lab No.	Depth (m)	TOC (wt. %)
Pr-23027	2240–2250	3.60
Pr-23028	2250–2260	3.16
Pr-23029	2260–2270	4.34
Pr-23030	2270–2280	4.50
Pr-23031	2280–2290	5.05
Pr-23032	2290–2300	3.70
Pr-23033	2300–2310	4.66

Pr-23034	2310–2320	3.30
Pr-23035	2320–2330	3.50
Pr-23036	2330–2340	2.88
Pr-23037	2340–2350	2.71
Pr-23038	2350–2360	3.24
Pr-23039	2360–2370	3.19
Pr-23040	2370–2380	3.20

Table 4.3(b) Total Organic Carbon (TOC), Mehar-1.

Lab No.	Depth (m)	TOC (wt. %)
Pr-22826	2357–2360	0.41
Pr-22827	2369–2372	0.43
Pr-22828	2375–2378	0.45
Pr-22829	2384–2387	0.32
Pr-22830	2393–2396	0.33
Pr-22831	2402–2405	0.36
Pr-22832	2411–2414	0.34
Pr-22833	2420–2423	0.32
Pr-22834	2429–2432	0.33
Pr-22835	2432–2435	0.32

TOC in Zamzama-5 ranges from 2.71 wt.% to 5.05 wt.%, corresponding to very good to excellent source rock richness using the standard classification of Peters and Cassa (1994): <0.5% poor; 0.5–1% fair; 1–2% good; 2–4% very good; >4% excellent.

All seven sampled depths in Zamzama-5 exceed the 2% threshold for good unconventional hydrocarbons, with three depths (2270 m, 2290 m and 2310 m) exceeding

4% (excellent) (Peters and Cassa, 1994; Peters et al., 2016). In contrast, TOC in Mehar-1 over the equivalent Ghazij interval (2357–2435 m) ranges from only 0.32 wt.% to 0.45 wt.%, classifying as poor source rock quality throughout (Fig. 4.2). This represents an order-of-magnitude reduction in organic richness relative to Zamzama-5 within the same stratigraphic unit, indicating significant lateral heterogeneity in the source rock potential of the Ghazij Formation across the field.

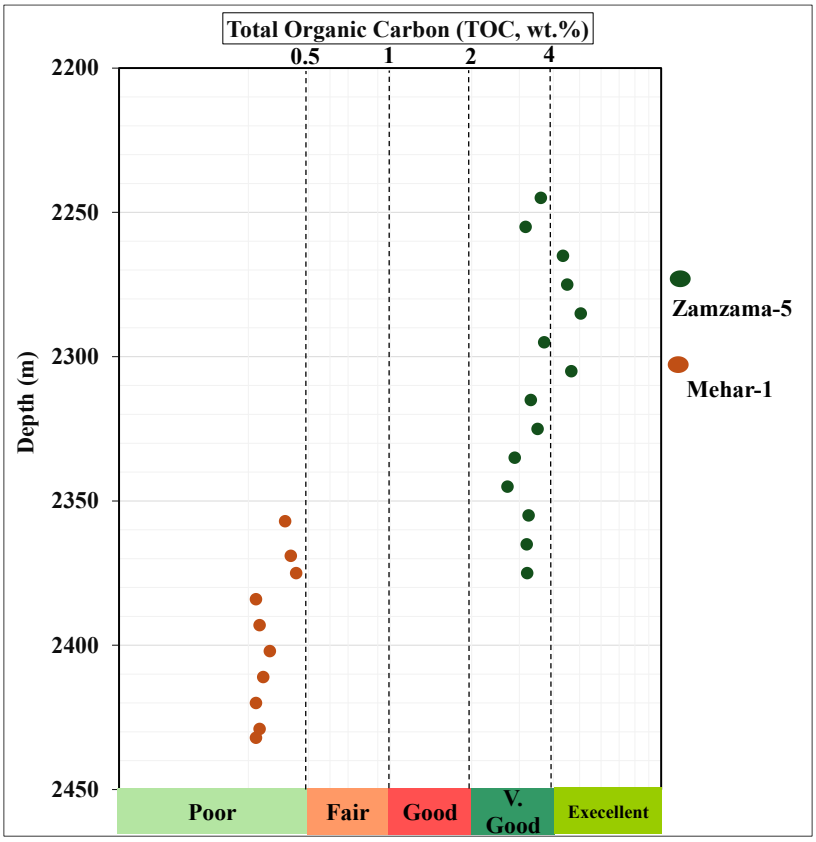


Figure 4.2 The distribution of TOC with respect to burial depth in both Zamzama-5 and Mehar-1 wells (plotted using the guidelines of Peters et al., 2005; Peters and Cassa, 1994).

In Zamzama-5, the TOC values are high enough to support the label of "bituminous limestone", since the rock shows high organic enrichment. At Mehar-1, however, the TOC values are too low to justify that same term, the more accurate description is "lean limestone", though this still assumes the rock is carbonate-dominated.

Several mechanisms may account for this lateral contrast: (i) a shift from a relatively restricted, organic matter-preserving depositional setting at Zamzama-5 to a shallower, better-oxygenated shelf or paleo-high setting at Mehar-1, where aerobic degradation of organic matter prior to and during burial would suppress TOC; (ii) dilution of the organic fraction at Mehar-1 by a higher rate of inorganic carbonate (bioclastic/skeletal) production, lowering TOC without necessarily implying lower original organic productivity; and (iii) genuinely lower primary organic productivity at Mehar-1, related to differences in water depth, distance from nutrient input, or basin configuration (Bohacs et al., 2005; Hedges and Keil, 1995; Peters and Cassa, 1994).

4.4 Kerogen Type and Hydrocarbon Generation Potential

Hydrogen Index (HI) values in Zamzama-5 range from 87.33 to 183.13 mg HC/g TOC. Applying the standard HI classification at low thermal maturity (Peters and Cassa, 1994: HI <50 Type IV; 50–200 Type III; 200–300 mixed Type II/III; 300–600 Type II; >600 Type I), all seven samples plot within the Type III (gas-prone) field, with the deepest sample (2380 m, HI = 183.13) approaching the Type II/III boundary (Figure 4.3). Table 4.4 presents the complete Rock-Eval pyrolysis dataset for Zamzama-5.

Table 4.4 Rock-Eval pyrolysis parameters, Zamzama-5 (Ghazij Formation).

Depth (m)	TOC (wt.%)	S_1 (mg/g)	S_2 (mg/g)	S_3 (mg/g)	GP (mg/g)	T_{max} (°C)	HI	OI	PI
2240–2250	3.60	0.25	3.50	0.87	3.75	438	97.22	24.17	0.07
2260–2270	4.34	0.14	3.79	0.99	3.93	436	87.33	22.81	0.04
2280–2290	5.05	0.17	5.16	1.62	5.33	433	102.18	32.08	0.03
2300–2310	4.66	0.21	4.73	3.15	4.94	431	101.50	67.60	0.04
2320–2330	3.50	0.61	5.32	1.64	5.93	432	152.00	46.86	0.10

2350–2360	3.24	0.57	4.09	1.11	4.66	430	126.23	34.26	0.12
2370–2380	3.20	1.25	5.86	1.28	7.11	428	183.13	40.00	0.18

These results are somewhat atypical given the carbonate-dominated, low-Al_2O_3 lithology established in Section 4.1, since marine carbonate source rocks more commonly host Type II (oil-prone, algal/bacterial) kerogen with HI in the 300-600 range. Possible explanations include: (i) mixing of terrigenous, higher-plant-derived organic matter into an otherwise marine carbonate depositional system, plausible if the Ghazij carbonate platform received episodic fluvial or deltaic input; (ii) partial oxidative degradation of the original marine organic matter prior to burial, which lowers HI without proportionally reducing TOC; and (iii) a degree of HI suppression by thermal maturity, since HI decreases progressively with increasing burial temperature even ahead of significant TOC loss (Espitalié et al., 1977; Peters and Cassa, 1994; Tissot and Welte, 1984).

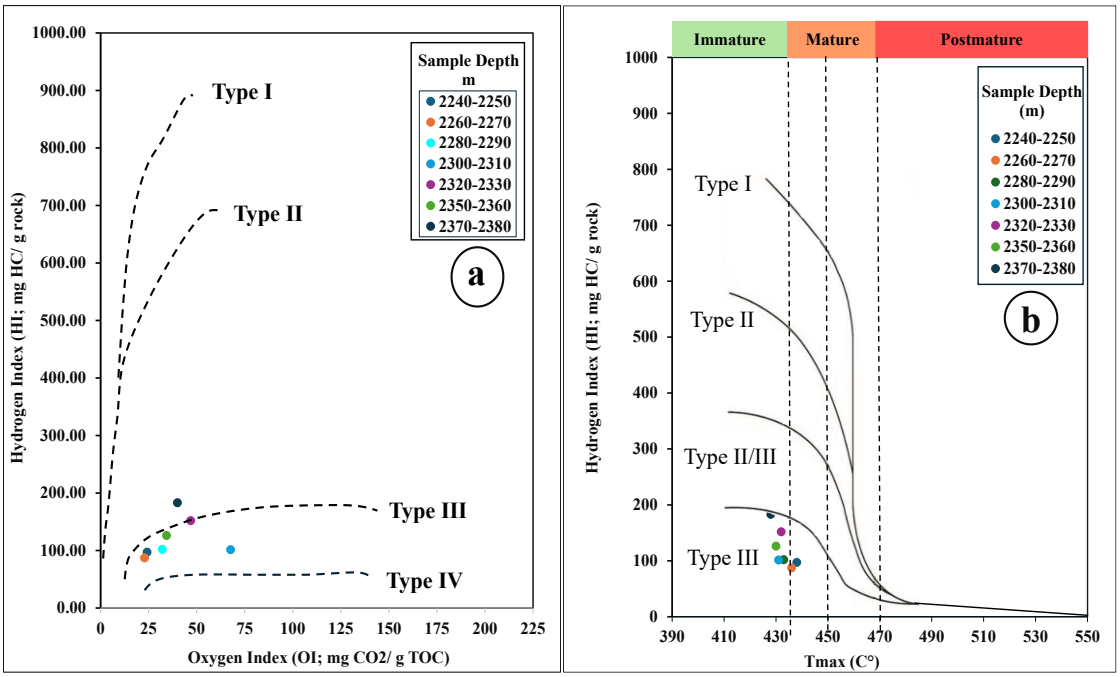


Figure 4.3 Modified Van Krevelen Diagrams of the tested Zamzama-5 Samples, (a) HI vs. OI to identify kerogen type. (b) HI vs. T_{max} to identify kerogen type and maturity (Adopted from Peters and Cassa, 1994).

Oxygen Index (OI) values are comparatively elevated (22.81–67.60 mg CO_2/g TOC), which would conventionally reinforce a Type III, oxidized organic matter interpretation. However, OI determined by Rock-Eval pyrolysis is known to be sensitive to mineral matrix effects in carbonate-rich rocks: CO_2 released during thermal decomposition of carbonate minerals within the S_3 measurement window can artificially inflate apparent OI, independent of the true oxidation state of the kerogen. Given the high and increasing CaO content with depth identified in Section 4.1, the OI values reported here should be treated with some caution as a secondary, supporting line of evidence rather than a primary kerogen-typing parameter; HI remains the more robust indicator in this lithology.

Genetic Potential (S_1+S_2) ranges from 3.75 to 7.11 mg HC/g rock, which, despite the gas-prone kerogen type, falls in the fair-to-excellent range (Peters and Cassa, 1994; Tissot and Welte, 1984) and is broadly consistent with the very good to excellent TOC values reported in Section 4.2. The Ghazij interval in Zamzama-5 can therefore be characterized as a gas-prone but volumetrically significant generative source rock.

4.5 Thermal maturity (T_{max} and production index) and its reliability

T_{max} values in Zamzama-5 decrease from 438°C at 2250 m to 428°C at 2380 m (Table 4.4). Using the standard T_{max} maturity classification (Peters and Cassa, 1994: <435°C immature; 435–445°C mature/peak oil generation; 445–470°C late mature; >470°C overmature), the uppermost two samples (2250 m, 2270 m) classify as mature, while the remaining five samples (2290–2380 m) classify as immature. This represents an

apparent reversal of the normal burial-maturation trend, in which thermal maturity is expected to increase, not decrease, with depth.

The Production Index (PI = $S_1/[S_1+S_2]$) provides an independent check on this trend, since it is a ratio of hydrocarbon species within the organic fraction itself and is comparatively insensitive to the mineral matrix effects that can bias T_{max} in carbonate-rich rocks. PI in Zamzama-5 increases from 0.03–0.07 in the upper four samples (2250–2310 m) to 0.10–0.18 in the lower three samples (2330–2380 m), the opposite trend to T_{max}, and consistent with the normally expected increase in maturity with depth. Using the standard PI classification of Peters (1986) (<0.10 immature; 0.10–0.40 oil generation zone/mature; >0.40 approaching exhaustion), the upper four samples are immature while the lower three samples have just entered the oil generation zone (Figure 4.4).

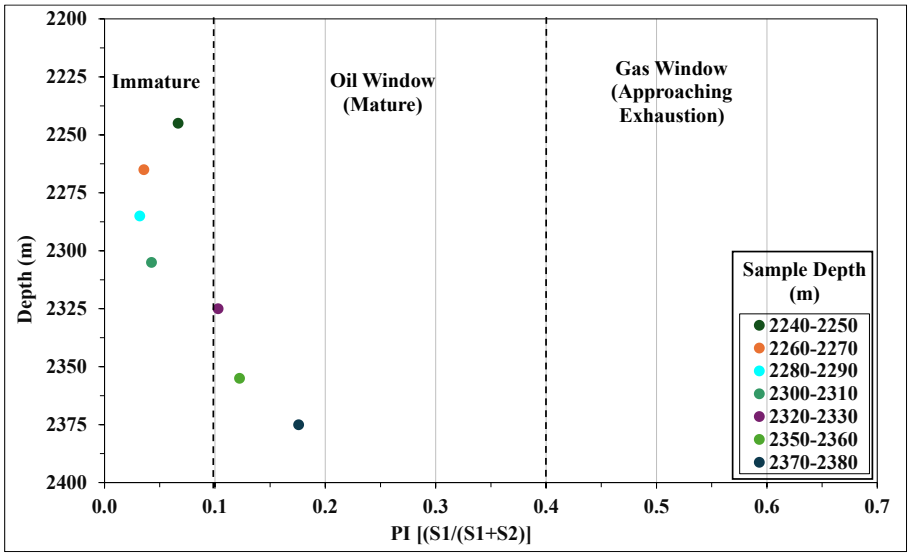


Figure 4.4 Production Index (PI) vs. depth plot showing maturation stages of the studied Zamzama-5 samples.

This discrepancy between T_{max} and PI suggests that the T_{max} values may be compromised by a mineral matrix effect rather than representing the true thermal history. This is consistent with the progressive increase in carbonate abundance and decrease in the

detrital Al_2O_3 component across the interval that was established in Section 4.1, indicating a substantial change in the mineral matrix across the sampled interval.

The reliability of T_{max} as a maturity indicator can be affected by several analytical and sample-related factors. Yang and Horsfield (2020) emphasized that T_{max} may be influenced by sample loading, mineral-matrix effects, clay minerals, oxidation, and other factors associated with Rock-Eval analysis. Such effects can produce anomalous T_{max} values that do not necessarily represent the true thermal maturity of the organic matter. In the present study, the anomalous decrease in T_{max} with depth is therefore interpreted cautiously and is not considered evidence of an actual reversal in geological maturity. Hence, the production index is considered the more reliable maturity indicator for this dataset, and the Ghazij Formation in Zamzama-5 is interpreted as immature to early mature, with maturity showing the expected increase with depth, rather than exhibiting a true maturity reversal.

An additional limitation arises from the use of drill-cuttings, which may contain caved material derived from shallower intervals during drilling. Jarvie (2015) noted that geochemical measurements from cuttings can be affected by the mixing of target-formation material with cavings from overlying organic-lean or organic-rich intervals. Such mixing may influence TOC and Rock-Eval parameters and introduce uncertainty in the assignment of geochemical values to their reported depths. In the present study, the samples were visually examined and cleaned to remove visible foreign material; however, minor downhole mixing or caving cannot be completely excluded. The T_{max} reversal is therefore interpreted cautiously in conjunction with PI and the other geochemical evidence.

4.6 Petroleum Source Rock Potential of the Ghazij Formation

Integrating the lithological, mineralogical, organic richness, kerogen type, and thermal maturity data, the Ghazij Formation in Zamzama-5 is classified as a bituminous (organic-rich) limestone: carbonate-dominated with confirmed calcareous quartzose to purer limestone mineralogy (Sections 4.1–4.2), very good to excellent TOC (Section 4.3), hosting indigenous Type III gas-prone kerogen with good-to-excellent generative potential (Section 4.4), and currently immature to early mature based on the Production Index (Section 4.5).

Table 4.5 Summary comparison of source rock characteristics, Zamzama-5 vs. Mehar-1.

Parameter	Zamzama-5	Mehar-1
Lithology	Carbonate-dominated limestone interval within shale-dominated Ghazij Formation; ranging from calcareous quartzose limestone at shallow depths to purer limestone at depth (XRF + XRD confirmed)	Mixed shale-limestone lithology based on visual cutting examination; TOC insufficient for further geochemical analysis
TOC	3.20–5.05 wt.% (very good-excellent)	0.32–0.45 wt.% (poor); below threshold for Rock-Eval analysis
Kerogen type (HI)	Type III (gas-prone, HI 87–183 mg HC/g TOC); approaching II/III boundary at base	Not determined

Thermal maturity	Immature to early mature (PI 0.03–0.18); T_{max} unreliable due to carbonate matrix effect	Not determined
Hydrocarbon origin	Indigenous (S_1 vs S_2 cross-plot)	Not determined
Overall classification	Bituminous (organic-rich) limestone; gas-prone, good-excellent generative potential	Lean (organic-poor), shale-limestone mixed lithology; poor source rock quality

The equivalent Ghazij interval in Mehar-1 records markedly lower TOC (0.32–0.45%, poor), and in the absence of XRF or Rock-Eval data for this well, is provisionally classified as a lean (organic-poor) limestone rather than the bituminous limestone seen in Zamzama-5. The cause of this lateral reduction in organic richness could be whether depositional (facies/redox change), diagenetic (dilution), or a genuine difference in primary productivity (Bohacs et al., 2005; Hedges and Keil, 1995; Peters and Cassa, 1994).

The cross-plot of HI versus TOC (Fig. 4.5 a) further confirms the gas-prone character of the Ghazij Formation at Zamzama-5, with the data clustering in a field consistent with good-to-excellent gas generation potential. The S_1 versus S_2 relationship indicates that the hydrocarbons present are indigenous to the source rock, ruling out contamination or migrated hydrocarbons (Fig. 4.5 b). Given that TOC values consistently exceed the 2% threshold, the Ghazij Formation at Zamzama-5 also qualifies as a favourable target for unconventional hydrocarbon exploration (Peters et al., 2016). Hence, these results indicate that the Ghazij Formation possesses significant petroleum source rock potential in at least part of the study area, as represented by Zamzama-5, but that this potential is not uniform across the field. The formation should therefore be regarded as a laterally variable, gas-prone carbonate source rock, with Zamzama-5 representing a more favourable interval and Mehar-1 representing a comparatively leaner equivalent.

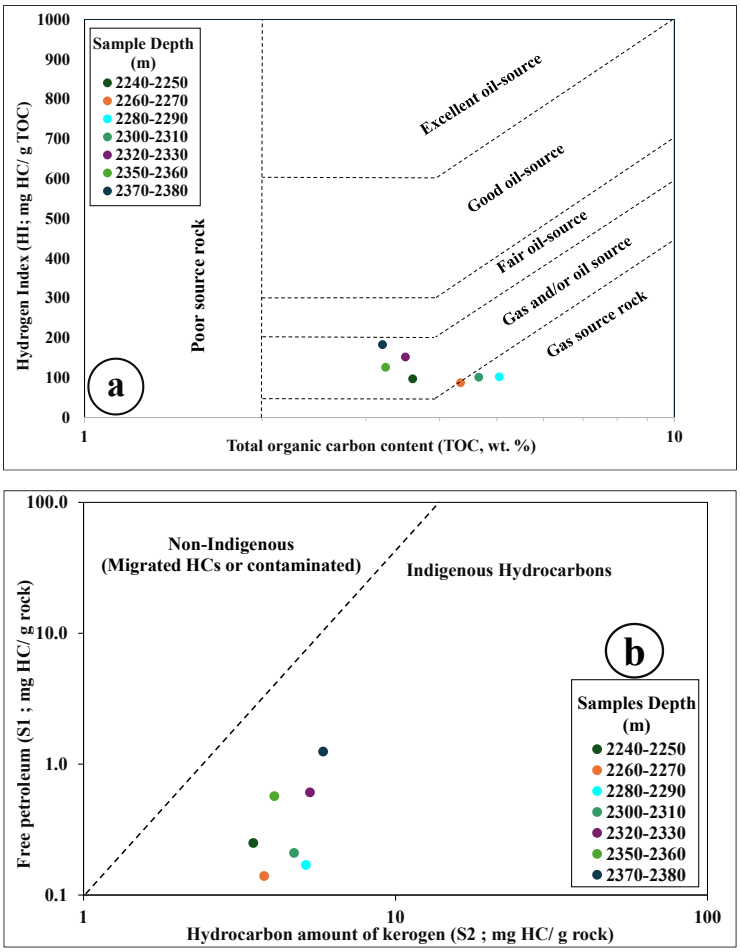


Figure 4.5 (a) Cross plot of HI vs. TOC suggests good to excellent gas generation potential, (b) S1 vs. S2 plot shows indigenous samples for Zamzama-5.

4.7 SEM-EDS Petrographic Characterization of the Ghazij Formation

Scanning Electron Microscopy coupled with Energy Dispersive X-ray Spectroscopy (SEM-EDS) was carried out on the same three samples used for XRF analysis (Pr-23027, Pr-23033 and Pr-23040), allowing micro-scale mineral identification

and pore fabric characterization to be directly correlated with bulk geochemical data. Secondary electron (SE) imaging documented pore types, matrix fabric, and diagenetic features across magnifications ranging from 750X to 3.67K, while EDS spot analyses provided elemental compositions at targeted mineral phases and grain boundaries.

4.7.1 Micro-scale mineral identification by EDS

EDS spot analyses confirmed the mineralogical framework established by XRF at the individual grain scale, while additionally resolving the specific mineral phases responsible for bulk elemental signals.

In Pr-23027 (2240–2250 m), three distinct mineral phases were identified across the analyzed spots. Spectrum 8 returned a calcite-dominated composition (Ca 38.7%, O 36.3%) with subordinate Si (11.9%), Al (4.8%), K (1.0%) and Mg (2.1%), indicating calcite as the primary phase with admixed illitic clay. Spectrum 9 yielded Si (43.8%) and O (52.0%) with negligible Ca and Al, identifying a pure detrital quartz grain, consistent with the SiO_2 (22.8%) recorded in bulk XRF. Spectrum 10 returned a mixed quartz-calcite composition with a notable Ba contribution (2.0%), confirming barite ($BaSO_4$) as an accessory diagenetic phase and directly accounting for the elevated BaO trend observed across XRF samples (Fig. 4.6) (Goldstein et al., 2018; Deer et al., 2013).

In Pr-23033 (2300–2310 m), Spectrum 7 yielded the purest calcite composition across the entire dataset (Ca 55.4%, O 32.3%), with only trace Si and Al, consistent with a clean microspar or bioclastic calcite grain. Spectrum 8 returned a clay-dominated composition with no Ca contribution (Si 24.0%, Al 16.3%, K 8.3%, O 45.6%, Fe 4.6%, Mg 1.2%), identifying illite as the specific clay mineral responsible for the Al_2O_3 signal in XRF (Moore and Reynolds, 1997; Goldstein et al., 2018). The high K content in particular is distinguishing illite from kaolinite or smectite in this sample. Spectrum 9 at the calcite-

clay interface recorded elevated Fe (7.8%), interpreted as pyrite or iron-rich clay, consistent with the anoxic, organic-preserving depositional conditions proposed in Section 4.2 and the elevated Fe_2O_3 in XRF (Fig. 4.7) (Berner, 1984; Goldstein et al., 2018).

In Pr-23040 (2370–2380 m), all three EDS spectra returned Si-Al-K-dominated compositions (Al 9.5–16.3%, K 1.8–8.3%) with subordinate Ca (1.3–7.2%), indicating clay-rich micro-zones despite this sample recording the highest bulk CaO (69.93%) in XRF. This apparent contradiction reflects micro-scale heterogeneity (Goldstein et al., 2018; Reed, 2005): the EDS beam sampled clay-rich pore-lining films and inter-grain clay coatings that are volumetrically minor but spatially concentrated, while XRF integrates the carbonate-dominant bulk matrix. The presence of Na (0.6%) alongside K-Al-Si in Spectra 8 and 10 suggests a minor smectite component within the clay assemblage (Moore and Reynolds, 1997), and Ti (0.5–0.8%) in Spectra 9 and 10 identifies detrital rutile or anatase (Deer et al., 2013), consistent with TiO_2 (0.576%) in XRF for this sample (Fig. 4.8).

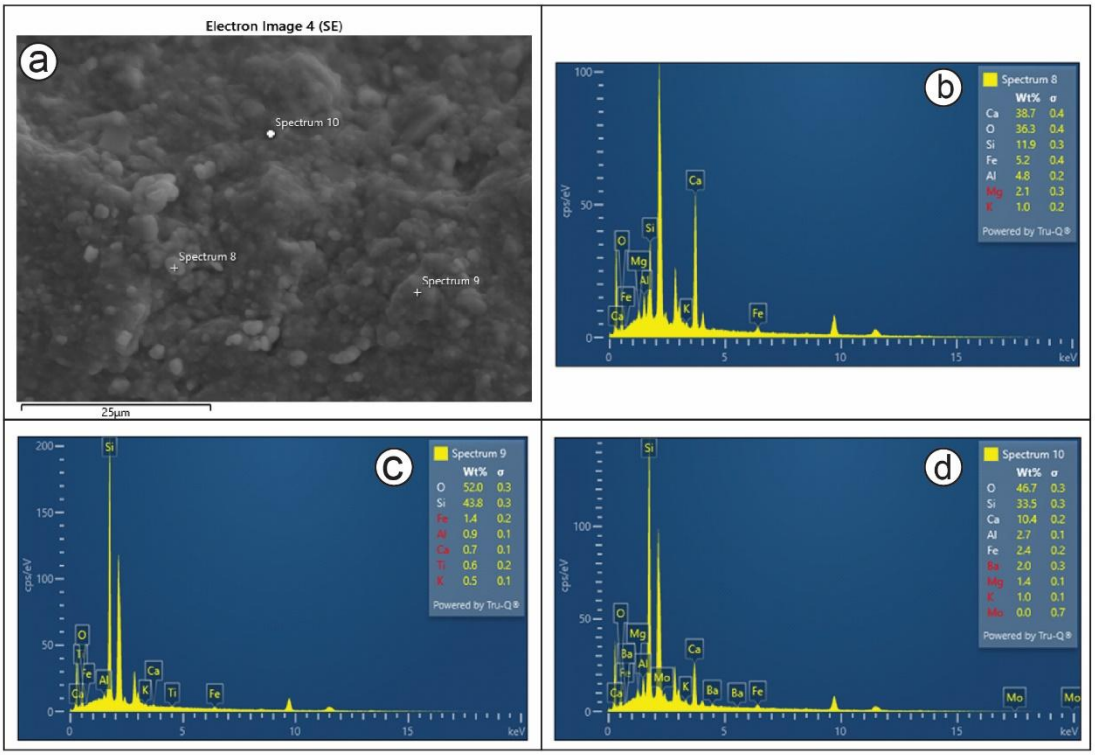


Figure 4.6 SEM-EDS analysis of Pr-23027 (2240–2250 m), Ghazij Formation, Zamzama-

5. (a) Secondary electron image at 25µm scale showing EDS spot locations. (b) Spectrum 8: calcite-dominated matrix with minor illite clay. (c) Spectrum 9: pure detrital quartz grain (Si 43.8%, O 52.0%). (d) Spectrum 10: mixed quartz-calcite zone with barite (Ba 2.0%) as an accessory diagenetic phase.

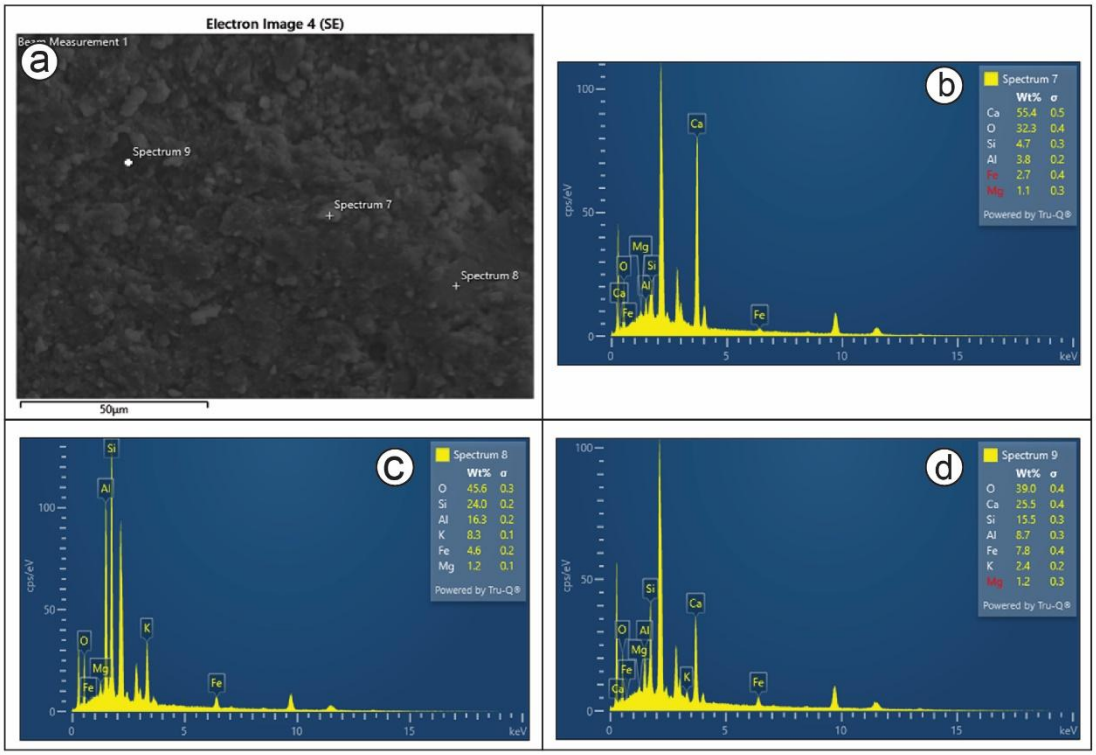


Figure 4.7 SEM-EDS analysis of Pr-23033 (2300–2310 m), Ghazij Formation, Zamzama-5. (a) Secondary electron image at 50µm scale showing EDS spot locations. (b) Spectrum 7: purest calcite composition in the dataset (Ca 55.4%). (c) Spectrum 8: illite clay phase (Al 16.3%, K 8.3%) with no carbonate contribution. (d) Spectrum 9: calcite-clay interface with elevated Fe (7.8%) interpreted as pyrite.

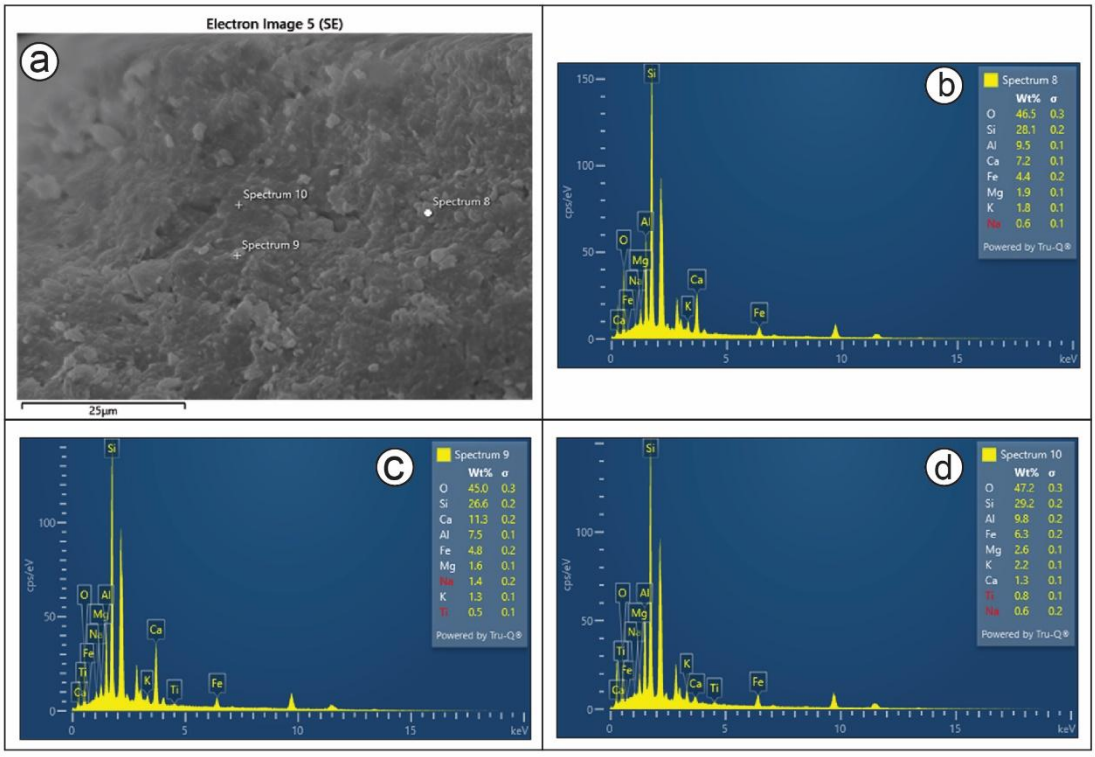


Figure 4.8 SEM-EDS analysis of Pr-23040 (2370–2380 m), Ghazij Formation, Zamzama-5. (a) Secondary electron image at 25µm scale showing EDS spot locations. (b) Spectrum 8: illite clay with minor calcite (Al 9.5%, K 1.8%, Ca 7.2%) and trace smectite indicated by Na (0.6%). (c) Spectrum 9: mixed illite-calcite zone with detrital rutile indicated by Ti (0.5%). (d) Spectrum 10: most clay-rich composition in the dataset (Al 9.8%, Fe 6.3%) with near-absent Ca (1.3%), representing pore-lining illite-smectite films.

4.7.2 Matrix fabric and organic matter distribution

SEM imaging of Pr-23027 at low-to-intermediate magnification (1.05K–1.44K, 10μm scale) reveals a dense micritic carbonate matrix with a granular to sub-rounded grain fabric and no preferred orientation (Figure 4.9 a), consistent with a low-energy carbonate mudstone to wackestone depositional texture (Dunham, 1962; Tucker and Wright, 1990). At higher magnification (3.67K, 1μm scale), a distinctive wavy to undulating surface texture is observed draped continuously across the carbonate matrix, interpreted as organic matter films or organic-mineral composite coatings based on their morphology and their spatial association with the carbonate matrix. This organic matter occurs as a surface coating along carbonate grain boundaries rather than as discrete pore-filling patches, consistent with localized organic-matter accumulation or coating along mineral surfaces, which could suggest adsorption onto carbonate grain surfaces during early diagenesis (Loucks et al., 2009; Bernard et al., 2012). A similar organic coating texture is observed in Pr-23033 at 1–2 μm scale (Figure 4.9 b), where wavy organic films are accompanied by brighter sub-micrometre patches interpreted as pyrite framboids, consistent with the elevated Fe_2O_3 and reducing/anoxic depositional conditions established in Section 4.2. The associated nanopores represent potential sites for gas sorption, whereas inorganic pores and natural fractures provide potential pore volume and transport pathways for free gas. However, SEM-EDS observations alone cannot directly distinguish or quantify free and sorbed gas; such differentiation requires independent gas-sorption and pore-characterization measurements. Therefore, the SEM results are interpreted as evidence of potential gas-storage domains and transport pathways rather than direct confirmation of the gas-storage state.

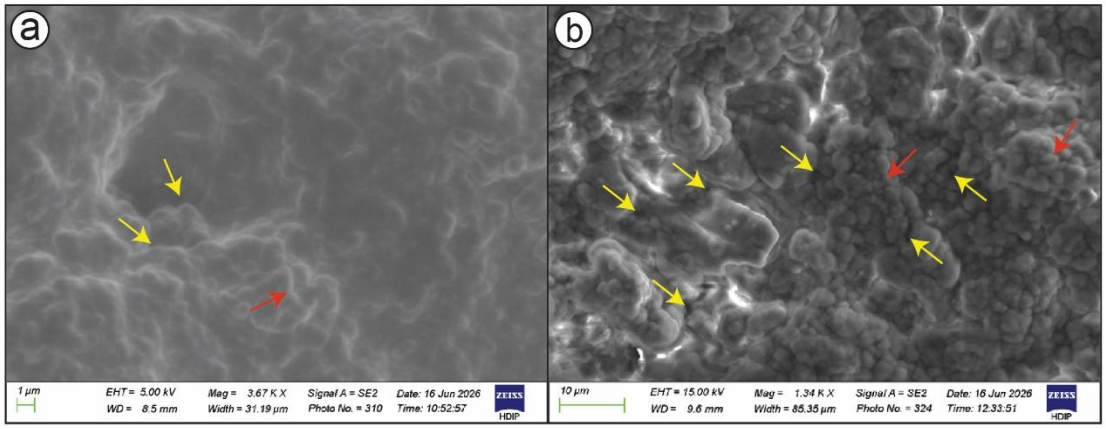


Figure 4.9 Organic matter distribution and associated porosity, Ghazij limestone, Zamzama-5. (a) Pr-23027 (2240–2250 m): wavy organic matter films coating carbonate grain surfaces (red arrow) with nano-scale pores developed within the organic matter (yellow arrows), representing potential sites for gas storage. (b) Pr-23033 (2300–2310 m): yellow arrows indicate organic matter-hosted and intercrystalline pores; red arrows indicate pyrite framboids within organic coating, consistent with reducing/anoxic depositional conditions.

4.7.3 Pore types

Five distinct pore types were identified across the three samples, constituting a multi-scale pore network spanning nanometre to micrometre dimensions. Micron-scale interparticle microporosity is the dominant pore type at shallow depth. In Pr-23027, pores between rounded micrite and calcite grains are clearly resolved at 2 µm scale (Mag 2.80K), with estimated pore dimensions of 1–5 µm. This pore type represents the primary matrix

storage porosity of the Ghazij limestone at this depth and is the most volumetrically significant pore type in the dataset (Fig. 4.10).

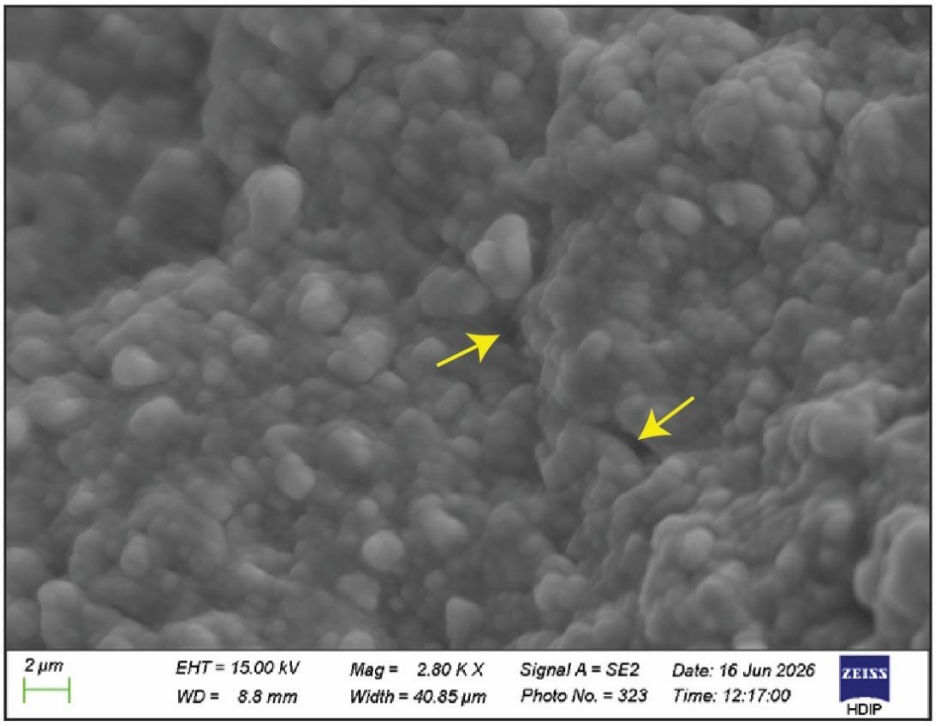


Figure 4.10 Micron-scale interparticle microporosity, Pr-23027 (2240–2250 m), Ghazij limestone, Zamzama-5. Rounded micrite grains at 2 µm scale with interparticle pores visible between grain boundaries (arrows), representing the primary matrix storage porosity at this depth.

Nano-scale interparticle porosity is most clearly developed in Pr-23033 at 1 µm magnification (Mag 3.56K), where pores between micrite grains are sub-micrometre in dimension (Fig. 4.11). Compared to Pr-23027, visible pore size has decreased, consistent with progressive compaction or carbonate cementation with increasing burial depth. While nano-scale pores contribute minimally to permeability independently, they represent significant gas storage capacity in tight carbonate unconventional systems.

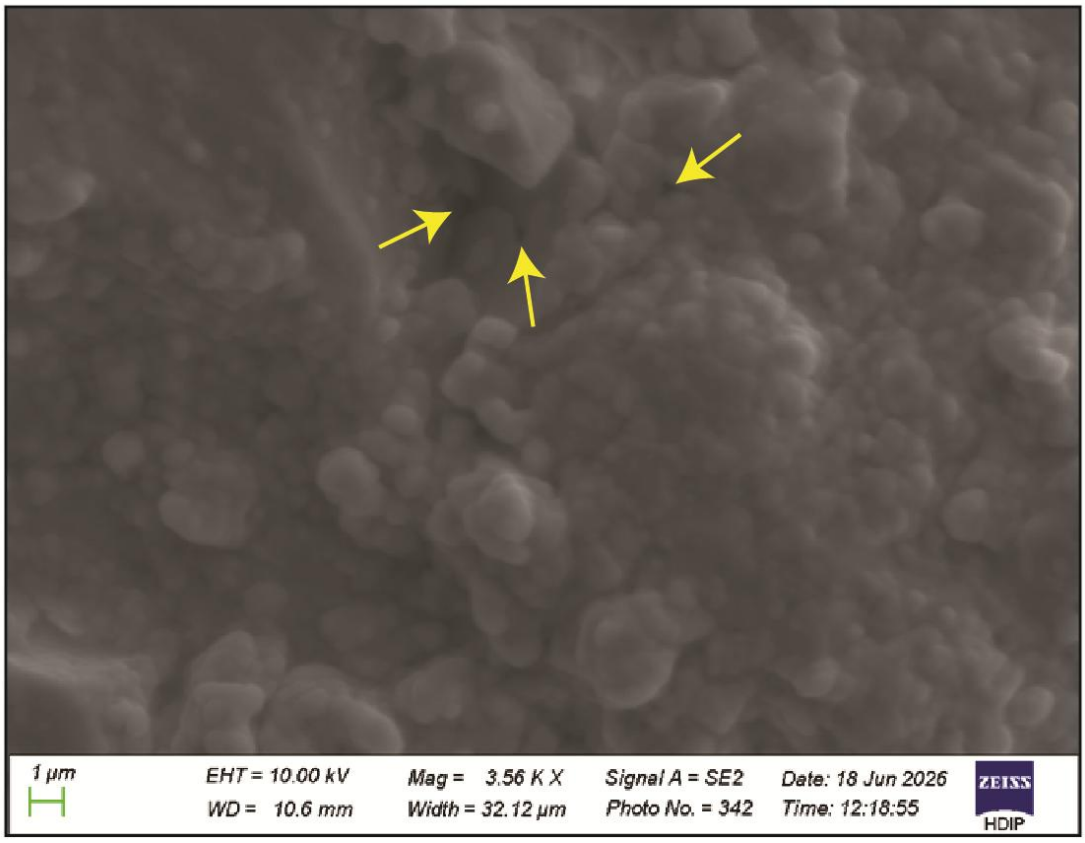


Figure 4.11 Nano-scale interparticle porosity, Pr-23033 (2300–2310 m), Ghazij limestone, Zamzama-5. Sub-micrometre pores between micrite grains at 1 µm scale (arrows), indicating progressive pore size reduction with depth due to compaction and carbonate cementation.

Organic matter-hosted porosity is observed within the wavy organic matter films identified in Pr-23027 and Pr-23033 (Fig. 4.9 a & b). Nano-scale pores developed within organic matter coatings contribute to both free gas storage within pore volume and adsorbed gas retention on organic surfaces, a dual storage mechanism directly analogous to organic-hosted porosity documented in unconventional tight carbonate and shale reservoirs globally.

Intercrystalline porosity is identified in Pr-23033 at 2µm scale (Mag 2.55K) between interlocking crystalline carbonate patches, representing a secondary storage pore type subordinate to interparticle porosity but contributing to overall pore network connectivity (Fig. 4.12).

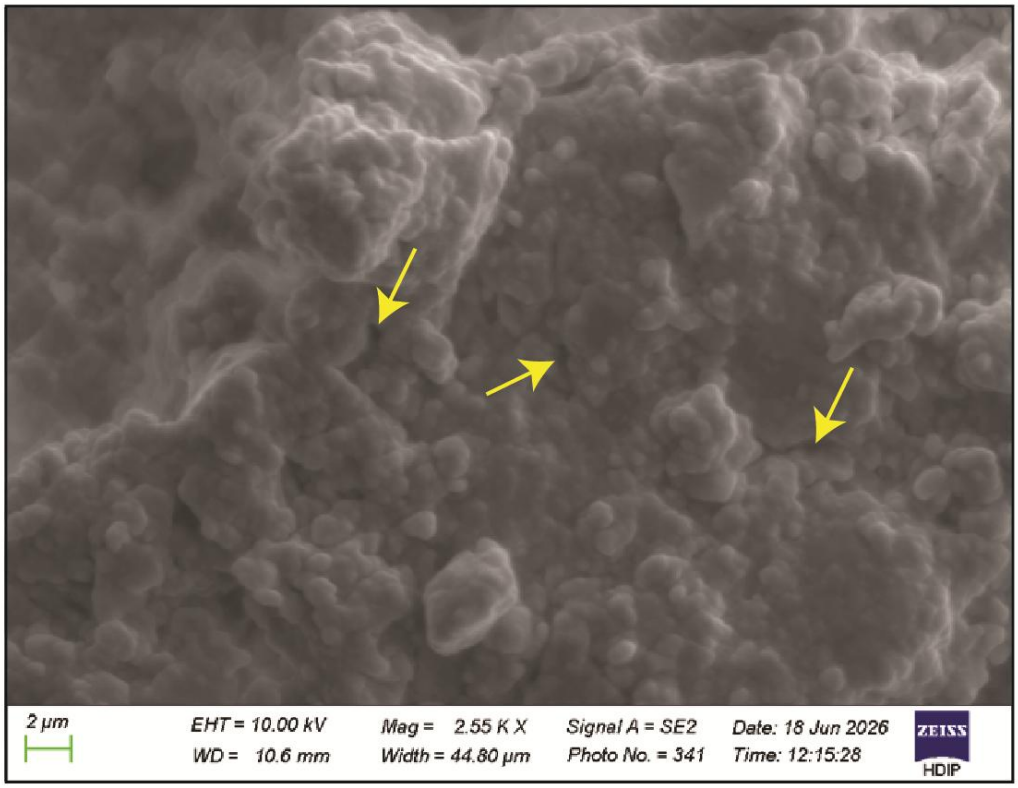


Figure 4.12 Intercrystalline porosity, Pr-23033 (2300–2310 m), Ghazij limestone, Zamzama-5. Pores developed between interlocking crystalline carbonate patches at 2 µm scale (arrows), representing a secondary storage pore type contributing to overall pore network connectivity at this depth.

Microfracture porosity is uniquely and clearly developed in the deepest sample Pr-23040 (2370–2380m), where a well-defined microfracture cuts diagonally across the matrix at 10µm scale (Mag 783X and 663X) (Following Figure 4.13). Granular debris and

partial clay or calcite infill along fracture walls is consistent with a natural fracture rather than an obvious sample-preparation artifact. A secondary minor fracture feature is additionally visible in the same sample at 10µm (Mag 1.79K). The development of microfractures at this depth, coinciding with reduced visible matrix porosity relative to shallower samples, identifies natural fractures as a potential high-permeability pathway in the deepest part of the analysed interval.

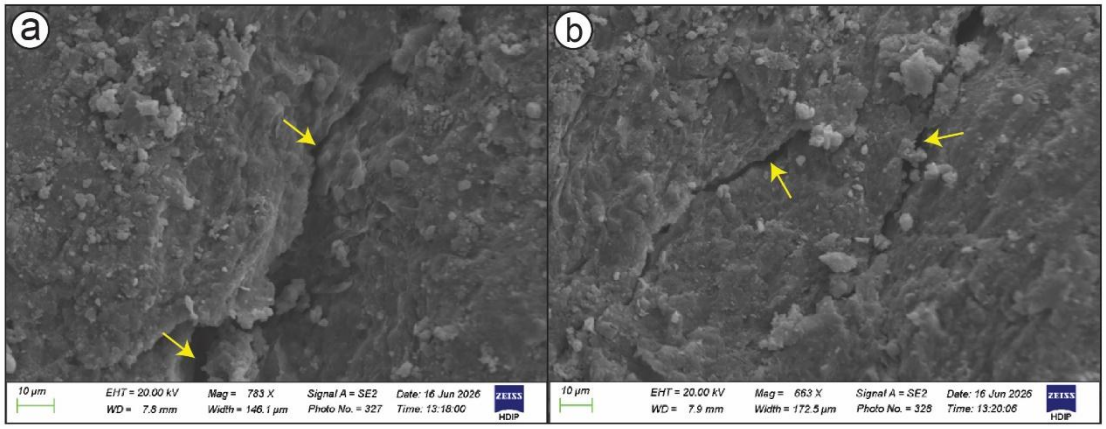


Figure 4.13 Microfracture porosity, Pr-23040 (2370–2380 m), Ghazij limestone, Zamzama-5. (a) Open microfracture cutting diagonally across the matrix at 10 µm scale (Mag 783X) (arrows). (b) Continuation of fracture network with partial calcite or clay diagenetic infill along fracture walls (arrows), confirming natural fracture origin and representing a potential permeability pathway at this depth.

4.7.4 Depth-related evolution of the pore system

Integrating SEM observations across the three samples reveals pore type variations with depth that are consistent with progressive changes in pore architecture, as summarized in table 4.6. Pore types were classified primarily according to their spatial relationship to mineral grains and organic matter, following the descriptive framework of Loucks et al. (2012), with carbonate-specific terminology for intercrystalline and fracture porosity following Choquette and Pray (1970). Accordingly, interparticle pores occur between mineral grains, organic-matter-hosted pores occur within or along organic matter domains, intercrystalline pores occur between adjacent mineral crystals, and fracture pores occur along discrete microfractures, pore size descriptors are used independently to describe the observed scale of the pore features.

Table: 4.6 Depth-related pore system evolution, Ghazij limestone, Zamzama-5.

Depth	Sample	Dominant Pore Type	Secondary Pore Type
2240–2250 m	Pr-23027	Micron-scale interparticle pores (1-5 μm)	Organic-matter-hosted nano-pores
2300–2310 m	Pr-23033	Nano-scale interparticle pores (<1 μm)	Intercrystalline and organic matter hosted pores
2370–2380 m	Pr-23040	Microfractures (>10 μm)	Minor interparticle pores

At the shallowest sampled interval, the observed pore system is dominated by relatively well developed interparticle pores, which may provide matrix storage space and potential fluid pathways (Fig. 4.14 a). At the intermediate interval, the observed interparticle pores occur predominantly at smaller scales, accompanied by intercrystalline and organic-matter-hosted pores (Fig. 4.14 b). At the deepest sampled interval, the

observed matrix pores are less prominent, whereas natural microfractures are more conspicuous and represent potential high permeability pathways (Fig. 4.14 c). These observations are consistent with progressive modification of the pore architecture by compaction and carbonate cementation with burial, although the limited number of SEM samples does not permit a definitive depth-dependent trend to be established. The observed combination of matrix pores and natural microfractures provides a petrographical basis for considering both storage and flow pathways in the evaluated carbonate interval.

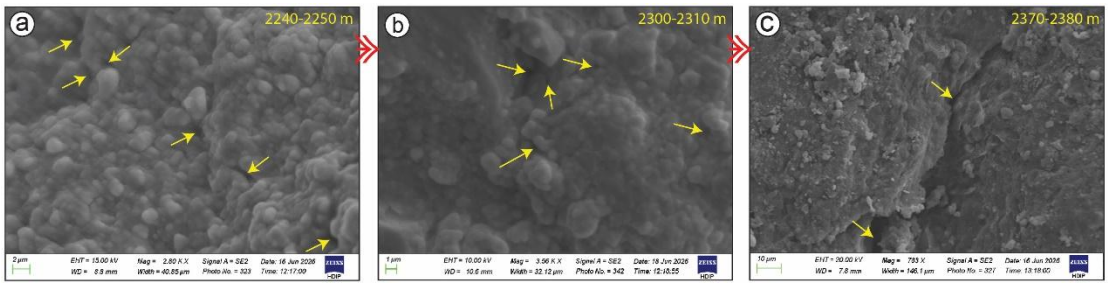


Figure 4.14 Depth-related evolution of pore types, Ghazij limestone, Zamzama-5. (a) Pr-23027 (2240–2250 m): micron-scale interparticle pores at approximately 2 µm scale (arrows). (b) Pr-23033 (2300–2310): nano- to submicron-scale interparticle pores at 1 µm scale (arrows), accompanied by organic-matter-hosted and intercrystalline pores. (c) Pr-23040 (2370–2380): natural, microfracture at 10 µm scale (arrows), representing a potential high-permeability pathway through the tight carbonate matrix.

4.8 Cross-validation of XRF, XRD and SEM-EDS

The three analytical methods applied to Zamzama-5, XRF, XRD and SEM-EDS, are independent techniques operating at different scales (bulk, mineral phase, and grain-scale respectively), and their convergence provides strong internal validation of the mineralogical framework established in this study. Table 4.7 summarizes the cross-validation of mineral phase identification across all three methods.

Table 4.7 Cross-validation of mineral phases across XRF, XRD and SEM-EDS, Ghazij Formation, Zamzama-5.

Mineral/Phase	XRF Signal	XRD Confirmation	SEM-EDS Evidence
Calcite (dominant)	High CaO (43–70%)	42–48% calcite confirmed	Ca-dominated EDS spectra; purest calcite in Pr-23033 (Ca 55.4%)
Quartz	High SiO_2 (9–23%)	28–38% quartz confirmed	Pure quartz grain identified (Si 43.8%, O 52.0%) in Pr-23027
Barite	Elevated BaO (4.36–7.02%)	4–5% barite confirmed	Ba (2.0%) detected in EDS Spectrum 10, Pr-23027
Clay minerals	Low Al_2O_3 (2–5%)	Clinochlore 4–5% (Pr-23027, Pr-23033)	Clay-rich pore-lining films detected at grain scale; K-Al-Si dominant EDS signal
Ankerite/Fe phases	Elevated Fe_2O_3 (4.8–14.4%)	Ankerite 21% in Pr-23040	Elevated Fe (4.4–6.3%) in EDS spectra of Pr-23040;

			resolved as Fe-carbonate by XRD
Dolomite	MgO present (0.8–1.5%)	12–14% dolomite (Pr-23027, Pr-23033)	Mg detected in EDS spectra; not resolved independently

The dominant calcite phase confirmed by XRD (42–48%) is directly reflected in high CaO values in XRF (43–70%) and Ca-dominated EDS spectra across all samples, with the purest calcite spot analysis recorded in Pr-23033 (Ca 55.4%), consistent with the highest XRD calcite proportion (48%) at this depth. Quartz confirmed by XRD (28–38%) accounts for the SiO_2 signal in XRF and is directly visualised as a discrete pure quartz grain in EDS Spectrum 9 of Pr-23027 (Si 43.8%, O 52.0%). Barite confirmed at 4–5% by XRD accounts for the elevated BaO trend in XRF across all three depths and is directly detected as Ba (2.0%) in EDS Spectrum 10 of Pr-23027.

The most important refinement that XRD provides over EDS is the definitive identification of clinochlore rather than illite as the clay phase. XRD is the authoritative method for clay mineral discrimination and confirms clinochlore as the correct identification; the K-Al-Si EDS signal previously interpreted as possibly illitic is consistent with clinochlore chemistry. This distinction has direct reservoir implications, since clinochlore is a non-swelling chlorite that does not impair permeability through hydration, in contrast to swelling clay minerals such as smectite or illite-smectite.

The most significant resolution that XRD provides over XRF alone is the identification of ankerite (21%) in Pr-23040, which directly explains the elevated Fe_2O_3 in XRF (4.78%) and Fe-dominated EDS signals (Fe 4.4–6.3%) in this sample that could not be attributed definitively to pyrite or clay from elemental data alone. This demonstrates the critical value of XRD as a complement to XRF for distinguishing between Fe-bearing mineral phases that yield identical or similar bulk elemental signals. Together, the three

methods provide a mutually consistent and fully validated mineralogical characterization of the Ghazij limestone at Zamzama-5.

4.9 Unconventional Hydrocarbon Reservoir Potential of the Ghazij Formation

The unconventional reservoir potential of the Ghazij Formation at Zamzama-5 is evaluated here by integrating all analytical results from Sections (4.1–4.8), lithology, mineralogy, organic geochemistry, thermal maturity, and petrographic pore characterization, against internationally recognized criteria for tight carbonate unconventional plays. An unconventional carbonate reservoir is defined here as a self-sourcing or tight formation where hydrocarbons are generated and retained within the same rock unit, requiring either natural fracture networks or hydraulic stimulation for economic production rather than buoyancy-driven migration into a separate structural trap (Jarvie, 2012; Schmoker, 2002; Law and Curtis, 2002).

4.9.1 Organic richness criterion

The fundamental prerequisite for an unconventional self-sourcing system is that the formation must be an active or capable source rock. TOC values of 3.20–5.05 wt.% throughout the Zamzama-5 interval comfortably exceed the 2% threshold widely adopted as the minimum for unconventional carbonate reservoir consideration (Jarvie, 2012; Peters

and Cassa, 1994; Peters et al., 2016; Hackley and Cardott, 2016). The S_1 versus S_2 cross-plot supports an indigenous origin for the hydrocarbons in the formation. Genetic Potential (S_1+S_2) values of 3.75–7.11 mg HC/g rock indicate fair-to-good generative capacity even at the current immature-to-early-mature thermal stage, meaning the formation may have greater generation potential if sufficient thermal maturity is attained. The type III kerogen confirmed from HI values (87.33–183.13 mg HC/g TOC) indicates gas-prone character, consistent with a gas-prone unconventional play with potential for thermogenic gas generation as thermal maturity increases.

4.9.2 Mineralogical criterion: brittleness index

A critical parameter distinguishing producible from non-producible unconventional reservoirs is rock brittleness, the capacity to fracture and maintain open fractures during hydraulic stimulation rather than deforming plastically. Brittleness in carbonate-rich unconventional rocks is influenced strongly by mineralogical composition, with quartz and carbonate minerals generally contributing to the brittle framework, whereas clay-rich compositions tend to promote more ductile behaviour. Two mineralogy-based brittleness indices were calculated from the XRD data: the original Jarvie et al. (2007) index developed for siliceous shale systems, and a modified mineralogical index adopted to the carbonate-rich mineral assemblage of the Ghazij Formation.

The Jarvie et al. (2007) Brittleness Index (BI_1) is defined as:

$$BI_1 = \text{Quartz} / (\text{Quartz} + \text{Calcite} + \text{Dolomite/Ankerite} + \text{Clay}) \times 100$$

This formula treats quartz as the sole brittle mineral, which is appropriate for siliceous shale systems but underestimates brittleness in carbonate-dominated rocks where

calcite and dolomite are also mechanically brittle. Applying this formula to the Ghazij limestone at Zamzama-5 yields BI_1 values of 39.6% (Pr-23027), 29.5% (Pr-23033) and 30.2% (Pr-23040). While these values fall in the moderate brittleness range and are lower than typical high-quartz shale plays, they should be regarded as conservative minimum estimates for this lithology given the formula's shale-specific derivation.

A modified mineralogical Brittleness Index (BI_2) was adopted to better account for the carbonate-rich mineral assemblage and the presence of feldspar in the studied samples. The previous version of this index was attributed to Wang and Gale (2009); however, the formulation used here has been revised and is based primarily on the mineralogical brittleness framework of Xu and Sonnenberg (2016), which includes quartz, carbonate minerals, and feldspar within the brittle fraction, while clay and TOC are included in the denominator. Jin et al. (2015) similarly considered feldspar and carbonate minerals as brittle components. The modified formulation used in this study is:

$$BI_2 = (\text{Quartz} + \text{Calcite} + \text{Dolomite/Ankerite} + \text{Feldspar}) / (\text{Quartz} + \text{Calcite} + \text{Dolomite/Ankerite} + \text{Feldspar} + \text{Clay} + \text{TOC}) \times 100$$

Accordingly, quartz, calcite, dolomite/ankerite, and feldspar are treated as brittle components, whereas clay minerals and TOC are included as non-brittle components. For Pr-23040, the 4% orthoclase identified by XRD is therefore included in the brittle fraction rather than being classified as clay. Applying the modified formulation yields BI_2 values of 92.4% (Pr-23027), 90.3% (Pr-23033), and 96.8% (Pr-23040) (Table 4.8). These high values reflect the dominance of quartz and carbonate minerals and the relatively low clay content of the analysed samples. These values indicate a highly brittle mineralogical framework throughout the sampled interval.

Table 4.8 Brittleness index calculations, Ghazij Formation, Zamzama-5.

Sample	Quartz (%)	Calcite (%)	Dol/Ank (%)	Fsp (%)	Clay (%)	TOC	BI_1 (%) Jarvie	BI_2 (%) (modified)
Pr-23027 (2240–2250 m)	38	42	12	0	4	3.60	39.6	92.4
Pr-23033 (2300–2310 m)	28	48	14	0	5	4.66	29.5	90.3
Pr-23040 (2370–2380 m)	29	42	21	4	0	3.20	30.2	96.8

It is important to acknowledge the limitations of both indices when applied to this lithology. The Jarvie et al. (2007) formula was specifically calibrated for the Barnett Shale, a siliceous mudrock, and underestimates true brittleness in carbonate systems by excluding calcite and dolomite/ankerite from the brittle fraction. Conversely, the modified BI_2 formula incorporates carbonate and feldspar minerals and is therefore more representative of the mineralogical composition of the studied Ghazij limestone. However, both indices remain mineralogical proxies rather than direct measurements of mechanical brittleness, and their values should be interpreted as indicative rather than definitive measures of fracture behaviour: BI_1 provides a more conservative mineralogical brittleness indication, whereas the modified BI_2 gives a higher mineralogical brittleness indication by incorporating carbonate and feldspar as brittle components.

Importantly, the natural microfractures documented by SEM in Pr-23040 (Section 4.7.3) provide complementary petrographic evidence of rock brittleness and fracture development that does not rely on mineralogical proxy formulae. The development of natural fractures in this interval confirms that the rock has already undergone brittle failure

under in-situ stress conditions, which is stronger direct evidence of brittleness than either index formula can provide. However, SEM observations alone cannot establish the timing or the in-situ stress conditions under which the fractures formed.

4.9.3 Pore fabric criterion: multi-scale pore network

Section 4.7 established that the Ghazij limestone hosts a multi-scale pore network comprising micron-scale interparticle microporosity, nano-scale interparticle porosity, organic matter-hosted nano-porosity, intercrystalline porosity, and natural microfractures. This pore architecture satisfies the dual requirement of unconventional tight carbonate reservoirs: sufficient matrix storage capacity combined with potential permeability pathways capable of sustaining economic flow rates.

The organic matter-hosted nano-porosity identified in Pr-23027 and Pr-23033 is particularly significant. In unconventional systems, the organic matter-hosted nanopores represent potential sites for gas sorption, whereas the observed inorganic pores and natural fractures provide potential pore volume and transport pathways for free gas. However, SEM observations alone cannot directly distinguish or quantify free and sorbed gas. The combined geochemical and petrographic observations are consistent with the coexistence of organic matter and potential storage domains within the same rock unit.

The natural microfractures documented in Pr-23040 represent the permeability component of the dual porosity system. Even partially occluded by diagenetic calcite or clay infill, natural fractures in tight carbonate reservoirs can provide substantially higher permeability than the surrounding matrix when sufficiently open and connected and serve as both natural production conduits and preferred pathways for hydraulic fracture

propagation during stimulation. Their development at the deepest sampled interval suggests that fracture density may increase further with depth, potentially improving reservoir deliverability in the deeper parts of the Ghazij section.

The Ghazij limestone at Zamzama-5 satisfies all principal criteria for unconventional tight carbonate gas reservoir potential: it is organically rich (TOC 3.2–5.05 wt.%, exceeding the 2% unconventional threshold) (Peters et al., 2016), hosts indigenous gas-prone kerogen (Type III, HI 87–183 mg HC/g TOC), is mineralogically brittle (high CaO, low Al_2O_3, non-swelling clinochlore clay), and possesses a multi-scale pore network combining organic-hosted nano-porosity and interparticle microporosity for gas storage with natural microfractures for permeability. Thermal maturity, while currently immature to early mature, indicates that the formation retains significant future generation potential as burial progresses.

The Ghazij limestone at Zamzama-5 is therefore proposed as a prospective unconventional tight carbonate gas play in the Southern Indus Basin, a characterization supported by independent convergence of geochemical, mineralogical, and petrographic evidence. The lateral variability in source rock quality documented between Zamzama-5 and Mehar-1 underscores that this unconventional potential is associated specifically with the carbonate-dominated limestone facies of the Ghazij Formation.

CONCLUSIONS

Integrated geochemical evidence from XRF, TOC, and Rock-Eval pyrolysis shows that the Ghazij Formation at Zamzama-5 is a carbonate-dominated bituminous limestone representing carbonate-rich facies within the regionally shale-dominated Ghazij sequence. It shows very good to excellent organic richness, with TOC values ranging from 2.71 wt.% to 5.05 wt.%, comfortably exceeding the 2% threshold typically required for good unconventional hydrocarbon potential. The kerogen present is indigenous and gas-prone (Type III), with good generative potential as confirmed by the S_1 versus S_2 cross-plot and HI values of 87–183 mg HC/g TOC. Thermal maturity, assessed from the production index as the more reliable indicator in this carbonate matrix, ranges from immature to early mature. The apparent T_{max} reversal with depth is interpreted cautiously and is considered more likely to reflect analytical and mineral-matrix effects, potentially compounded by the inherent uncertainties of drill-cutting samples, rather than a true geological maturity reversal. Together, these properties make the Ghazij limestone at Zamzama-5 a favourable target for unconventional hydrocarbon exploration. At Mehar-1, TOC values of 0.32–0.45 wt.% throughout the sampled interval classify the equivalent Ghazij section as a lean, organic-poor, shale-limestone mixed facies, confirming that the source rock potential of the Ghazij Formation is not uniform across the study area but is associated specifically with the carbonate-dominated facies represented at Zamzama-5.

XRD analysis confirms that the Ghazij limestone at Zamzama-5 is dominated by calcite (42–48%) with significant quartz (28–38%), dolomite at shallow depths transitioning to ankerite (21%) at the deepest interval, a diagenetic signature confirming burial-related iron enrichment under reducing conditions. The clay phase is clinochlore, a

non-swelling chlorite occurring at only 4–5%, which is mineralogically favourable for reservoir quality. Cross-validation across XRF, XRD and SEM-EDS provides strong internal consistency, with XRD resolving the clinochlore identification and ankerite phase that could not be definitively established from elemental data alone. SEM-EDS confirms the carbonate and quartz framework at the grain scale and additionally resolves the spatial distribution of organic matter coatings, pore-lining clay films, and accessory phases. Organic matter occurs as continuous grain-surface coatings hosting nano-scale porosity, confirming that gas generation and retention are occurring within the same rock unit. Five pore types were identified, defining a multi-scale pore system showing depth-related variation, from micron-scale interparticle microporosity at shallow depths, through nano-scale pores at intermediate depths, to natural microfractures as the dominant permeability pathway at the deepest interval. The Ghazij limestone at Zamzama-5 satisfies the principal organic, mineralogical, and pore-system criteria for an unconventional tight carbonate gas reservoir, including organic richness above the unconventional threshold, indigenous gas-prone kerogen, carbonate-dominated mineralogy, and a multi-scale pore network providing potential storage capacity and fracture-controlled permeability. However, the sampled intervals are currently immature to early mature, making thermal maturity the principal limitation to their present thermogenic hydrocarbon potential. More thermally mature Ghazij intervals may occur in deeper parts of the Southern Indus Basin where greater burial has occurred. Investigation of deeper and more mature wells is therefore required to determine whether the favourable source-rock and reservoir characteristics identified in this study extend into a thermally mature hydrocarbon-generating interval. Ghazij Formation is proposed as a prospective unconventional tight carbonate gas play in the Southern Indus Basin.

RECOMMENDATIONS

1. Additional and deeper Ghazij intervals from more mature wells should be investigated to evaluate the thermal maturity and hydrocarbon potential of the formation, particularly in the deeper parts of the Southern Indus Basin.
2. Quantitative reservoir measurements including helium porosimetry, pulse-decay permeametry, and mercury injection capillary pressure (MICP) should be carried out on the Zamzama-5 samples to quantify the storage and flow capacity of the multi-scale pore network identified by SEM, enabling a full quantitative assessment of unconventional production feasibility.
3. Direct mechanical testing (uniaxial compressive strength, Young's modulus, Poisson's ratio) is recommended as future work to independently quantify mechanical brittleness and validate the mineralogical proxy estimates presented here.

REFERENCES

Afzal, J., Williams, M., & Aldridge, R. J. (2009). Revised stratigraphy of the lower Cenozoic succession of the Greater Indus Basin in Pakistan. Journal of Micropalaeontology, 28(1): 7-23.

Ahmad, N., Mateen, J., Shehzad, K. C., Mehmood, N., and Arif, F. (2012 & 2013). Shale gas potential of Lower Cretaceous Sembar Formation in Middle and Lower Indus Basin, Pakistan. Pakistan Journal of hydrocarbon Research, Volumes 22 & 23: 51-62.

Ahmad, N., Fink, P., Sturrock, S., Mahmood, T., and Ibrahim, M., (2012). Sequence stratigraphy as predictive tool in Lower Goru Fairway, Lower and Middle Indus Platform, Pakistan. AAPG, Search and Discovery Article, no. 10404.

Ahmad, R., and Afzal, J. (2012). Sequence stratigraphy of the mixed carbonate-siliciclastic system of the Eocene Nisai Formation, Pishin Basin: Distribution of source rocks and reservoir facies. AAPG, Search and Discovery Article, no. 10406.

Ahmed, A., Hakimi, M. H., Jahandad, S., Lashin, A., Rahim, A., Naseem, W., Nurgaliev, D. K., Khan, M. A., and Munir, M. N. (2025). Geochemical characteristics and 1-D basin modelling study of the Early Cretaceous and Paleogene succession in the Southern Indus Basin, Southern Pakistan. Geological Journal, 60(9): 2213-2231.

Amjad, M. R., Khan, S., Nisar, U. B., Shakir, U., and Ahmed, K. A. (2022). Exploring the untapped gas potential of Ghazij shale in Pirkoh area, Pakistan: Integrated approach of attribute analysis and maturity modelling. Turkish Journal of Earth Sciences, 31(1): 1-19.

Bannert, D., and Raza, H. A. (1992). The segmentation of Indo-Pakistan Plate. Pakistan Journal of Mineral Research, 4(2): 5-18.

Behar, F., Beaumont, V., and De B. Penteado, H. L. (2001). Rock-Eval 6 technology: Performance and developments. Oil & Gas Science and Technology – Revue De L'IFP, 56(2): 111-134.

Bernard, S., Horsfield, B., Schulz, H. M., Schreiber, A., and Wirth, R. (2012). Geochemical evolution of organic-rich shales with increasing maturity: A STXM and TEM study of the Posidonia Shale. Marine and Petroleum Geology, 31(1): 70-89.

Berner, R. A. (1984). Sedimentary pyrite formation: An update. Geochimica et Cosmochimica Acta, 48(4): 605-615.

Boggs, S. Jr. (2012). Principles of sedimentology and stratigraphy (5th ed.). Harlow, England: Pearsons Education Limited.

Bohacs, K. M., Grabowski, G. J., Carroll, A. R., Mankiewicz, P. J., Miskell-Gerhardt, K. J., Schwalbach, J. R., Wegner, M. B., and Simo, J. A. (2005). Production, destruction, and dilution- the many paths to source-rock development. In N. B. Harris (Ed.), The deposition of organic-carbon-rich sediments: Models, Mechanisms, and consequences (SEPM Special Publication, 82: 61-101).

Carvajal-Ortiz, H., Gentzis, T. (2018). Geochemical screening of source rocks and reservoirs: The importance of using the proper analytical program. International Journal of Coal Technology, 190: 56-69.

Choquette, P. W., and Pray, L. C. (1970). Geologic nomenclature and classification of porosity in sedimentary carbonates. The American Association of Petroleum Geologists Bulletin, 54(2): 207-250.

Dar, Q. Z., Renhai, P., Ghazi, S., Ahmed, S., Ali, R. I., and Mehmood, M. (2023). Depositional facies and reservoir characteristics of the Early Cretaceous Lower Goru Formation, Lower Indus Basin, Pakistan: Integration of petrographic and gamma-ray log analysis. Petroleum, 9(2): 331-341.

Deer, W. A., Howie, R. A., and Zussman, J. (2013). An introduction to the rock-forming minerals (3rd ed.). London: The mineralogical Society.

Dunham, R. J. (1962). Classification of carbonate rocks according to depositional texture. In W. E. Ham (Ed.), Classification of carbonate rocks (AAPG Memoir 1: pp. 108-121).

Energy Information Administration (EIA). (2015). Technically recoverable shale oil and shale gas resources: Pakistan. U.S. Department of Energy. https://www.eia.gov

Espitalie, J., Madec, M., Tissot, B., Mennig, J. J., and Leplat, P. (1977). Source rock characterization method for petroleum exploration. Offshore Technology Conference, Houston, Texas, OTC 2935.

Goldstein, J. I., Newbury, D. E., Michael, J. R., Ritchie, N. W. M., Scott, J. H. J., and Joy, D. C. (2018). Scanning electron microscopy and X-ray microanalysis (4th ed.). USA: Spinger.

Hackley, P. C., and Cardott, B. J. (2016) Application of organic petrography in North American shale petroleum systems: A review. International Journal of Coal Geology, 163: 8-51.

Hedges, J.I., and Keil, R. G. (1995). Sedimentary organic matter preservation: An assessment and speculative synthesis. Marine Chemistry, 49: 81-115.

Hupp, B. N., and Donovan, J. J. (2018). Quantitative mineralogy for facies definition in the Marcellus Shale (Appalachian Basin, USA) using XRD-XRF integration. Sedimentary Geology, 371: 16-31.

Immenhauser, A. (2022) On the delimitation of the carbonate burial realm. The Depositional Record, 8: 524-574.

Jadoon, I. A. K., Lawrence, R. D., and Lillie, R. J. (1994). Seismic data, geometry, evolution, and shortening in the active Sulaiman Fold-and-thrust Belt of Pakistan, Southwest of the Himalayas. AAPG Bulletin, 78(5): 758-774.

Jarvie, D. M. (2012). Shale resource systems for oil and gas: Part 2, Shale-oil resource systems. In J. A. Breyer (Ed.), Shale Reservoirs-Giant Resources for the 21st Century (AAPG Memoir 97: pp. 89-119).

Jarvie, D. M., Hill, J. M., Ruble, E. T., and Pollastro, M. R. (2007). Unconventional shale-gas systems: The Mississippian Barnett Shale of north-central Texas as one model for thermogenic shale-gas assessment. AAPG Bulletin, 91(4): 475-499.

Ji, L. M., Qui, J. L., Xia, Y. Q., and Zhang, T. W. (2012). Micro-pore characteristics and methane adsorption properties of common clay minerals by electron microscope scanning, Acta Petrolei Sinica, 33(2): 249-256.

Jin, X., Shah, S. N., Roegiers, J. C., and Zhang, B. (2015). An integrated petrophysics and geomechanics approach for fracability evaluation in shale reservoirs. SPE Journal, 20(3): 518-526.

Johnson, E. A., Warwick, P. D., Roberts, S. B., and Khan, I. H. (1999). Lithofacies, depositional environments, and regional stratigraphy of the Lower Eocene Ghazij Formation, Balochistan, Pakistan. U.S. Geological Survey Professional Paper 1599. U.S. Government Printing Office.

Kadri, I. B. (1995). Petroleum geology of Pakistan. Pakistan Petroleum Limited, Karachi.

Kassi, A. M., Qureshi, A. R., and Kakar, D. M. (1987). Sedimentology of the Ghazij Formation, Kuch Area, Baluchistan. Geological Bulletin, University of Peshawar, 20: 53-62.

Kakar, D. M., and Kassi, A. M. (1997). Lithostratigraphy, sedimentology and petrology of the Ghazij Formation, Sor Range area, Quetta District, Pakistan. Acta Mineralogica Pakistanica, 8: 73-85.

Kazi, A. (1968). Sedimentology of the Ghazij Formation, Harnai, Baluchistan. Geologic Magazine, 105(1), 35-45.

Kazimi, A. H., and Abbasi, S. A. (2008). Stratigraphy and historical geology of Pakistan. Department of Geology, University of Karatchi.

Kazimi, A. H., and Jan, M. Q. (1997). Geology and tectonics of Pakistan. Graphic Publishers, Karachi.

Khalid, A., Ahmad, S., Ali, A., Rehman, G., and Yaseen, M. (2023). Structural analysis of Kirthar Fold Belt, Lower Indus Basin, Balochistan, Pakistan, Pakistan: Implications from compression and inversion tectonics. Sains Malaysiana, 52(2): 417-430.

Khan, M., and Liu, Y. (2019). Geodynamic evolution of the offshore Indus basin Pakistan: The western Indian Plate passive continental margin. Geophysical Journal International, 217(2): 1366-1386.

Law, B. E., and Curtis, J. B. (2002). Introduction to unconventional petroleum systems. AAPG Bulletin, 86(11): 1851-1852.

Loucks, R. G., Reed, R. M., Ruppel, S. C., and Jarvie, D. M. (2009). Morphology, genesis, and distribution of nanometer-scale pores in siliceous mudstones of the Mississippian Barnett Shale. Journal of Sedimentary Research, 79(12): 848-861.

Loucks, R. G., Reed, R. M., Ruppel, S. C., and Hammes, U. (2012). Spectrum of pore types and networks in mudrocks and a descriptive classification for matrix-related mudrock pores. AAPG Bulletin, 96(6): 1071-1098.

Malkani, M. S., and Mahmood, Z. (2017). Stratigraphy of Pakistan. Geological Survey of Pakistan, Memoir 24.

Moore, C. H., and Wade, W. J. (2013). Burial diagenetic environment. In Developments in sedimentology (Vol. 67: pp. 239-284). Elsevier.

Moore, D. M., and Reynolds, R. C. (1997). X-ray diffraction and the identification and analysis of clay minerals (2nd ed.). New York: Oxford University Press.

Mughal, M. R., and Akhtar, G. (2021). Predicting the Gas resource potential in reservoir C-sand interval of Lower Guro Formation, Middle Indus Basin, Pakistan. Open Geosciences 13(1): 49-71.

Nosheen, S., and Giao, P. H. (2017). Evaluation of shale gas potential in the Lower Cretaceous Sembar Formation, the Southern Indus Basin, Pakistan. Journal of Natural Gas Science and Engineering, 44: 162-176.

Peters, K. E. (1986). Guidelines for evaluating petroleum source rock using programmed pyrolysis. AAPG Bulletin, 70(3): 318-329.

Peters, K. E., and Cassa, M. R. (1994). Applied source rock geochemistry. In L. B. Magoon and W. G. Dow (Eds.), The petroleum system-From source to trap (AAPG Memoir 60: pp. 93-120).

Peters, K. E., Walters, C. C., and Moldowan, J. M. (2005). The biomarker guide (Volume 1): Biomarkers and isotopes in the environment and human history (2nd ed.). Cambridge University Press.

Peters, K. E., Xia, X., Pomerantz, A. E., and Mullins, O. C. (2016). Geochemistry applied to evaluation of unconventional resources. In Z. Ma and S. Holditch (Eds.), Unconventional oil and gas resources handbook (pp. 71-126). Elsevier.

Qureshi, K. A., Arif, M., Basit, A., Ahmad, S., Janjuhah, H. T., and Kontakiotis, G. (2023). Sedimentological controls on the reservoir characteristics of the Mid-Triassic Tredian Formation in the Salt and Trans-Indus Surghar Ranges, Pakistan: Integration of Outcrop, Petrographic, and SEM Analysis. Journal of Marine Sciences and Engineering, 11(5): 1019.

Raza, H. A., Ahmed, R., Ali, S. M., and Ahmad, J. (1989). Petroleum prospects of the Sulaiman Sub-Basin, Pakistan. Pakistan Journal of Hydrocarbon Research, 1: 21-56.

Raza, H. A., Ali, S. M., and Ahmed, R. (1990). Petroleum geology of Kirthar sub-basin and part of Kutch Basin. Pakistan Journal of Hydrocarbon Research, 2(1): 29-73.

Reed, S. J. B. (2005). Electron microprobe analysis and scanning electron microscopy in geology (2nd ed.). United Kingdom: Cambridge University Press.

Rollinson, H. R. (1993). Using geochemical data: Evaluation, presentation, interpretation. London, United Kingdom: Longman Scientific & Technical.

Ross, D. J. K., and Bustin, R. M. (2009). The importance of shale composition and pore structure upon gas storage potential of shale gas reservoirs. Marine and Petroleum Geology, 26(6): 916-927.

Sahir, N. (2018). The comparison of the retained gas in shale (RGIS) between the Paleocene Ranikot Formation and the Lower Cretaceous Sembar Formation, the Southern Indus Basin, Pakistan. International Journal of Geoinformatics and Geological Science, 5(3), 33-38.

Schenk, C. J., Klett, T. R., Charpentier, R. R., Cook, T. A., Pitman, J. K., Pollastro, R. M., Schuenemeyer, J. H., Tennyson, M. E., and Whidden, K. J., (2017). Assessment of undiscovered oil and gas resources of the Lower Indus Basin, Pakistan. U.S. Geological Survey Fact Sheet 2017-3034.

Schmoker, J. W. (2002). Resource-assessment perspectives for unconventional gas systems. AAPG Bulletin, 86(11): 1993-1999.

Shah, F., Miraj, M. A. F., Ali, A., Ahsan, N., Mehmood, T., Sajid, M., Salaam, A., and Fazal, A. G. (2023). Tectonics of Jacobabad-Khairpur High and its Impact on Petroleum Fields of the Region, Southern Indus Basin, Pakistan: A Case Study. Geotectonics, 57(3): 346-358.

Shah, S. M. I. (2009). Stratigraphy of Pakistan. Geological Survey of Pakistan Memoirs, Vol. 22.

Slatt, R. M., and O'Brien, N. R. (2011). Pore types in the Barnett and woodford gas shales: Contribution to understanding gas storage and migration pathways. AAPG Bulletin, 95(12): 2017-2030.

Tissot, B. P., and Welte, D. H. (1984). Petroleum formation and occurrence (2nd ed.). Germany: Springer-Verlag.

Tucker, M. E. (2001) Sedimentary Petrology: An introduction to the origin of sedimentary rocks (3rd ed.). United Kingdom: Blackwell Science.

Tucker, M. E., and Wright, V. P. (1990). Carbonate sedimentology. United Kingdom: Blackwell Scientific Publication.

Wandrey, C. J., Law, B. E., and Shah, H. A. (2004). Sembar Goru/Ghazij composite total petroleum system, Indus and Sulaiman-Kirthar geologic provinces, Pakistan and India (USGS Bulletin 2208-C). U.S. Geological Survey.

Wang, F. P., and Gale, J. F. W. (2009). Screening criteria for shale-gas systems. Gulf coast Association of Geological Societies Transactions, 59: 779-793.

Warwick, P. D., Johnson, E. A., and Khan, I. H. (1998). Collision-induced tectonism along the northwestern margin of the Indian subcontinent as recorded in the Upper Paleocene

to Middle Eocene strata of central Pakistan (Kirthar and Sulaiman Ranges). Palaeogeography, Palaeoclimatology, Palaeoecology, 142: 201-216.

Worden, R. H., and Morad, S. (Eds.). (2003). Clay mineral cements in sandstones. International Association of Sedimentologists Special Publication No. 34. United Kingdom: Blackwell Publishing.

Xu, J., and Sonnenberg, S. (2016). Brittleness and rock strength of the Bakken Formation, Williston Basin, North Dakota. Unconventional Resources Technology Conference (URTeC: 2460490).

Yang, S., and Horsfield, B. (2020). Critical review of the uncertainty of Tmax in revealing the thermal maturity of organic matter in sedimentary rocks. International Journal of Coal Technology, 225, 103500.

Zhao, C., Jiang, Y., Liu, J., Liu, M., and Wang, L. (2022). Occurrence and origin of chlorite and associated impact on tight sandstone reservoir quality: A case study of the Xujiahe Formation (NE Sichuan Basin, China). Journal of Petroleum Science and Engineering, 209(1): 109859.

Zou, C. (2017). Unconventional Petroleum Geology (2nd ed.) Elsevier.

17% Overall Similarity

The combined total of all matches, including overlapping sources, for each database.

Filtered from the Report

- Bibliography
- Quoted Text

Match Groups

235 Not Cited or Quoted 12%
Matches with neither in-text citation nor quotation marks

108 Missing Quotations 5%
Matches that are still very similar to source material

0 Missing Citation 0%
Matches that have quotation marks, but no in-text citation

0 Cited and Quoted 0%
Matches with in-text citation present, but no quotation marks

Top Sources

12% Internet sources
11% Publications
13% Submitted works (Student Papers)

Integrity Flags

0 Integrity Flags for Review

Our system's algorithms look deeply at a document for any inconsistencies that would set it apart from a normal submission. If we notice something strange, we flag it for you to review.

A Flag is not necessarily an indicator of a problem. However, we'd recommend you focus your attention there for further review.

Match Groups

- **235** Not Cited or Quoted 12%
  Matches with neither in-text citation nor quotation marks
- **108** Missing Quotations 5%
  Matches that are still very similar to source material
- **0** Missing Citation 0%
  Matches that have quotation marks, but no in-text citation
- **0** Cited and Quoted 0%
  Matches with in-text citation present, but no quotation marks

Top Sources

12% Internet sources
11% Publications
13% Submitted works (Student Papers)

Top Sources

The sources with the highest number of matches within the submission. Overlapping sources will not be displayed.

1	Internet	
www.mdpi.com		<1%
2	Student papers	
Higher Education Commission Pakistan on 2015-01-21		<1%
3	Internet	
pubs.usgs.gov		<1%
4	Student papers	
Higher Education Commission Pakistan on 2023-03-03		<1%
5	Internet	
mdpi-res.com		<1%
6	Internet	
www.researchgate.net		<1%
7	Internet	
www.frontiersin.org		<1%
8	Internet	
docplayer.net		<1%
9	Internet	
etheses.dur.ac.uk		<1%
10	Student papers	
Higher Education Commission Pakistan on 2025-08-12		<1%

11	Student papers	
Higher Education Commission Pakistan on 2014-07-09		<1%
12	Publication	
Arif Nazir, Fraz Khalid, Saeed Abbas, Qaiser Hussain, Muhammad Deen, Abid Ali, ...		<1%
13	Internet	
www.science.gov		<1%
14	Student papers	
Higher Education Commission Pakistan on 2011-11-14		<1%
15	Internet	
hdl.handle.net		<1%
16	Internet	
ediss.uni-goettingen.de		<1%
17	Internet	
prr.hec.gov.pk		<1%
18	Student papers	
Higher Education Commission Pakistan on 2018-09-04		<1%
19	Internet	
shareok.org		<1%
20	Internet	
aj.tubitak.gov.tr		<1%
21	Internet	
public-pages-files-2025.frontiersin.org		<1%
22	Publication	
Adeeb Ahmed, Tahseenullah Khan, Khairul Azlan Mustapha, Samina Jahandad. "N...		<1%
23	Student papers	
Higher Education Commission Pakistan on 2022-03-25		<1%
24	Internet	
phd-dissertations.unizik.edu.ng		<1%

25	Internet	
ra.azu.edu.ly		<1%
26	Internet	
lra.le.ac.uk		<1%
27	Internet	
pure.manchester.ac.uk		<1%
28	Student papers	
Eiffel Corporation on 2019-04-29		<1%
29	Student papers	
Higher Education Commission Pakistan on 2020-08-25		<1%
30	Internet	
ir.lib.uwo.ca		<1%
31	Publication	
Robson, Micaela Jeanette. "Integrating Heterotrophic Nitrification - Aerobic Denit...		<1%
32	Internet	
pmc.ncbi.nlm.nih.gov		<1%
33	Student papers	
Federal University of Technology on 2019-08-31		<1%
34	Student papers	
Higher Education Commission Pakistan on 2011-08-23		<1%
35	Internet	
scholars.unh.edu		<1%
36	Internet	
www.geojournals.cn		<1%
37	Student papers	
University of Newcastle upon Tyne on 2015-11-18		<1%
38	Internet	
doi.org		<1%

39	Publication	
Momotaj Begum, Mahmood Reza Yassin, Hassan Dehghanpour. "Effect of keroge...		<1%
40	Publication	
Shilin Wang, Ahmed Mansour, Cong Li, Peidong Su, Lingjian Meng, Mohamed S. A...		<1%
41	Internet	
repository.mines.edu		<1%
42	Internet	
studentsrepo.um.edu.my		<1%
43	Student papers	
Indian School of Mines on 2019-06-16		<1%
44	Publication	
Nosheen Sheikh, Pham Huy Giao. "Evaluation of shale gas potential in the Lower ...		<1%
45	Internet	
api-depositonce.tu-berlin.de		<1%
46	Internet	
ejurnal.itats.ac.id		<1%
47	Internet	
id.scribd.com		<1%
48	Student papers	
lms20261 on 2026-10-08		<1%
49	Student papers	
Higher Education Commission Pakistan on 2026-08-13		<1%
50	Publication	
Srivastava, Pankaj, Subhra Patel, Nandita Singh, Toshienla Jamir, Nandan Kumar, ...		<1%
51	Student papers	
University Der Es Salaam on 2024-03-13		<1%
52	Internet	
cedar.wwu.edu		<1%

53	Student papers	
University of Limpopo on 2021-02-03		<1%
54	Publication	
Xiaoqi Ban, Jin Yao, Wanzhong Yin, Shenda Chen, Wenju Sun, Taozhong Zhang, W...		<1%
55	Internet	
espace.curtin.edu.au		<1%
56	Internet	
worldwidescience.org		<1%
57	Internet	
www.e-publicacoes.uerj.br		<1%
58	Student papers	
Higher Education Commission Pakistan on 2025-02-07		<1%
59	Student papers	
King Fahd University for Petroleum and Minerals on 2026-05-02		<1%
60	Student papers	
University of Malaya on 2026-08-26		<1%
61	Internet	
d-nb.info		<1%
62	Internet	
etheses.durham.ac.uk		<1%
63	Internet	
gyan.iitg.ac.in		<1%
64	Internet	
services.bgr.de		<1%
65	Internet	
www.hdip.com.pk		<1%
66	Publication	
Aya Raafat, Sameh S. Tahoun, Moataz El-Shafeiy, Thomas Gentzis, Walid H. Tawfik...		<1%

67	Publication	
Bodhisatwa Hazra, David A. Wood, Devleena Mani, Pradeep K. Singh, Ashok K. Sin...		<1%
68	Student papers	
Higher Education Commission Pakistan on 2015-05-13		<1%
69	Student papers	
Sriwijaya University on 2023-05-29		<1%
70	Internet	
www.semanticscholar.org		<1%
71	Publication	
Adeeb Ahmed, Tahseenullah Khan, Samina Jahandad, Mohammed Hail Hakimi, Ar...		<1%
72	Publication	
Esther B. Owusu, Haylay Tsegab, Chow Weng Sum, Eswaran Padmanabhan. "Orga...		<1%
73	Student papers	
Higher Education Commission Pakistan on 2013-04-20		<1%
74	Student papers	
Higher Education Commission Pakistan on 2015-06-19		<1%
75	Student papers	
Higher Education Commission Pakistan on 2018-10-25		<1%
76	Publication	
Subhrangsu K. Acharyya, Puspendu Saha. "Himalayan Paleogene Foreland Basin, ...		<1%
77	Student papers	
University of Houston, Downtown on 2026-05-06		<1%
78	Student papers	
University of Mosul on 2022-11-27		<1%
79	Internet	
repository.derby.ac.uk		<1%
80	Publication	
Abheek Sarkar, Janardhan Damodhar Gajbhiye, Gourab Rana, Deepika Arora, Lov...		<1%

81	Student papers	
Asian Institute of Technology on 2017-04-07		<1%
82	Student papers	
Higher Education Commission Pakistan on 2021-06-21		<1%
83	Student papers	
Higher Education Commission Pakistan on 2025-02-03		<1%
84	Publication	
Rizwan Sarwar Awan, Bo Liu, Qamar Yasin, David A. Wood et al. "Paleoenvironme...		<1%
85	Internet	
cp.copernicus.org		<1%
86	Internet	
file.scirp.org		<1%
87	Internet	
frackinginquiry.nt.gov.au		<1%
88	Internet	
open.uct.ac.za		<1%
89	Internet	
umpir.ump.edu.my		<1%
90	Internet	
www.scirp.org		<1%
91	Publication	
Muyyassar Hussain, Urooj Shakir, Zohaib Naseer, Muhammad Raiees Amjad, Faro...		<1%
92	Student papers	
Universiti Teknologi Petronas on 2015-07-09		<1%
93	Student papers	
University of Nottingham on 2026-04-22		<1%
94	Publication	
Waqas Naseem, Irfan Ullah Jan, Mohammed Hail Hakimi, Khairul Azlan Mustapha...		<1%

95	Internet	
actampcem.net		<1%
96	Internet	
ddd.uab.cat		<1%
97	Internet	
eprints.kfupm.edu.sa		<1%
98	Internet	
livrepository.liverpool.ac.uk		<1%
99	Internet	
theses.lib.sfu.ca		<1%
100	Publication	
Bei Liu, Juergen Schieber, Maria Mastalerz, Juan Teng. "Variability of rock mechan...		<1%
101	Publication	
Black, Dawn Ebony. "Stratigraphic Characterisation of the Collingham Formation ...		<1%
102	Publication	
Syed Bilawal Ali Shah. "Shale gas potential of Sembar Formation, Punjab Platform...		<1%
103	Student papers	
Universiti Brunei Darussalam on 2021-11-18		<1%
104	Internet	
agupubs.onlinelibrary.wiley.com		<1%
105	Internet	
baadalsg.inflibnet.ac.in		<1%
106	Internet	
digital.library.adelaide.edu.au		<1%
107	Internet	
etheses.whiterose.ac.uk		<1%
108	Internet	
pdffox.com		<1%

109	Internet	
www.gamtostyrimai.lt		<1%
110	Publication	
Gaibor, J.. "Hydrocarbon source potential of the Santiago Formation, Oriente Basi...		<1%
111	Student papers	
Higher Education Commission Pakistan on 2017-12-19		<1%
112	Publication	
Peter D Warwick, Edward A Johnson, Intizar H Khan. "Collision-induced tectonism ...		<1%
113	Publication	
Tewari, Anuradha, Suryendu Dutta, and Tanmoy Sarkar. "ORGANIC GEOCHEMICA...		<1%
114	Student papers	
University of Ghana on 2020-06-30		<1%
115	Student papers	
University of Newcastle upon Tyne on 2011-08-18		<1%
116	Student papers	
University of Nottingham on 2023-04-21		<1%
117	Student papers	
Univerza v Ljubljani on 2023-05-03		<1%
118	Publication	
Wnuk, Christopher. "Coal resource potential of Afghanistan", International Geolo...		<1%
119	Internet	
bahria.edu.pk		<1%
120	Internet	
prism.ucalgary.ca		<1%
121	Internet	
pure.uva.nl		<1%
122	Internet	
revistas.ufrj.br		<1%

123 Internet
www.etesters.com <1%

124 Publication
Celeste D. Lohr, Matthew D. Merrill. "Comparison of measured versus modeled T... <1%

125 Student papers
Cranfield University on 2010-10-18 <1%

126 Publication
Cunfei Ma, Chunmei Dong, Chengyan Lin, Derek Elsworth, Guoqiang Luan, Xiaolo... <1%

127 Student papers
Federal University of Technology on 2013-07-10 <1%

128 Student papers
Heriot-Watt University on 2017-11-07 <1%

129 Student papers
Higher Education Commission Pakistan on 2011-08-22 <1%

130 Student papers
Higher Education Commission Pakistan on 2014-07-22 <1%

131 Student papers
Higher Education Commission Pakistan on 2021-06-10 <1%

132 Student papers
Imperial College of Science, Technology and Medicine on 2009-06-22 <1%

133 Publication
Khurram Shahzad, Christian Betzler, Nadeem Ahmed, Farrukh Qayyum, Silvia Spe... <1%

134 Student papers
King Abdullah University of Science and Technology (KAUST) on 2026-05-17 <1%

135 Publication
Syed Muhammad Ibad, E. Padmanabhan. "Methane sorption capacities and geoc... <1%

136 Student papers
Universiti Kuala Lumpur on 2026-06-29 <1%

137 Student papers
Universiti Teknologi Petronas on 2021-05-10 <1%

138 Student papers
University of Derby on 2009-09-24 <1%

139 Student papers
University of Newcastle upon Tyne on 2006-08-21 <1%

140 Internet
africadailynews.net <1%

141 Internet
archive.org <1%

142 Internet
coek.info <1%

143 Internet
core.ac.uk <1%

144 Internet
dokumen.pub <1%

145 Internet
dr.ddn.upes.ac.in:8080 <1%

146 Internet
ia600201.us.archive.org <1%

147 Internet
www.bioregionalassessments.gov.au <1%

148 Internet
www.scbaghdad.edu.iq <1%

149 Student papers
Central University Of Jharkhand on 2026-05-21 <1%

150 Publication
Christopher M. Agyingi, Noel C. Tangko, Emmanuel Eseme. "Bulk petroleum geoc... <1%

151 Student papers
Curtin University of Technology on 2016-11-03 <1%

152 Publication
Goswami, Himakshi. "Geological Carbon Storage in Deep, Low Permeable Shale R... <1%

153 Publication
Grégoire Métais, Pierre-Olivier Antoine, S.R. Hassan Baqri, Jean-Yves Crochet et al... <1%

154 Publication
Gurgey, K.. "Origin of petroliferous bitumen from the Buyuk Menderes-Gediz g... <1%

155 Student papers
Higher Education Commission Pakistan on 2015-08-01 <1%

156 Student papers
Higher Education Commission Pakistan on 2017-08-11 <1%

157 Student papers
King Abdullah University of Science and Technology (KAUST) on 2025-12-03 <1%

158 Student papers
KoE on 2026-06-10 <1%

159 Publication
Liangwei Xu, Yang Wang, Luofu Liu, Lei Chen, Ji Chen. "Evolution characteristics a... <1%

160 Publication
Maqsood Ur Rahman, Muhammad Hanif, Tao Jiang, Wang Qianru, Fulong Ning, M... <1%

161 Publication
Muhammad Aslam Khan, Chenglin Liu, Zhengang Ding, Wang Haidong, Tian Anqi.... <1%

162 Publication
Paul C. Hackley, Clifford C. Walters, Simon R. Kelemen, Maria Mastalerz, Heather ... <1%

163 Publication
Peerzada Danish, Anil Sagar Srinivasa, Jasir Mushtaq, Ganesh G. Mohan, A.S. Sant... <1%

164 Publication
Penglin Zhang, Qingtao Meng, David Misch, Reinhard F. Sachsenhofer, Zhaojun Li... <1%

165	Publication	
Roger Slatt. "Important geological properties of unconventional resource shales"...		<1%
166	Publication	
Tianbo Liang, Dongya Wei, Fujian Zhou, Xiuhui Li, Lishan Yuan, Bo Wang, Jun Lu. "...		<1%
167	Student papers	
Universiti Brunei Darussalam on 2015-10-17		<1%
168	Student papers	
University College London on 2013-10-13		<1%
169	Student papers	
University of Greenwich on 2025-11-28		<1%
170	Student papers	
University of Newcastle upon Tyne on 2016-08-19		<1%
171	Student papers	
University of South Florida on 2020-11-06		<1%
172	Student papers	
University of York on 2016-08-03		<1%
173	Internet	
archives.datapages.com		<1%
174	Internet	
commons.und.edu		<1%
175	Internet	
delsuelib.com.ng		<1%
176	Internet	
edepositireland.ie		<1%
177	Internet	
egusphere.net		<1%
178	Internet	
escholarship.org		<1%

179	Internet	
hal.univ-lorraine.fr		<1%
180	Internet	
jksus.org		<1%
181	Internet	
link.springer.com		<1%
182	Internet	
ontariotechu.scholaris.ca		<1%
183	Internet	
openaccess.medipol.edu.tr		<1%
184	Internet	
ourspace.uregina.ca		<1%
185	Internet	
pu.edu.pk		<1%
186	Internet	
real-phd.mtak.hu		<1%
187	Internet	
researcharchive.vuw.ac.nz		<1%
188	Internet	
ruj.uj.edu.pl		<1%
189	Internet	
theses.hal.science		<1%
190	Internet	
ualberta.scholaris.ca		<1%
191	Internet	
ucalgary.scholaris.ca		<1%
192	Internet	
vital.seals.ac.za		<1%

193	Internet	
www.degruyter.com		<1%
194	Internet	
www.ijsrp.org		<1%
195	Publication	
Adeeb Ahmed, Tahseenullah Khan, Khairul Azlan Mustapha, Samina Jahandad, Ah...		<1%
196	Student papers	
Higher Education Commission Pakistan on 2012-08-16		<1%
197	Student papers	
Higher Education Commission Pakistan on 2017-07-05		<1%
198	Student papers	
Higher Education Commission Pakistan on 2019-09-24		<1%
199	Student papers	
Sabanci Universitesi on 2026-10-06		<1%
200	Publication	
William, Masen S.. "Stress Corrosion Cracking and Hydrogen Embrittlement of Ba...		<1%
201	Internet	
journalarticle.ukm.my		<1%
202	Internet	
nora.nerc.ac.uk		<1%
203	Internet	
www.engineering10.com		<1%
204	Internet	
zaguan.unizar.es		<1%
205	Publication	
"Advances in Petroleum Source Rock Characterizations: Integrated Methods and ...		<1%
206	Publication	
"Encyclopedia of Geochemistry", Springer Science and Business Media LLC, 2018		<1%

207	Publication	
Aijaz Ali Halepoto, Muhammad Hassan Agheem, Asghar A.A.D. Hakro, Shabeer Ah...		<1%
208	Student papers	
Higher Education Commission Pakistan on 2012-06-22		<1%
209	Student papers	
Higher Education Commission Pakistan on 2013-03-11		<1%
210	Student papers	
Higher Education Commission Pakistan on 2016-08-10		<1%
211	Student papers	
Higher Education Commission Pakistan on 2018-06-01		<1%
212	Publication	
Moamen Ali. "Three dimensional structural modelling and source rock evaluation...		<1%
213	Publication	
Monalisa Mallick, Runcie Paul Mathews, Nihar Ranjan Kar, Barnita Banerjee et al. ...		<1%
214	Publication	
Nhamutole, Nelson Ernesto. "Palynology and Organic Geochemistry Analysis of B...		<1%
215	Publication	
Perveiz Khalid, Asam Farid, Muhammad Tayyab Naseer, Qamar Yasin, Shazia Nas...		<1%
216	Publication	
Rizwan Sarwar Awan, Bo Liu, Hongxia Li, Sajjad Ali, Muhammad Amar Gul, Lingsh...		<1%
217	Student papers	
Troy University on 2023-08-05		<1%
218	Student papers	
Universiti Teknikal Malaysia Melaka - Library on 2026-07-07		<1%
219	Student papers	
University of Mosul on 2021-07-25		<1%
220	Student papers	
University of Newcastle upon Tyne on 2008-08-13		<1%

221 Publication

V.P. Chabalala, N. Wagner, N. Malumbazo, C.F. Eble. "Geochemistry and organic p... <1%

222 Internet

research.manchester.ac.uk <1%